OPTICAL AND ELECTROCHEMICAL ANION SENSORS
BASED ON METALLOPORPHYRINS AND METALLOTEXAPHYRINS

by

Young-Jea Kang

A dissertation submitted in partial fulfillment
of the requirements for the degree of
Doctor of Philosophy
(Chemistry)
in The University of Michigan
2008

Doctoral Committee:

    Professor Mark E. Meyerhoff, Chair
    Professor Edward T. Zellers
    Associate Professor Zhan Chen
    Assistant Professor Marc J. A. Johnson

To my mother and father

Acknowledgements

I would like to thank all the people who helped me during the dissertation work. Most of all, I would like to appreciate Dr. Meyerhoff, my research advisor, for his concern, patience, and encouragement on me whenever I was lost in the middle of dark. I would like to thank Dr. Zellers, Dr. Chen, and Dr. Johnson for their deep interests and feedback on my work as dissertation committee members. I would like to give special thanks to my 'teachers' who gave me valuable comments on the research: Prof. Ibrahim Badr, Prof. Youngmi Lee, Prof. Elzbieta Malinowska, Prof. Sungbae Park, Prof. Wei Qin, Dr. Wansik Cha, Dr. Sangyeul Hwang, Dr. Bongkyun Oh, and Mr. Seunghyuk Choi.

Table of Contents

List of Figures

Figure

List of Tables

List of Schemes

Scheme

Chapter 1

Introduction

1.1 Principles of ion-selective electrodes and optical ion sensors

Since the 1960s, ion-selective electrodes have contributed significantly to sensor - based measurements with a wide range of applications for detecting various ions important in the clinical, environmental, and industrial areas [1, 2]. In this introductory chapter, response mechanisms of ion-selective electrodes and related ionophore-based optical sensors are briefly covered, and the principles of anion sensors based on metalloporphyrin ionophores in polymeric films are discussed.

1.1.1 Ion-selective electrode

The concentration cell (Fig. 1.1) is an electrochemical cell where the concentration difference of the same ion creates a potential difference between two electrodes across two aqueous phases that are connected via a salt bridge. The potential developed is described by the Nernst equation :

$$E = K - \frac{RT}{z_I F} \ln \frac{a_{I(phase1)}}{a_{I(phase2)}} \qquad (Eq. 1.1)$$

where E is the measured electrochemical potential, K is the sum of all constant potentials of the cell (e.g., E^o values for electrodes and corresponding redox couple), R is the gas constant, T is temperature, z_I is the charge of the ion I, F is the Faraday constant and a_I is the activity of the ion I in each aqueous phase. The salt bridge physically connects the two separate phases, maintaining ionic conductivity via the diffusion of electrolytes

through the salt bridge. An electric current must be generated between the two electrodes in order for the two phases to have the same concentration of the ion at equilibrium. This concentration cell is a fundamental precursor of the ion-selective electrode.

The concentration cell can be configured to perform as a sensor if one of the aqueous phases is considered an unknown sample and the other as a known internal phase. When the concentration of an ion in the internal side is fixed, a potential change dependent solely on the concentration change of the ion in the sample side will be observed.
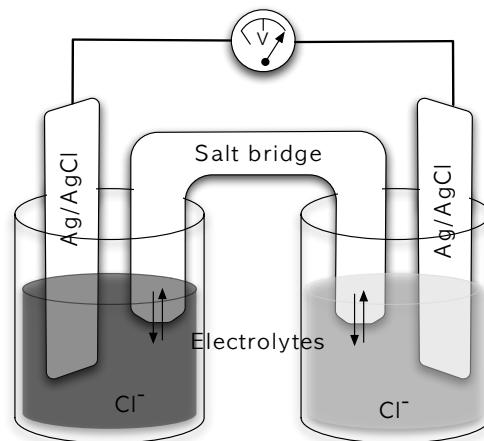
Figure 1.1 An example of a chloride concentration cell. The dark solution (left) indicates higher concentration of chloride than the bright solution (right).

When two phases are immiscible, an interface is formed between the two phases. This interface can replace the salt bridge in the concentration cell because it separates the two phases and allows the ion-transport that makes the cell conductive. Therefore, the electrochemical potential developed across the interface is described by Eq. 1.1 where phase 1 is the aqueous phase and the phase 2 is the organic phase. However, the diffusion of ions across the interface must be limited because, depending on their solvation energies, the free movement of ions across the interface would allow spontaneous distribution of ions in each phase. This type of ion partitioning in each phase prohibits the use of this configuration as a sensor. A change of concentration in one phase immediately causes a corresponding change in the other phase and the following equation is valid

when the partitioning process governs ion distribution across the interface:

$$p = \frac{a_{I(aq)}}{a_{I(org)}} = \text{constant} \qquad\qquad (\text{Eq. 1.2})$$

In Eq. 1.1, the ratio of activities can be substituted with partitioning coefficient (p), and thus the overall potential E of the cell is constant regardless of $a_{I(aq)}$ or $a_{I(org)}$. However, addition of a lipophilic ion-exchanger in the organic phase can make E in Eq. 1.1 a function of $a_{I(aq)}$ only.
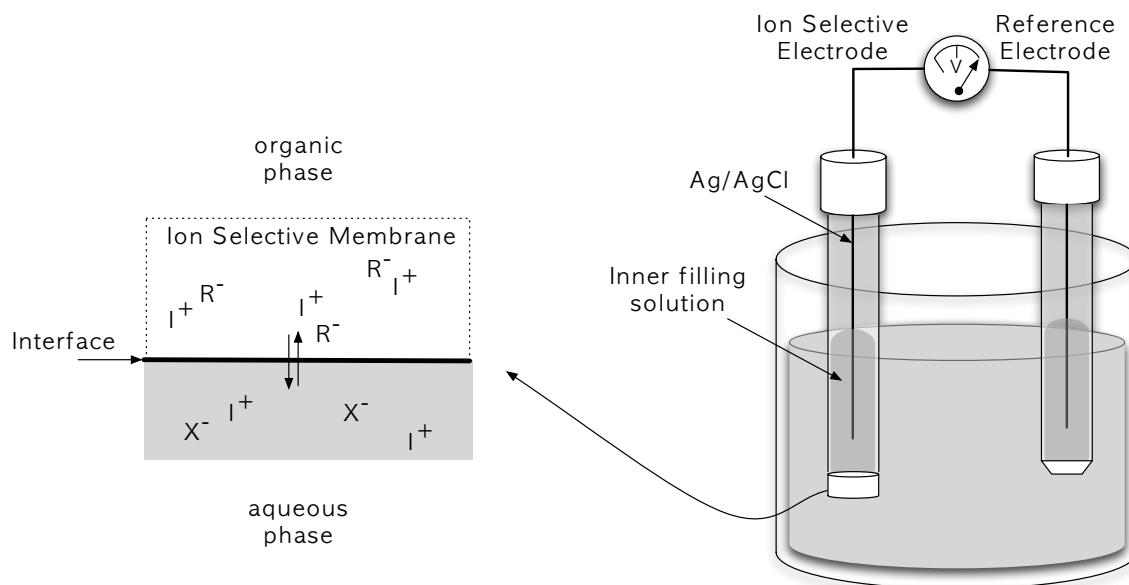
Figure 1.2 Ion-selective electrode based on the cation-exchanger. Note that the free cation concentration (I^+) in the membrane is equal to the concentration of the ion-exchanger (R^-) regardless of the concentration of I^+ in the aqueous phase.

Lipophilic ion-exchangers are ionic species that do not partition into the aqueous phase nor bind with counter ions to become a neutral complex. If the organic phase is doped with a particular lipophilic ion-exchanger, the concentration of counter ions will be equal to the concentration of the lipophilic ion-exchanger in the organic phase. In other words, a concentration change of an ion in the aqueous phase does not affect its concentration in the organic phase. Therefore, in Eq. 1.1, $a_{I(org)}$ is now constant. In the sensor configuration shown in Fig. 1.2, the potential across the interface changes only as

3

a function of the activity of the ion in the aqueous phase. This behavior can be represented by Eq. 1.3:

$$E = E' - \frac{RT}{z_I F} \ln(a_{I(aq)}) \qquad \text{(Eq. 1.3)}$$

$$\text{and } E' = K + \frac{RT}{z_I F} \ln(a_{I(org)}) \quad , \quad a_{I(org)} = z_I [R^{\pm}_{(org)}]$$

where $[R^{\pm}_{(org)}]$ is the concentration of the lipophilic ion-exchanger in the organic phase.

With an ion-exchanger, the sensor responds to ions that counter-balance the charge of the ion-exchanger (i.e., an anion-exchanger (lipophilic cationic species) will respond to anions, and vice versa). Therefore, the degree of response between ions will depend on how well the ion of interest is solvated in the organic phase and how well it is de-solvated from the aqueous phase. Since differences of hydration energies of ions are much greater than differences of solvation energies in the organic solvents [1], the tendency of ions to partition from the aqueous phase to the organic phase follows the trend in hydration energy of ions. The selectivity pattern according to this trend is called the "Hofmeister selectivity pattern" [3]:

Cations : $MeNH_3^+ > NH_4^+ > K^+ > Na^+ > Li^+ > Mg^{2+} > Ca^{2+}$

Anions : $ClO_4^- > SCN^- > salicylate > I^- > NO_3^- > Br^- > NO_2^- > Cl^- > HCO_3^- > F^-$
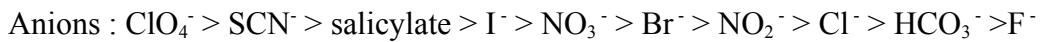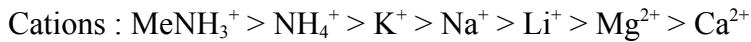
It is also possible to control the selectivity of a sensor by incorporating an ion recognition unit (i.e., ionophore) that selectively binds with the ion of interest in the organic phase. Therefore, the selectivity of such a sensor now depends on how well the ion is solvated into the given organic phase, and how strongly it binds with the ionophore. In fact, the response obtained from a sensor is a collective response for every ion present in the sample solution. Eq. 1.3 should be modified in order to include the responses from each ion as follows:

$$E = E' - \frac{RT}{z_I F} \ln \left[a_{I(aq)} + \sum_J k_{I,J}^{pot} a_J{}^{z_I / z_J} \right] \qquad \text{(Eq. 1.4)}$$

where $k^{pot}{}_{I,J}$ is the selectivity coefficient of ion I over ion J. Eq. 1.4 is called the Nikolskii-Eisenman equation [4] and the selectivity coefficient in this equation represents the degree of response for each ion when they each possess the same activity in the sample phase. Therefore, a selectivity coefficient is a guideline on how much an ion-selective electrode suffers from interference by other ions of the same charge as the analyte. For practical applications, the selectivity coefficients for the ion of interest over interfering ions should be low enough to ignore responses from the interferent species.
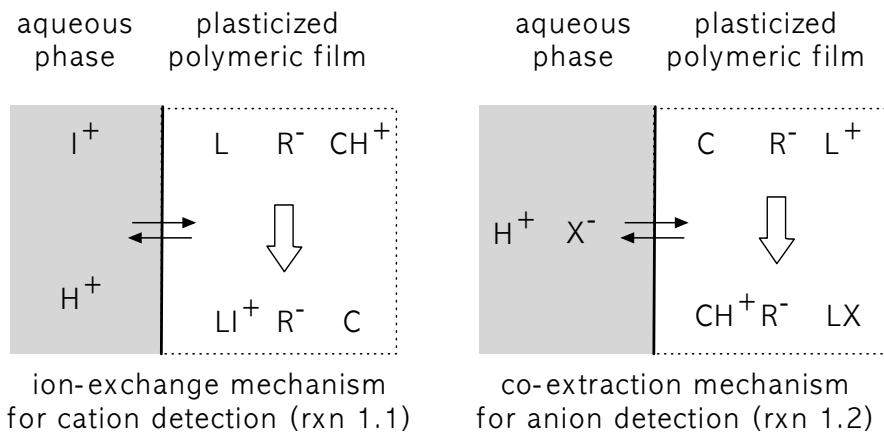
Figure 1.3 Response mechanisms of ion-Selective optical sensors.

1.1.2   Ion-selective optical sensor

Optical ion sensors described in this thesis are often called "bulk optodes," which consist of a plasticized polymeric phase doped with ionophores and chromoionophores [1, 5]. The optical signal is obtained by monitoring absorbance changes of the film upon contact with the aqueous sample phase. The absorbance of the film originates from the lipophilic dye solvated in the plasticized film. The dyes, called chromoionophores, are usually lipophilized pH indicators that change absorbance in the visible spectral region

upon protonation and deprotonation. Ionophores doped in the film facilitate an extraction of ions of interest into the film and a concomitant protonation or deprotonation of the chromoionophore takes place to maintain charge neutrality in the film. For example, a Na^+ optical sensor extracts the Na^+ into the film and a proton in the film leaves into aqueous phase via an ion exchange process (Fig. 1.3). The amount of cation extracted into the film is equal to the amount of proton that exited the film. Therefore, the degree of protonation (or deprotonation) of dye is a quantitative measure for the degree of extraction of the ion of interest as can be seen in the following equilibrium:

$$CH^+R^- + L + I^+_{(aq)} \rightleftharpoons C + LI^+R^- + H^+_{(aq)} \qquad \text{(rxn 1.1)}$$
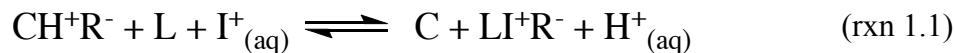
where C is the chromoionophore, R^- is the anionic site, L is the ionophore for ion I^+, and species in the organic phase are denoted without any subscript. While optodes for cations utilize the ion exchange mechanism, in the case of anion-selective optical sensors, anions are co-extracted into the film along with a proton because the anion ionophore is typically a charged carrier type species (Fig. 1.3). Therefore, the equilibrium is usually as follows:

$$C + L^+R^- + H^+_{(aq)} + X^-_{(aq)} \rightleftharpoons CH^+R^- + LX \qquad \text{(rxn 1.2)}$$

where L^+ is the ionophore for anion X^-. Since the ion-selective optical sensor involves proton response, pH should be fixed during the measurement by using an appropriate buffer as a sample phase. The above mechanisms are presented to demonstrate how the ion-selective optical sensor works. There are many variations of these principles in the literature based on the charges of ionophores and chromoionophores as well as on whether or not the ionophores themselves also exhibit optical properties [1].

An optical response of a sensor is also a collective response of all the ions in the sample phase. The degree of response of ions at the same concentration depends on how well the ion is solvated in the organic phase from aqueous phase and how strongly it binds with the ionophore in the organic phase. Therefore, the selectivity coefficient can
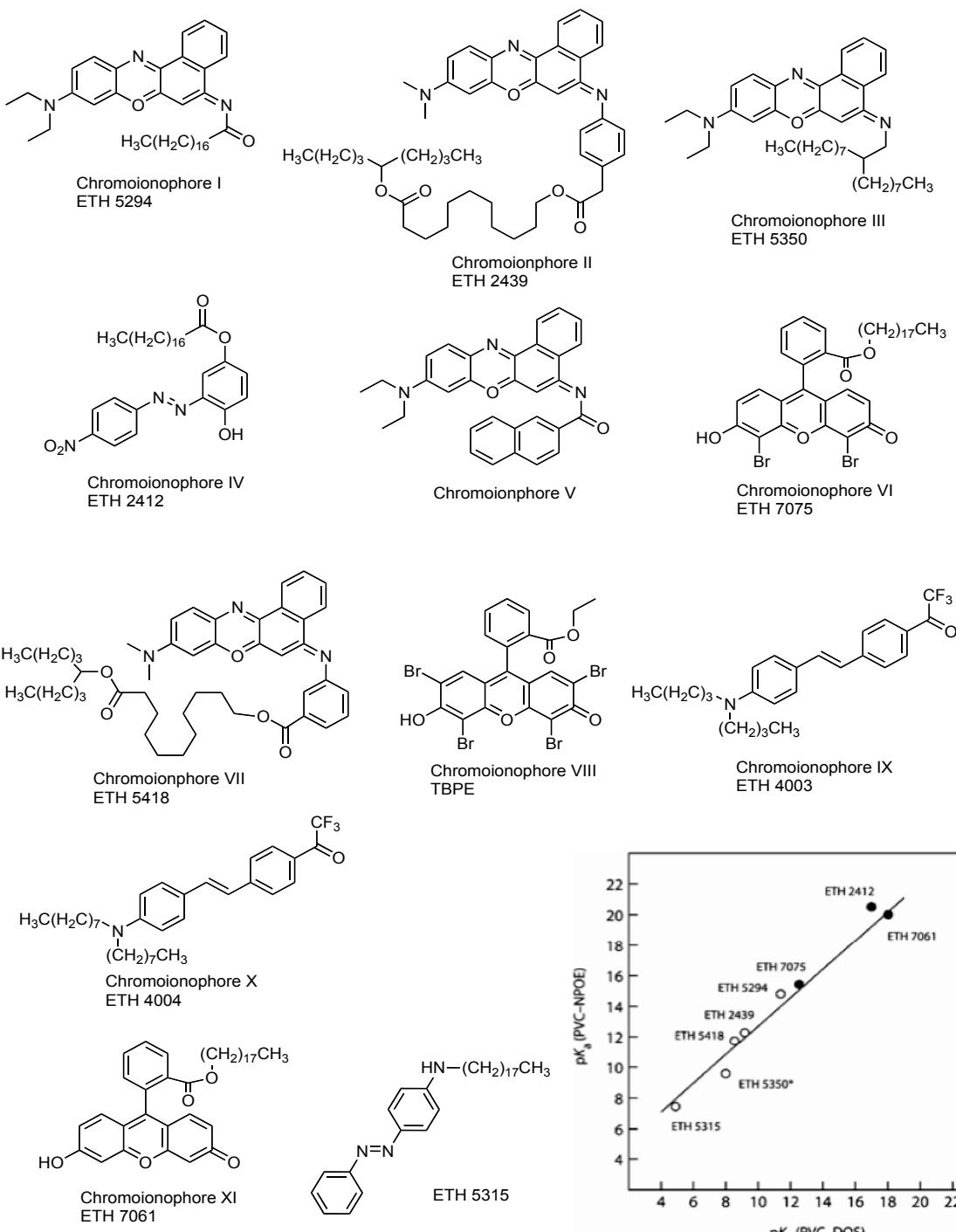
Figure 1.4 Chromoionophores employed in ion-selective optical sensors. The inset graph correlates pK$_a$s in the NPOE(o-nitrophenyl ether)/PVC with pK$_a$s in the DOS(bis(2-ethylhexyl) sebacate)/PVC of certain chromoionophores [6].

be defined in the same way as done for the organic membrane based ion-selective electrodes:

$$a_{overall} = a_I + \sum_J k_{I,J}^{Osel} a_J \qquad \text{(Eq. 1.5)}$$

While ion-selective optodes share many components with ion-selective electrodes such as polymeric supports, plasticizers, and ionophores, it is the chromoionophore that makes the ion-selective optode unique. Fig. 1.4 shows the structures of several commercially available chromoionophores from Fluka. They are lipophilized derivatives of fluorescein, azobenzene, nile blue, and stilbene. Depending on the binding strength of a chromoionophore with a proton (i.e., pKa), the detection range of a sensor can be modulated. For example, in rxn. 1.1, if a chromoionophore with a low pKa value is employed, the equilibrium shifts to the right and sensitivity toward cation I will be improved [5]. The pKas of some chromoionophores in the polymeric phase are illustrated in Fig. 1.4 [6, 7].

There are other factors to be considered to optimize an optical ion sensor such as the interaction between the ionophore and the chromoionophore, an ionic strength change in the organic film, water dissociation by an anion ionophore and a chromoionophore, etc. Among these, the change of ionic strength should be carefully considered [8, 9]. When the ionic strength increases dramatically, it can create osmotic flow of water from the aqueous phase into the organic film and form microscopic water droplets in the film. This makes the film turbid and increases the background signal in the absorption spectrum. In this case, the sample solution should be buffered with high ionic strength solution or appropriate membrane components should be chosen to minimize the ionic strength effect on water uptake by the film.

1.2   Metalloporphyrins for anion sensors

Monitoring anions is important in many areas including clinical and environmental analysis. The study of anion recognition has been a critical part in the most recent research in the area of host-guest chemistry [10]. Certain chemical interactions such as a coulombic dipolar interaction, hydrogen bonding, and coordination bonding have been utilized to improve attractive interactions between hosts and anion species. In order to differentiate a target anion from others, the host molecule must be carefully designed, considering not only the structural complementary interaction between the ion-molecule pair, but also interactions with solvent molecules. As a result, many of the host molecules for anion recognition comprise at least one interaction site that improves the selective interaction for the target anion and overcomes the solvation energy of the target anion in the aqueous phase. Among these host molecules, metal ion-organic ligand complexes have received considerable interest because they can provide dedicated single-point interactions with the capability to further modify the host molecular structure. One of the most successful examples of anion ionophores are metalloporphyrins (Fig. 1.5).

In(III)OEP-OH   In(III)TPP-OH
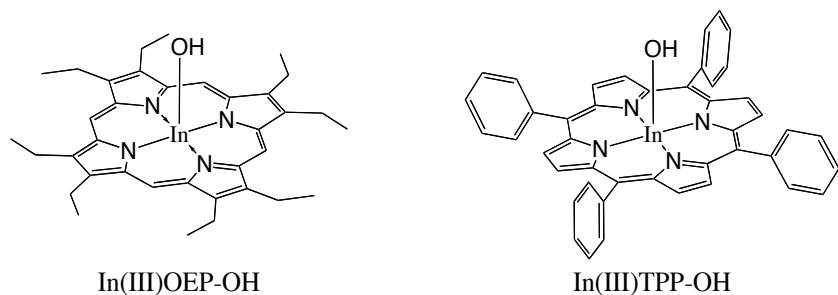
Figure 1.5 Structures of a indium(III) octaethylporphyrin (OEP) and a indium(III) tetraphenylporphyrin (TPP). In(III) porphyrins are useful for chloride-selective membrane electrodes and optodes.

A metalloporphyrin is a metal ion complex comprised of a metal ion center strongly chelated by four nitrogens in the ligand. This forms a planar structure with two openings in the axial positions. It can be solvated by water or toluene, depending on the pendent groups of the porphyrin ring. Selectivity can be engineered by placing an

appropriate metal ion within the core and adding side structures around the ring. In particular, tetraphenylporphyrin derivatives can be easily prepared with desired peripheral structures [11-13]. In addition, porphyrin itself can be employed as a signal transducer or tailored with an additional unit for the signal transduction [14]. For these reasons, metalloporphyrins were first successfully adopted for use in anion-selective electrodes in 1988 by the Meyerhoff group [11, 15, 16].

1.2.1 Metalloporphyrins in ion-selective electrodes

Metalloporphyrins meet the critical requirements of ionophores for the development of new anion-selective electrodes. Common porphyrins that are commercially available or easily prepared in the lab (i.e., octaethylporphyrin and tetraphenylporphyrin) are lipophilic enough for direct use as ionophores without further modification. Porphyrins form stable complexes with many metal ions, which do not demetallate until heated in a strong acid (i.e., conc. H_2SO_4 or HCl solution) [17]. A unique anion selectivity pattern can be achieved by an appropriate choice of central metal

Table 1.1 Metalloporphyrins employed in anion-selective electrodes. Note that metalloporphyrins selective for soft anions (○) mostly have partially filled outermost d-electrons and metalloporphyrins for hard anions (☐) have d^0 or d^{10} in their outmost electron shells.

10
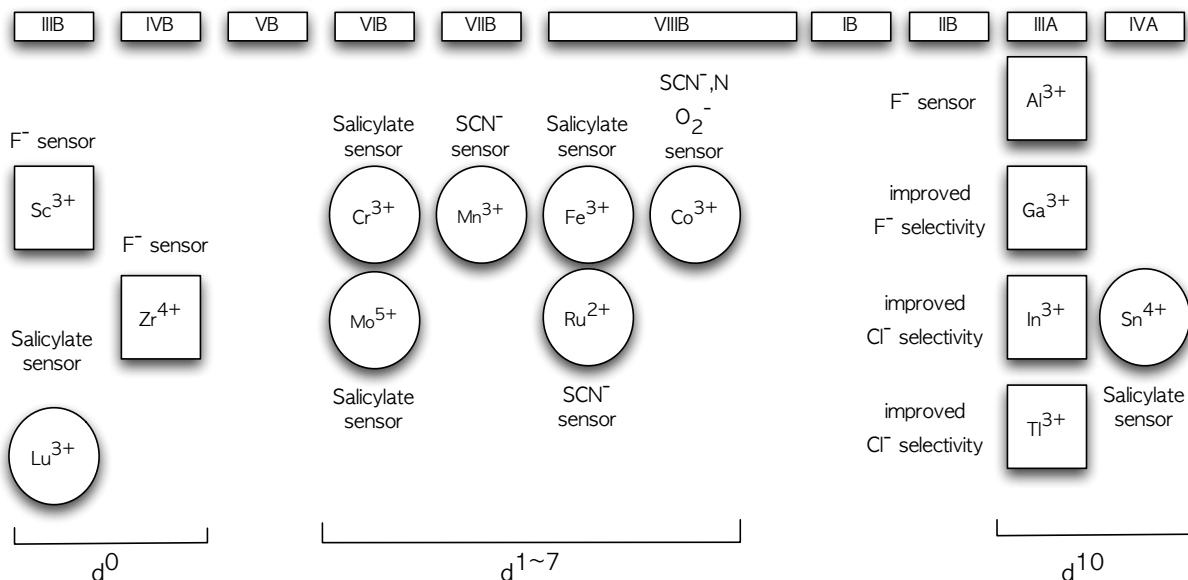
ion in the core of the porphyrin. An additional functional unit can be attached in the porphyrin structure for the purpose of immobilizing the ionophore to a polymeric backbone, or in order to impart size selectivity by attaching bulky side structures (e.g., t-butyl, etc.) [13].

If we expect a metal ion-dependent selectivity with metalloporphyrin ionophores, then metal ions should behave differently enough to exhibit varied interactions with anions. However, it is also possible that these differences may not be sufficient and may result in similar response patterns. Table 1.1 lists the metal ions that have been incorporated in porphyrin structures and their application for the detection of anions. As can been seen, ion-selective electrodes based on metalloporphyrins have been applied for detection of fluoride [13, 18-21, 21-23], chloride [24-28], nitrite [29-34], thiocyanate [34-39], salicylate [40-45], and organic anions [46-49]. In this table, metal ions that are selective for fluoride and chloride have d^0 or d^{10} electron configurations in their outermost shells (i.e., Sc(III) [23], Zr(III) [19, 20, 22], Al(III) [13, 21, 50, 51], Ga(III) [18, 32, 52], In(III) [18, 24-28, 32, 53]), while metal ions that bind nitrite, thiocyanate, and salicylate have partially filled d shells (i.e., Cr(III) [43], Mn(III) [11, 16, 35-37, 45, 48, 49, 54, 55], Fe(III) [49, 56, 57], Co(III) [29, 31-34, 58, 59], Mo(V)=O [42, 60], Ru(II) [30]) except for tin(IV) [15, 40-42, 46, 50, 58] and lutetium(III) [44].

In order to understand trends over the periodic table, it is beneficial to invoke the hard-soft acid-base convention [61]. Soft bases are ligands relatively less charged, large, more polarizable, and less electronegative. Nitrite, thiocyanate, and salicylate can be classified as relatively soft bases compared to fluoride and chloride. As can be seen in the Hofmeister selectivity series, they are also lipophilic anions that yield good responses in ion-selective electrodes based on lipophilic anion-exchangers. Fluoride and chloride are generally classified as hard bases and they have high negative Gibbs free energies of hydration and thus are difficult to extract into organic phases. In the case of cations, the hardness of acids is not easily predicted because metal ions are ligated with the highly conjugated porphyrin ring and thus their hardness will be changed accordingly. Correlating metalloporphyrin-based ISEs with their target anions in their applications

reveals a tendency that soft anions are mostly associated with metal ions of partially filled d-electron configuration and hard anions selectively interact with metal ions with d^0 or d^{10} configurations (see Table 1.1). This tendency clearly shows that the hard-soft character of metal ion in the porphyrin structure provides selective binding with an anionic ligand based on the hard-soft interaction.

In the case of hard anions (F^-, Cl^-), the affinity toward these hard bases should be significant enough to overcome poor partitioning into the sensing membrane. Group IIIA metal ions (see Fig. 1.6) fit, to some degree, with the hard-soft acid-base concept. Moving from Tl^{3+} to Al^{3+}, the hardness increases with selectivity for F^- over Cl^- (note that hardness of F^- is higher than Cl^-). Moving from Al^{3+} to Tl^{3+}, softness increases and selectivity for Br^- is clearly improved. As a result, aluminum(III) porphyrins exhibit excellent selectivity for F^- over Cl^- compared to gallium(III) porphyrins. However, indium(III) porphyrins exhibit the best selectivity for Cl^- over F^- and Br^- than other group IIIA metalloporphyrins. It is also noteworthy that zirconium(IV) porphyrins have been found to be fluoride selective ionophores where hardness would be higher than porphyrins with trivalent metal ion centers.
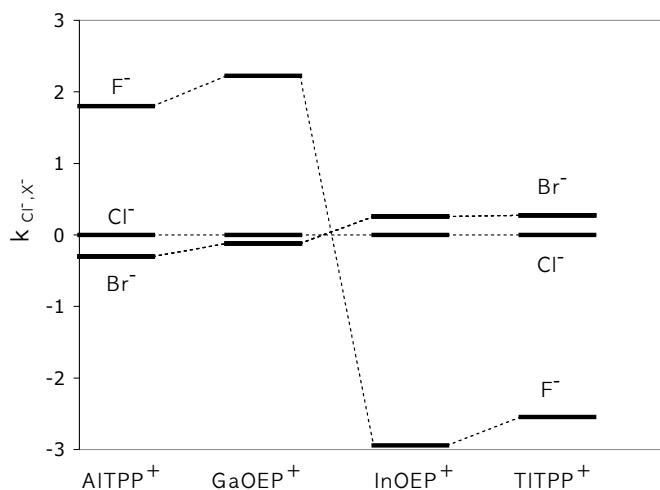
Figure 1.6 Selectivity change for halogen anions using metalloporphyrins with Group IIIA metal ions as ionophores in polymeric membrane ISEs. For clarity, potentiometric selectivity coefficients for other anions are omitted.

1.2.2 Metalloporphyrins in ion-selective optodes

Metalloporphyrins are also useful as optical sensor components. Fig. 1.7 shows that the absorbance of porphyrins consist of two strong bands: the Soret band (around 400 nm) and Q-bands (500 nm - 600 nm). The λ_{max} and intensity of these absorbance bands can change corresponding to the combination of metal ions, axial ligands, and conformation. It is possible that metalloporphyrins can behave as chromophores or fluorophores [14]. However, ligation of anions with the metal ion center usually does not alter the spectrum significantly. Thus most optical anion sensors use metalloporphyrin ionophores and chromoionophores in the plasticized films [62]. However, recently, the first report of chloride selective optical sensor based on dimer-monomer equilibrium of In(III)OEP was published by our group in which the metalloporphyrin serves as both the ionophore and chromophore for optical detection [26].
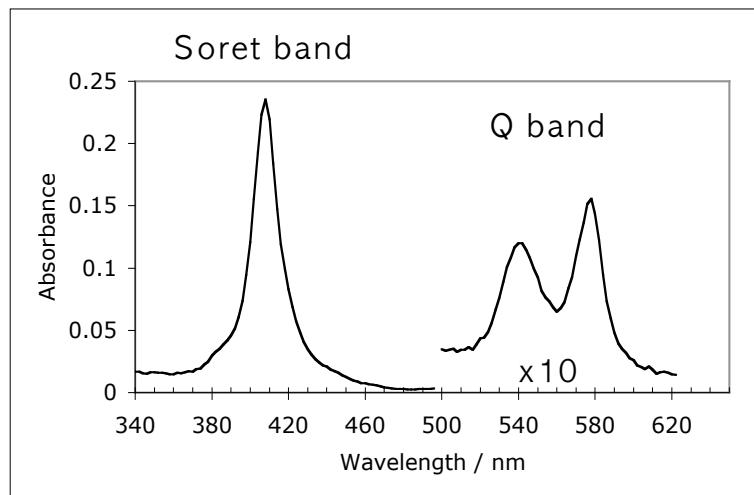
Figure 1.7 UV-Vis spectrum of Sc(III)[OEP]OH in CHCl₃.

1.3   Dimer-monomer equilibrium of metalloporphyrins

In general, the response slope of ion-selective electrodes is called "Nernstian" if the observed response follows the theoretical response function (Eq. 1.3). In early studies of anion-selective electrodes based on metalloporphyrins, super-Nernstian responses were often observed [24]. Subsequent optical studies and mechanistic considerations proved

that this abnormal behavior was the consequence of the following dimer-monomer equilibrium of the metalloporphyrin within the polymeric membrane [18, 24, 52]:

$$LOH + L^+ R^- \rightleftharpoons L_2OH^+ R^-$$

<div align="right">(rxn 1.3)</div>

where LOH is the hydroxide ligated metalloporphyrin (L^+) and L_2OH^+ is a hydroxo-bridged dimer. This dimer-monomer equilibrium becomes a critical issue when a metalloporphyrin is to be employed as an ionophore in an ion-selective electrode.

1.3.1   μ-Hydroxo-dimer of indium(III) octaethylporphyrin(OEP)

Fig. 1.8 shows the X-ray crystal structure of $\{In(III)OEP\}_2\mu\text{-}(OH)^+$ [63]. The bond angle of In-O-In is larger than the angle of H-O-H of H_3O^+ due to the bulkiness of porphyrin ring. The bridging ligand displaces two porphyrin rings about 4 Å, which prevents π-π stacking of the two conjugated planar structures. One of the important features of dimerization is the absorbance change. In general, the Soret band (strong and sharp band at about 400 nm) of the porphyrin slightly shifts about 5 nm depending on the axial ligand, whereas the Q-band pattern (500 ~ 600 nm) dramatically changes upon metallation of the porphyrin ligand (i.e., a free porphyrin has four Q-bands, whereas In(III) porphyrin has two Q-bands). The conformational change, such as the dimerization,
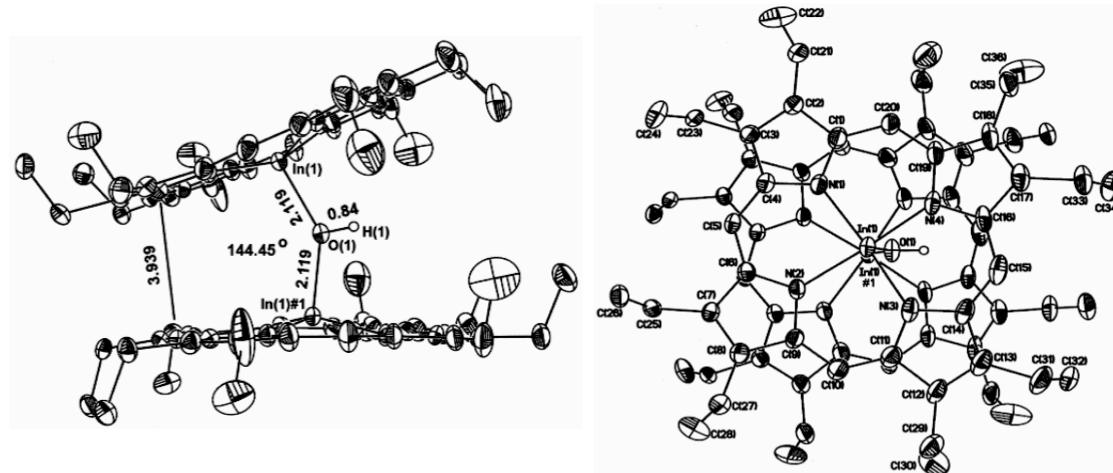
Figure 1.8 ORTEP diagram of $\{In(III)OEP\}_2(\mu\text{-}OH)^+$. [63]

causes a significant shift of the Soret absorbance band. For example, In(III)OEPCl exhibits the Soret band at 408 nm, whereas the corresponding μ-hydroxo-dimer exhibits a Soret band at 390 nm [26, 63].

The conceptual explanation of this hypsochromic shift of the Soret band has been discussed in the literature [64, 65]. As illustrated in Fig. 1.9, when two dyes represented by two dipole moments are placed close enough to each other, they begin to behave as one optical entity. When two dipoles are placed edge-to-edge and aligned in the same direction, the dyes are optically active. Since this alignment of two dipoles is electrostatically more stable than the alignment of the opposite direction, this orientation results in a red-shift of the absorbance band. However, when two dipoles are facing each other and aligned in the same direction, they are optically active but electrostatically less favored than in the opposite direction. This results in blue-shift of the absorbance band. In the case when the two dyes are placed at a distance comparable to their size, thorough computation is required to obtain a reliable quantitative prediction. However, the conceptual consideration is still valid for correlation of the direction of absorbance λ_{max} shift with conformational change. Therefore, blue-shift of the Soret band of metalloporphyrins that are larger than 10 nm can be used to suggest the likelihood of formation of a bridged face-to-face dimer structure.
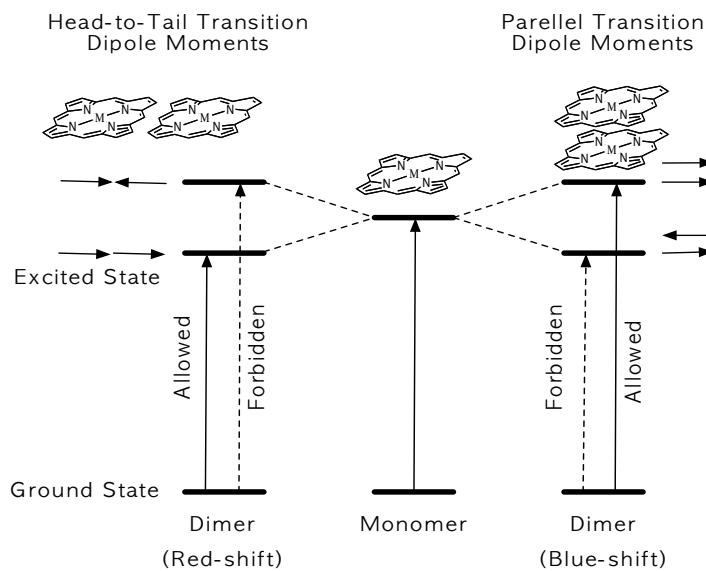
Figure 1.9 Kasha point-dipole model for exciton coupling of electronic transition in dimers.

1.3.2 Dimer-monomer equilibrium in ion-selective electrodes

The origin of super-Nernstian response of the chloride sensor based on In(III) porphyrin was ascribed to dimer-monomer equilibrium in the polymeric membrane [52]. As discussed previously, Nernstian response is observed when the membrane potential across the sample-organic interface is only dependent on the analyte activity on the sample side since the analyte activity in the organic phase should be constant. In the case of a charged carrier mechanism of metalloporphyrins, the following equilibrium is established in the membrane:

$$L^+ + X^- \rightleftharpoons LX \qquad \text{(rxn 1.4)}$$

with the equilibrium constant for this reaction given as the following:

$$\beta_{LX} = \frac{[LX]}{[L^+][X^-]} \qquad \text{(Eq. 1.6)}$$

The total amount (L_T) of lipophilic metalloporphyrin does not change during the measurement and the amount of L^+ is also fixed by introducing a certain amount of lipophilic anionic sites (R^-) into the membrane (e.g., about 20 mol% to metalloporphyrin). Since $LX = L_T - L^+$ and $L^+ = R^-$, both LX and L^+ are fixed, and thus X^- in the membrane is fixed by Eq. 1.1. Therefore, ISEs based on this mechanism should exhibit Nernstian response.

However, if dimerization occurs simultaneously with the response, then $X^-_{(org)}$ is dependent on the dimerization. In the presence of 20 mol% of lipophilic anionic sites, about 40 mole% of the monomer (to total amount of metalloporphyrin) forms positively charged dimers (i.e., 20 mol%) and 60 mole% remains as a monomer in the organic membrane at equilibrium (Rxn 1.3). Since L_2OH^+ does not possess a sufficient binding capability with the analyte anion (e.g., Cl⁻), the effect of dimerization is a reduction of the

real ionophore (L^+) in the membrane. As the chloride concentration increases in the aqueous phase, the dimers are broken into monomers via the following ion-exchange reaction:

$$L_2OH^+ R^- + Cl^-_{(aq)} \rightleftharpoons LCl + L^+ R^- + OH^-_{(aq)} \quad \text{(rxn 1.5)}$$

The consequence of the monomer formation is an increase of L^+ in the membrane phase followed by reduction of free Cl^- concentration in the membrane; the increase of L^+ and LCl by rxn. 1.5 results in a decrease in the ratio of LCl/L^+ in Eq. 1.6 (note that $LCl > L^+$ when R^- is less than 50 mol%), and thus it causes the decrease of Cl^-. In Eq. 1.1, since the increase of $Cl^-_{(aq)}(=a_{I(phase1)})$ results in the decrease of $Cl^-_{(org)}(=a_{I(phase2)})$, the response slope becomes higher than that of a Nernstian response.

The possible benefits of this super-Nernstian response have been discussed [66]. Even though the sensitivity may increase due to this abnormally high response slope, the response time has been observed to be on the order of a few minutes or longer. This is the time required to reach the steady-state of the dimer-monomer process in the viscous membrane phase where the diffusion coefficient is normally ca. 10^{-8} cm^2/sec [67]. It is quite disadvantageous to have the dimer-monomer equilibrium during the measurement when most of the conventional ion-selective electrodes reach their steady-state in a few seconds to tens of seconds. To avoid this dimerization, a porphyrin ring with bulky side groups (e.g., picket-fence porphyrin [13]) can be employed or the metalloporphyrin can be immobilized on the polymeric backbone [53].

1.3.3 Dimer-monomer equilibrium in optical sensors

The Soret band shift upon dimer-monomer equilibrium provides a good optical transduction scheme. Indeed, the activity of Cl^- in aqueous phase can be quantified by using In(III)OEP and monitoring the absorbance change of either the dimeric form (390 nm) or monomeric form (408 nm) as a function of chloride activity [26]. The degree of

monomer formation from dimer in rxn 1.5 corresponds to how much Cl$^-$ is present in the aqueous solution compared to OH$^-$. Since the response depends on the ratio of Cl$^-$/OH$^-$, the concentration of OH$^-$ is fixed by using an appropriate buffer for the measurement of Cl$^-$. In this case the metalloporphyrin acts as an ionophore as well as a chromoionophore via the dimer-monomer mechanism. This is advantageous over the conventional optical sensors where an additional dye is required to monitor analyte-ionophore binding. This dimer-monomer scheme has also been successfully applied for optical gas sensing [68]. Amine vapors in the gas phase can diffuse into the polymeric film with In(III)OEP and anionic sites and break the dimer into monomers by the following equilibrium:

$$L_2OH^+ R^- + \text{amine}_{(g)} \rightleftharpoons LOH + (L\text{-amine})^+ R^- \qquad \text{(rxn 1.6)}$$

1.3.4 Other dimeric metalloporphyrins and their applications

The bridged dimers of various metalloporphyrins other than indium(III) have also been reported in the membranes of ion-selective sensors. Positively charged dimers like In(III) porphyrin were found with Mn(III) [69, 70], Ga(III) [63], and Sn(IV) [42]. Their chemistry and X-ray structures in the literature exhibit a great resemblance to In(III) porphyrins: the Soret band shift and super-Nernstian response of ion-selective electrodes based on the dimer-monomer equilibria. Other than these metalloporphyrins, there have been different types of dimers examined in the study of ion-selective sensors.

The neutral dimer, (Fe(III)TPP)$_2$O, was used to prepare a SCN$^-$-selective electrode [71]. In the suggested mechanism, the oxo-dimer itself serves as an ionophore rather than any dimer-monomer mechanism. Zirconium(IV) porphyrins, used to prepare fluoride-selective electrodes, have been found to exhibit much more complicated dimer formation due to the high valency of Zr(IV) and the ability to have two or three ligands only on one side of metal ion center [72]. Aluminum(III) porphyrins were also found to form oxo-(or hydroxo-)bridged dimers and close investigation is under way by this group to clarify this dimer-monomer process [21]. Unprecedented selectivity for fluoride was demonstrated

with Al(III)OEP and a fluoride-bridged dimer was suggested to explain the response mechanism based on a shift in the Soret band upon fluoride complexation to form the dimer.

This dissertation describes the investigation of Sc(III)porphyrins as ionophores in fluoride-selective optical and electrochemical sensors. The X-ray structure of the fluoride-bridged dimer was observed and thus it strongly supports a fluoride-bridged dimer of metalloporphyrins. Other than hydroxo-, oxo-, and fluoro-bridged dimers, metalloporphyrin dimers via difunctional ligands have also been studied for the detection of this bridging ligand. For example, a zinc(II) porphyrin covalently connected with a fluorophore exhibits great selectivity for detecting imidazole over other non-bridging ligands using a optical transduction mode [73].

1.4   Statement of purpose

Metalloporphyrins have been shown to function as analytically useful anion ionophores, and have been the subject of considerable sensor research. The importance of dimer-monomer equilibria of metalloporphyrins in organic polymeric membranes is now well understood. This process is not desirable in ion-selective electrodes while it can be beneficial (e.g., serves as transduction mechanism) in the design of new optical anion sensors. This thesis provides additional fundamental and applied studies relating to the development of optical and electrochemical sensors based on metalloporphyrins that can exhibit dimer-monomer equilibria in polymeric films.

Chapter 2 describes fast-responding anion/gas sensitive optical sensors based on the dimer-monomer equilibrium of In(III)OEP in a waveguide configuration by employing ultra-thin films. It is shown that the response time is limited by the diffusion rate of the analyte species in the film and not by the dimer-monomer reaction kinetics. The waveguide configuration allows use of a very thin film for the fast response as well as increasing sensitivity by multiple reflections through the waveguide. Related experimental issues such as loss of the plasticizer and humidity effects are discussed.

Chapter 3 describes optical and electrochemical fluoride sensors based on scandium(III) porphyrins. The success of Al(III)OEP for a fluoride sensor suggests that Sc(III) porphyrins may be a good candidate to be examined based on the similarity between aluminum(III) and scandium(III) ligation chemistry [74]. Plasticized films doped with Sc(III)OEP and Sc(III)TPP are prepared and both optical and electrochemical configurations are examined to assess selectivity patterns and to understand the response mechanisms.

Chapter 4 describes optical and electrochemical sensors based on indium(III) Texaphyrins. Certain metals are unstable within the porphyrin ring partially because the ionic radius of the metal does not fit in the cavity of the porphine ring. This is especially true for the large cations such as yttrium and lathanides. Expanded porphyrins such as Texaphyrins may serve as better chelating ligands for such metal ions. However, metallated expanded porphyrins have not yet been explored as ionophores. In this chapter, In(III) Texaphyrins are prepared and examined as anion ionophores in both optical and electrochemical sensing configurations. Based on the selectivity of these sensors, In(III)Texaphyrins are compared to In(III) porphyrins.

Chapter 5 describes fluoride sensors based on gallium(III) porphyrins. The gallium(III) porphyrins have been reported to exhibit an enhanced fluoride selectivity. However, they suffer significant interferences from thiocyanate and salicylate. In this chapter, various approaches are examined to enhance the fluoride selectivity and lower the detection limit. Different anionic sites and membrane compositions are employed for this purpose. In addition, the observation of a fluoro-bridged dimer of Ga(III)TPP in the membrane phase leads to an attempt to examine covalently linked porphyrin dimers in order to enhance the fluoride selectivity.

Chapter 6 summarizes this dissertation work and suggests future research directions.

1.5   References

[1] Bakker, E.; P. Bühlmann; E. Pretsch, Chem. Rev. 97 (1997) 3083.

[2] Bühlmann, P.; E. Pretsch; E. Bakker, Chem. Rev. 98 (1998) 1593.

[3] Hofmeister, F., Arch. Exp. Pathol. Pharmakol. 24 (1888) 247.

[4] Umezawa, Y., Handbook of Ion-Selective Electrodes: Selectivity Coefficients, CRC Press, Roca Raton, FL, 1990,

[5] Seiler, K.; W. Simon, Anal. Chim. Acta 266 (1992) 73.

[6] Qin, Y.; E. Bakker, Talanta 58 (2002) 909.

[7] Bakker, E.; M. Lerchi; T. Rosatzin; B. Rusterholz; W. Simon, Anal. Chim. Acta 278 (1993) 211.

[8] Li, Z.; X. Li; S. Petrovic; D.J. Harrison, Anal. Chem. 68 (1996) 1717.

[9] Li, Z.; X. Li; M. Rothmaier; D.J. Harrison, Anal. Chem. 68 (1996) 1726.

[10] Schmidtchen, F.P.; M. Berger, Chem. Rev. 97 (1997) 1609.

[11] Chaniotakis, N.A.; A.M. Chasser; M.E. Meyerhoff; J.T. Groves, Anal. Chem. 60 (1988) 185.

[12] Amemiya, S.; P. Bühlmann; Y. Umezawa; R.C. Jagessar; D.H. Burns, Anal. Chem. 71 (1999) 1049.

[13] Mitchell-Koch, J.T.; M. Pietrzak; E. Malinowska; M.E. Meyerhoff, Electroanalysis 18 (2006) 551.

[14] Kadish, K.M.; M.K. Smith, R. Guilard, The porphyrin handbook, Academic Press, San Diego, 2000,

[15] Ma, S.C.; N.A. Chaniotakis; M.E. Meyerhoff, Anal. Chem. 60 (1988) 2293.

[16] Meyerhoff, M.E.; D.M. Pranitis; N.A. Chaniotakis, Advances in Instrumentation 42 (1987) 469.

[17] Kadish, K.M.; M.K. Smith, R. Guilard, The porphyrin handbook, Academic Press, San Diego, 2000,

[18] Steinle, E.D.; U. Schaller; M.E. Meyerhoff, Anal. Sci. 14 (1998) 79.

[19] Malinowska, E.; L. Gorski; M.E. Meyerhoff, Anal. Chim. Acta 468 (2002) 133.

[20] Gorski, L.; M.E. Meyerhoff; E. Malinowska, Talanta 63 (2004) 101.

[21] Badr, I.H.A.; M.E. Meyerhoff, Anal. Chem. 77 (2005) 6719.

[22] Gorski, L.; E. Malinowska, Anal. Chim. Acta 540 (2005) 159.

[23] Kang, Y.; J.W. Kampf; M.E. Meyerhoff, Anal. Chim. Acta 598 (2007) 295.

[24] Park, S.B.; W. Matuszewski; M.E. Meyerhoff; Y.H. Liu; K.M. Kadish, Electroanalysis 3 (1991) 909.

[25] Wang, E.; C. Romero; D. Santiago, Abstracts of Papers, 220th ACS National Meeting, Washington, DC, United States, August 20-24, 2000 (2000) ANYL.

[26] Zhang, W.; E. Rozniecka; E. Malinowska; P. Parzuchowski; M.E. Meyerhoff, Anal. Chem. 74 (2002) 4548.

[27] Brasuel, M.G.; T.J. Miller; R. Kopelman; M.A. Philbert, Analyst 128 (2003) 1262.

[28] Pimenta, A.M.; A.N. Araujo; M.C.B.S.M. Montenegro; C. Pasquini; J.J.R. Rohwedder; I.M. Raimundo, J. Pharm. Biomed. Anal. 36 (2004) 49.

[29] Hodinar, A.; A. Jyo, Anal. Chem. 61 (1989) 1169.

[30] Huser, M.; W.E. Morf; K. Fluri; K. Seiler; P. Schulthess; W. Simon, Helv. Chim. Acta 73 (1990) 1481.

[31] Li, X.; D.J. Harrison, Anal. Chem. 63 (1991) 2168.

[32] Malinowska, E.; J. Niedziolka; M.E. Meyerhoff, Anal. Chim. Acta 432 (2001) 67.

[33] Cosnier, S.; C. Gondran; R. Wessel; F.-P. Monfforts; M. Wedel, Sensors 3 (2003) 213.

[34] Vlascici, D.; E. Fagadar-Cosma; O. Bizerea-Spiridon, Sensors 6 (2006) 892.

[35] Brown, D.V.; N.A. Chaniotakis; I.H. Lee; S.C. Ma; S.B. Park; M.E. Meyerhoff; R.J. Nick; J.T. Groves, Electroanalysis 1 (1989) 477.

[36] Zhou, Z.X.; T.S. Li; Y.Z. Wang; Y.J. Wu, Chin. Chem. Lett. 8 (1997) 997.

[37] Khorasani, J.H.; M.K. Amini; H. Motaghi; S. Tangestaninejad; M. Moghadam, Sens. Actuators B B87 (2002) 448.

[38] Vlascici, D.; E. Fagadar-Cosma; O. Spiridon-Bizerea; A. Pascariu; A. Chiriac, Rev. Chim. (Bucharest) 56 (2005) 224.

[39] Vlascici, D.; O.S. Bizerea; E. Fagadar-Cosma, J. Optoelec. Adv. Mat. 8 (2006) 883.

[40] Kibbey, C.E.; S.B. Park; G. Deadwyler; M.E. Meyerhoff, J. Electroanal. Chem. 335 (1992) 135.

[41] Torihara, M.; S. Kamata, Bunseki Kagaku 42 (1993) 375.

[42] Malinowska, E.; J. Niedziolka; E. Rozniecka; M.E. Meyerhoff, J. Electroanal. Chem. 514 (2001) 109.

[43] Shahrokhian, S.; A. Hamzehloei; M. Bagherzadeh, Anal. Chem. 74 (2002) 3312.

[44] Steinle, E.D.; S.W. Scranton; M.N. Kinde; J.M. Hastings, Abstracts, 39th Midwest Regional Meeting of the American Chemical Society, Manhattan, KS, United States, October 20-22 (2004) MID04.

[45] Radecka, H.; I. Grzybowska; J. Radecki; P. Jakubowski; S. Loteran; C. Orlewska; W. Maes; W. Dehaen, Anal. Lett. 40 (2007) 387.

[46] Badr, I.H.A.; M.E. Meyerhoff; S.S.M. Hassan, Anal. Chim. Acta 321 (1996) 11.

[47] Zhang, X.-B.; C.-C. Guo; J.-B. Xu; G.-L. Shen; R.-Q. Yu, Analyst 125 (2000) 867.

[48] Santos, E.M.G.; C.M.C.M. Couto; A.N. Araujo; M.C.B.S.M. Montenegro; B.F. Reis, J. Braz. Chem. Soc. 15 (2004) 701.

[49] Amini, M.K.; S. Shahrokhian; S. Tangestaninejad, Analyst 124 (1999) 1319.

[50] Rakhman'ko, E.M.; A.A. Rat'ko, Vestnik Belorusskogo Gosudarstvennogo Universiteta, Seriya 2: Khimiya, Biologiya, Geografiya (2001) 16.

[51] Badr, I.H.A.; M.E. Meyerhoff, J. Am. Chem. Soc. 127 (2005) 5318.

[52] Steinle, E.D.; S. Amemiya; P. Bühlmann; M.E. Meyerhoff, Anal. Chem. 72 (2000) 5766.

[53] Qin, Y.; E. Bakker, Anal. Chem. 76 (2004) 4379.

[54] Hong, Y.K.; Y.R. Kang; D.H. Shin; D.S. Shin; G.S. Cha; H. Nam, Anal. Sci. Tech. 9 (1996) 270.

[55] Shamsipur, M.; G. Khayatian; S. Tangestaninejad, Electroanalysis 11 (1999) 1340.

[56] Shahrokhian, S.; H. Seifi; M. Bagherzadeh; S.R. Mousavi, ChemPhysChem 5 (2004) 652.

[57] Santos, E.M.G.; A.N. Araujo; C.M.C.M. Couto; M.C.B.S.M. Montenegro, J. Pharm. Biomed. Anal. 42 (2006) 535.

[58] Avlasevich, Y.S.; A.A. Rat'ko; V.V. Egorov, J. Appl. Spectrosc. 69 (2002) 554.

[59] Shamsipur, M.; M. Javanbakht; A.R. Hassaninejad; H. Sharghi; M.R. Ganjali; M.F. Mousavi, Electroanalysis 15 (2003) 1251.

[60] Abe, H.; E. Kokufuta, Bull. Chem. Soc. Jpn. 63 (1990) 1360.

[61] Pearson, R.G., J. Am. Chem. Soc. 85 (1963) 3533.

[62] Wang, E.; C. Romero; D. Santiago; V. Syntilas, Anal. Chim. Acta 433 (2001) 89.

[63] Ab, P.G.P.; J.W. Kampf; E. Rozniecka; Y. Kondratenko; E. Malinowska; M.E. Meyerhoff, Inorg. Chim. Acta 355 (2003) 302.

[64] Kasha, M., Radiat. Res. 20 (1963) 55.

[65] Hunter, C.A.; J.K.M. Sanders; A.J. Stone, Chem. Phys. 133 (1989) 395.

[66] Gorski, L.; E. Malinowska; P. Parzuchowski; W. Zhang; M.E. Meyerhoff, Electroanalysis 15 (2003) 1229.

[67] Eugster, R.; T. Rosatzin; B. Rusterholz; B. Aebersold; U. Pedrazza; D. Ruegg; A. Schmid; U.E. Spichiger; W. Simon, Anal. Chim. Acta 289 (1994) 1.

[68] Qin, W.; P. Parzuchowski; W. Zhang; M.E. Meyerhoff, Anal. Chem. 75 (2003) 332.

[69] Cheng, B.; F. Cukiernik; P.H. Fries; J.-C. Marchon; W.R. Scheidt, Inorg. Chem. 34 (1995) 4627.

[70] Cheng, B.; P.H. Fries; J.-C. Marchon; W.R. Scheidt, Inorg. Chem. 35 (1996) 1024.

[71] Gao, D.; J. Li; R. Yu; G. Zheng, Anal. Chem. 66 (1994) 2245.

[72] Huhmann, J.; J. Corey; N. Rath; C. Campana, J. Organomet. Chem. 513 (1996) 17.

[73] Zhang, Y.; R. Yang; F. Liu; K. Li, Anal. Chem. 76 (2004) 7336.

[74] Cotton, F.A., G. Wilkinson, Advanced Inorganic Chemistry, 3rd, Interscience, New York, 1972, 10.

Chapter 2.

Rapid Response Optical Ion/Gas Sensors Using Dimer-Monomer Metalloporphyrin Equilibrium in Ultrathin Polymeric Films Coated on Waveguides

2.1 Introduction

Recent studies in this laboratory and elsewhere [1-5] have demonstrated that certain metalloporphyrins can undergo a reversible dimer-monomer equilibrium reaction within plasticized polymeric films, and that such reactions can be useful in the design of anion and gas selective optical sensors owing to the difference in the porphyrin's visible absorption spectrum in the dimer vs. monomer state [1, 2]. At the same time, the discovery of this dimer-monomer chemistry has helped explain the super-Nernstian response characteristics of potentiometric anion sensors that utilize these same metalloporphyrins as anion selective ionophores in organic membrane electrodes [4]. The dimer-monomer equilibrium reaction displayed by given metalloporphyrins involves formation of a hydroxo-bridged dimer species that can be broken into monomeric porphyrins as hydroxide ion is replaced by an analyte ion or a gas molecule that coordinates the metal ion center of the porphyrin. To date, it has been shown that aluminum(III) [6, 7], gallium(III) [8, 9], indium(III) [5], tin(IV) [3], and zirconium(IV) [10-13] porphyrins can form dimers in plasticized poly(vinyl chloride) films, especially when lipophilic tetraphenylborate derivatives are added to optimize anion selectivity when the films are employed to prepare potentiometric anion selective membrane electrodes.

While the existence of the dimer-monomer equilibrium reaction can cause super-Nernstian behavior and slow response times when the metalloporphyrins are employed to prepare anion selective electrodes [10, 14], such reactions provide a new transduction

chemistry for corresponding optical sensors, where film thicknesses can be much thinner. Indeed, formation of hydroxo-bridged dimers yields a hypsochromic shift of the Soret absorption band of the metalloporphyrins of about 10-20 nm from that of the monomeric species [4, 5, 8, 15]. Considering the narrow bandwidth of Soret band, a 10-20 nm shift is sufficient to distinguish the dimeric species from the monomeric species in the polymeric film. Therefore, unlike the conventional bulk optodes that typically employ ionophores and lipophilic pH indicators in the polymeric films [16-18], the innate dimer-monomer reactions of certain metalloporphyrins allow the development of optical anion sensors that do not require any additional pH indicator. Indeed, the first anion optical sensor based on this dimer-monomer chemistry was successfully demonstrated for the selective detection of chloride in aqueous phase using indium(III) octaethylporphyrin (In(III)[OEP]) as the ionophore [2]. This same system was subsequently shown to be useful for selectively detecting amines in gas phase [1]. Fig. 2.1 schematically illustrates the chemistry that takes place within the thin sensing films when the dimer-monomer chemistry of metalloporphyrins is employed for gas or anion sensing.
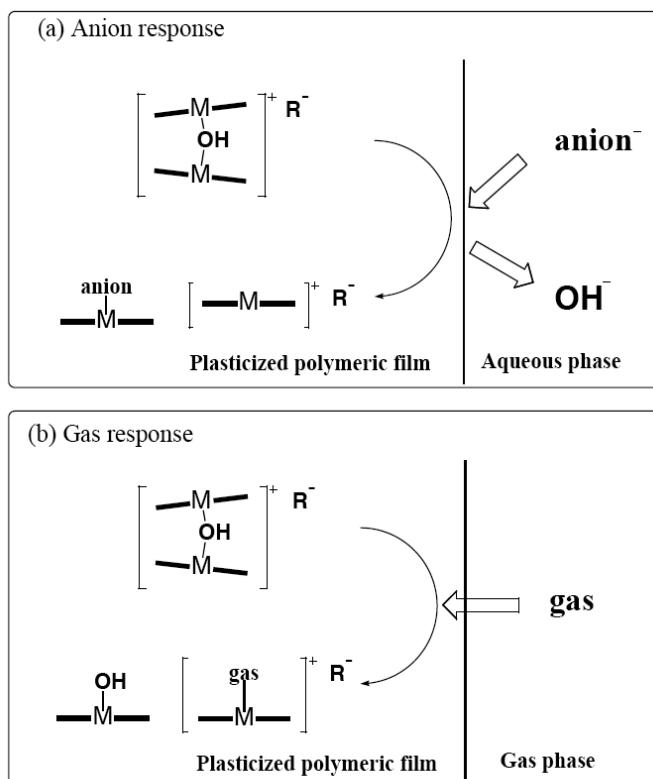
Figure 2.1 Response mechanism of dimer-monomer equilibrium in the presence of analyte. (a) anions in aqueous phase; and (b) neutral molecules in gas phase.

Waveguide type optical chemical sensors with thin polymer films (i.e., optical fibers [19-21] and planar waveguides) have been widely studied due to the advantages of such configurations in many applications. Among them, planar waveguide arrangements have been examined for use in flow-through detection systems [22-25]. These types of sensors are potentially useful as in-line detectors for gas and liquid chromatography, as well as flow-injection analysis (FIA) systems. The combination of the planar waveguides with bulk optode polymeric films for ion detection (with ionophore doped films) has great advantages over the conventional transmission mode measurements owing to the potential to employ ultrathin films on planar waveguides (using a spin coating process), without loss in analyte sensitivity owing to the multiple reflections of the source light that provides a large pathlength for the absorbance measurements. Further, since the films can be quite thin, such sensors will consume less analyte ion by the extraction chemistry (and thus require reduced sample volumes). Most importantly, equilibrium between the sample and polymeric phase will be achieved much more quickly. Since Simon et al. first employed a planar waveguide based bulk optode film sensor for ion detection using a sapphire crystal [26, 27], many different types of planar waveguide based ion-selective optical sensors have been suggested. However, to date, the use of a dimer-monomer equilibrium reaction of metalloporphyrins has not yet been demonstrated in such practical configurations. Herein, we describe the first fast-responding thin film optical sensors based on dimer-monomer equilibrium of In(III)[OEP] by employing the planar waveguide configuration. Optical chloride and amine vapor sensors based on In(III)[OEP]Cl are prepared and assessed with respect to their speed of response. It will be shown that the dimer-monomer chemistry in the films is fast enough to enable preparation of waveguide-based sensors that yield equilibrium response in < 2 s, suggesting possible applications of such sensors as detectors in FIA as well as liquid and gas chromatography.

2.2 Experimental

2.2.1 Reagents and instruments

Poly(vinyl chloride) (PVC), potassium tetrakis[3,5-bis(trifluoromethyl)phenyl] borate (KTFPB), *o*-nitrophenyl octyl ether (*o*-NPOE), [12-(4-ethylphenyl)dodecyl] 2-nitrophenyl ether (ETH 8045) and dodecyl *o*-nitrophenyl ether (DNPE) were used as received from Fluka (Ronkonkoma, NY). Tetrahydrofuran (THF) was from Aldrich and distilled before use. Chloro(2,3,7,8,12,13,17,18-octaethylporphyrinato)indium(III) (In(III)[OEP]Cl) was obtained from MidCentury (Posen, IL). Sodium hydroxide, hydrochloric acid, sodium chloride, methylammonium chloride, sodium phosphate monobasic, and phosphoric acid were obtained from Aldrich and used without further purification.

2.2.2 Film preparation and thickness measurement

Optical film cocktails were prepared by dissolving In(III)[OEP]Cl (1.0 mg), KTFPB (45 mole % relative to In(III)[OEP]Cl for chloride sensor and 45 and 80 mol % for amine sensor), plasticizer (66 mg), and PVC (33 mg) in 5 mL THF. A fused silica glass slide (75 mm x 25 mm x 1 mm, Chemglass) was immersed in a chromate-sulfuric acid solution overnight, thoroughly washed with distilled water, and dried in the desiccator. The film was formed on the slide by using a spin coating device (model SCS-G3-8, Cookson Electronics). The spin chamber was saturated with THF by placing a THF soaked paper towel at the bottom. The glass slide was washed once with THF while spinning. Then, 150 μL of film cocktail was added on the slide and spun at 1500 rpm for 30 s. The film was dried in the desiccator overnight before testing. The film thickness was determined by measuring fringe pattern in the transmission spectrum [28]. The blank film (only *o*-NPOE and PVC without In(III)[OEP]Cl and KTFPB) was used to obtain the fringe pattern in the 500 nm - 1100 nm range. Based on the thickness measurement, the correlation between the thickness and the absorbance at 332 nm (absorbance of *o*-NPOE)

was established. This correlation was used to estimate the thickness of chloride and amine sensing films by measuring the absorbance of *o*-NPOE. Thicknesses of films prepared via this method were reproducible within the range of 0.2 - 0.3 μm.

2.2.3 Planar waveguide configuration and optical measurement

Efficient light coupling into the waveguide is critical to obtain high quality optical response with the sensing films coated on the fused silica slides. Due to high efficiency and simplicity, a prism coupling scheme was chosen for use in this study. A schematic diagram of the waveguide sensor in a flow system arrangement is shown in Fig. 2.2. The light from a deuterium-tungsten lamp (DT-1000, Ocean Optics) was guided by an optical fiber and coupled into the silica waveguide through a collimating lens and the prism. The light was coupled out by a second prism and collected into another optical fiber by a collimating lens on the other side. A CCD detector (USB 2000, Ocean Optics) connected to the output optical fiber was employed to obtain an spectrum from 200 nm to 800 nm. In the optimized configuration with a distance between prisms of approx. 30 mm and a polymer film thickness of 0.2 - 0.3 μm, an absorbance change of 1.0 at 400 nm in the waveguide mode corresponded to an absorbance change of 0.05 in the transmission mode measured by a UV-Vis spectrophotometer (Lambda 35, Perkin Elmer). This 20-fold increase in signal results from the increased pathlength due to multiple reflections of the light as it passes from the first prism to the second down the waveguide.
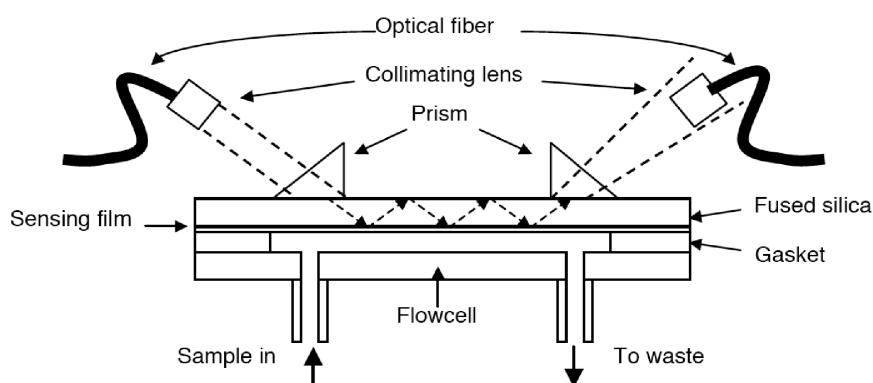
Figure 2.2 Schematic diagram of planar waveguide-type optical sensor based on thin polymeric film containing In(III)[OEP] within low volume flowcell.

29

2.2.4 Detection of chloride in solution phase and methylamine in gas phase

The thickness of a gasket in the flow-cell (see Fig. 2.3) for chloride detection was about 0.18 mm and the cell volume was measured to be ca. 40 μL. To determine the response time, a six-way valve (Fig. 2.3(a)) was connected to the flow-through set-up, where the volume for the connection tube between the valve and the flow-cell was minimized (ca. 10 μL). Switching the position of the valve enabled a sudden change in the solution composition (different chloride levels) that passed through the flow cell. In the FIA arrangement with a 50 μL of sample loop (Fig. 2.3(b)), sample solutions containing various levels of chloride prepared in 0.05 M phosphate buffer (pH 3.0) were injected while the spectral change was recorded at 392 nm (dimer) and 408 nm (monomer), as well as 450 nm and 700 nm (background), simultaneously. The background shift originating from bubbles and osmolarity changes of sample solution [29, 30] was corrected by using the absorbance changes at 450 nm and 700 nm.

The generation of various organic amine gas vapors is well described in the literature [1]. As illustrated in Fig. 2.3(c), to make methylamine standards, a solution containing methylammonium chloride and 2 M NaOH solution was introduced around a gas permeation tube through which a nitrogen gas stream (60 mL/min) flowed. The nitrogen gas stream carries the methylamine vapor into the main nitrogen gas stream (1~2 L/min, humidified), which dilutes the analyte by the ratio of analyte-stream flow rate to total flow rate. The concentration of methylamine in the analyte carrier stream was determined by trapping the amine from this line in a 1 mM HCl solution with the pH increase of this solution monitored. The degree of pH change in the acid solution after a fixed flow of analyte gas phase can be used to determine the gas phase amine level. All tubings in the final sensing arrangement were made of stainless steel and the gasket in the flow cell was 1 mm thick glass. The outlet from the flow cell was introduced into the 1 M sulfuric acid trap.
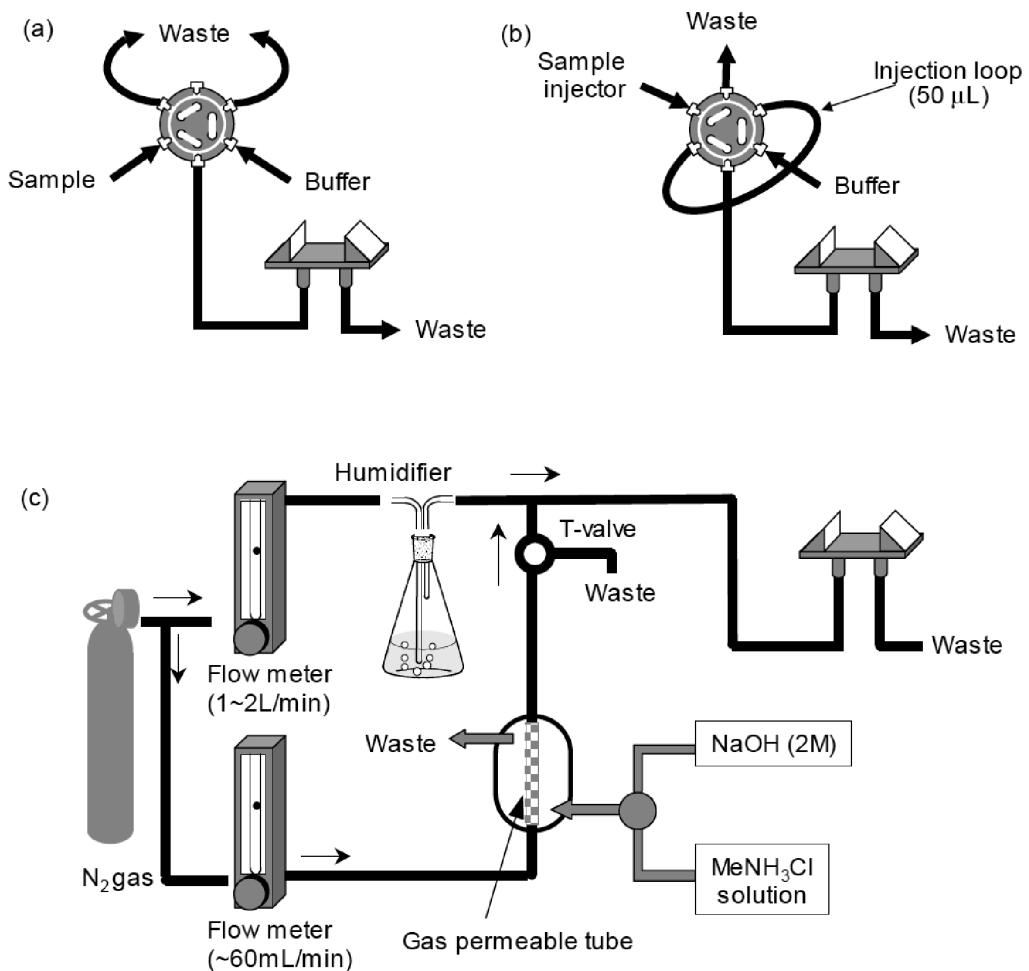
Figure 2.3 Schematic diagram of flow system for aqueous chloride detection and amine vapor detection: (a) two-way flow configuration with switch valve for response time measurement; (b) flow injection analysis configuration; (c) schematic of gas flow system for methylamine detection in the humidified nitrogen stream.

2.3 Results and discussion

2.3.1 Waveguide chloride optical sensor in FIA arrangement

The previously reported optical chloride sensor based on the dimer-monomer equilibrium of In(III)[OEP]OH exhibited a detection range from $10^{-5.5}$ to 10^{-1} M in pH 3.0 phosphate buffer with response times (t_{90}) of about 60 seconds using 5-10 μm thick films [2]. Although crystallization of metalloporphyrin in the films was observed, and was cited as the primary factor that limits the sensor lifetime, the system was shown to yield reproducible analytical results during short-term experiments (within a day) and the inherent optical properties of metalloporphyrin were fully utilized for sensing without need for an additional chromoionophore in the polymeric film. In order to further evaluate this novel sensing mechanism, the waveguide configuration was employed to assess the kinetic aspects of the multiple sensing equilibria involved, in terms of response time and lifetime. The kinetic aspects of the transduction chemistry (e.g., "on" and "off" rate constants for ion/gas-ionophore interactions, etc.) can be a limiting factor in whether ion- (and gas) sensing bulk-optodes can be used as detectors in flow-through systems once the diffusional distances are reduced using ultrathin films on planar waveguides.

2.3.1.1 Response time

Initial results of FIA experiments for chloride response, using 0.3 μm thick films and a flow-rate of 1 mL/min, are shown in Fig. 2.4. The response range for chloride concentrations (at absorbance of monomer band at 408 nm) mirrors that which was observed previously using much thicker films operated in the transmission mode [2]. Therefore, even with the much thinner film, the polymer film acts as a bulk phase where the response behavior originates from partitioning of the chloride in the film rather than purely a surface interaction. As shown in the Fig. 2.5, the response time of the thin film - based optical chloride sensor is fast enough to yield full equilibrium optical response for
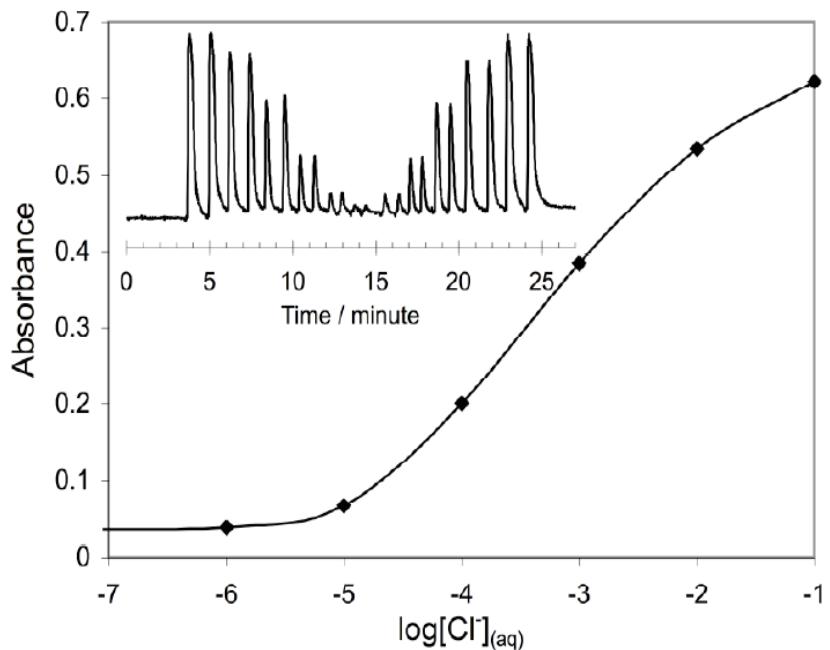
Figure 2.4 Calibration curve for optical chloride response in 0.05 M phosphate buffer (pH 3.4). Response to chloride in the FIA configuration (inset).
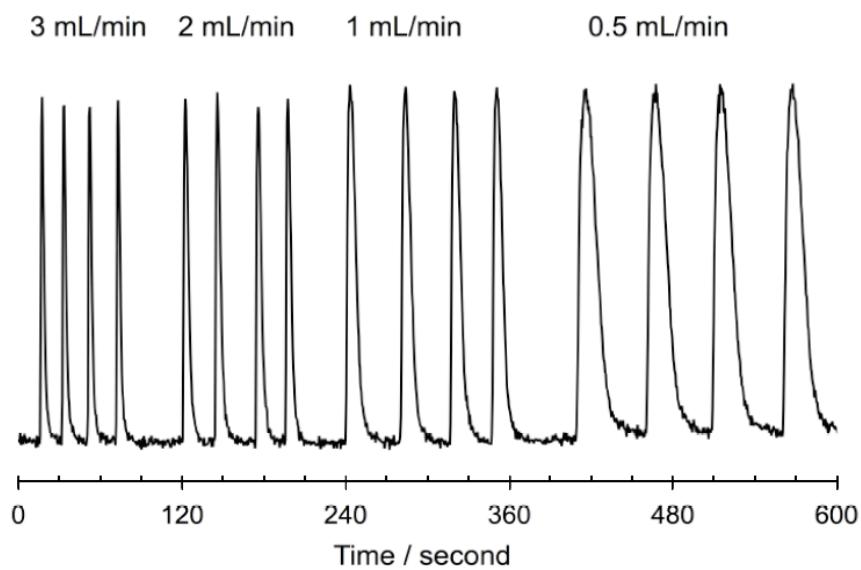
Figure 2.5 Response to [Cl⁻] = 1.0 x 10⁻³ M in 0.05 M phosphate buffer (pH 3.4) in FIA system at various flow rates (0.5 mL/min, 1 mL/min, 2 mL/min, and 3 mL/min).

each sample injection even when the flow rate is increased to 3 mL/min. Indeed, the response height for each injected chloride standard is independent of the flow-rate. In separate experiments, the measured t_{95} value (95% of equilibrium response time) when switching from a steady-flow stream of 10^{-1} M and 10^{-3} M was found to be less than 2 s, using a 6-way switch valve to change between blank buffer and analyte stream to minimize diffusion at the interface between them (data not shown). This response time is comparable to potentiometric sensors developed for LC detectors (< 2 s) [31, 32]. Therefore, the multiple equilibria involved in the dimer-monomer reaction to yield optical chloride response are kinetically fast enough to be adopted for practical applications such as an FIA system (for chloride measurements) and potentially as an ion-selective LC detector.

2.3.1.2 Drift and lifetime

One critical limitation of the ultrathin polymer films containing In(III)[OEP] on planar waveguides for use in FIA arrangement is their short lifetime. The slope of chloride response was reduced to about 45 % of its original value after 10 h of continuous buffer flow (flow rate = 0.5 mL/min). Although such changes in sensitivity can be accounted for by frequent one-point calibrations, eventually this deterioration in the response curve will prevent accurate and precise analytical results after 1-2 days. The loss of sensitivity may be attributed to the leaching of components, crystallization of the metalloporphyrin [2], and degradation of the lipophilic borate [33, 34]. Among these factors, the fast loss of o-NPOE was most evident. Figure 2.6 shows the absorbance decrease of a very thin film (thickness ~ 0.2 μm) under the flow of a 1.0 x 10^{-3} M chloride solution in pH 3 phosphate buffer (flow rate = 1.0 mL/min), which clearly indicates the leaching of the plasticizer at the rate of ca. 11 %/h based on absorbance change at 332nm, the λ_{max} for o-NPOE. Attempts to use more lipophilic plasticizers including ETH 8045, chloroparaffin, and DOS did not resolve the leaching problem. This fast leaching rate is explained by the reduced thickness of the film that is necessary to achieve rapid response times. The rate of concentration decrease of the components due to leaching is inversely proportional to the volume of the film, and the volume is

proportional to the film thickness. Therefore, the leaching rate is inversely proportional to the film thickness and this process limits the lifetime of the sensor. The leaching of film components is further accelerated by continuous flow of sample solution over the film. Therefore, to increase the lifetime of the chloride optical sensor in a flowing arrangement, it will be necessary to use a more lipophilic In(III) porphyrin that has a greater partition coefficient for the organic film phase (but is still capable of undergoing the dimer-monomer equilibrium reaction) in conjunction with more lipophilic plasticizers and/or polymer matrixes that do not need exogenous plasticizer (e.g., polyurethanes with appropriate soft-segment composition [9]).
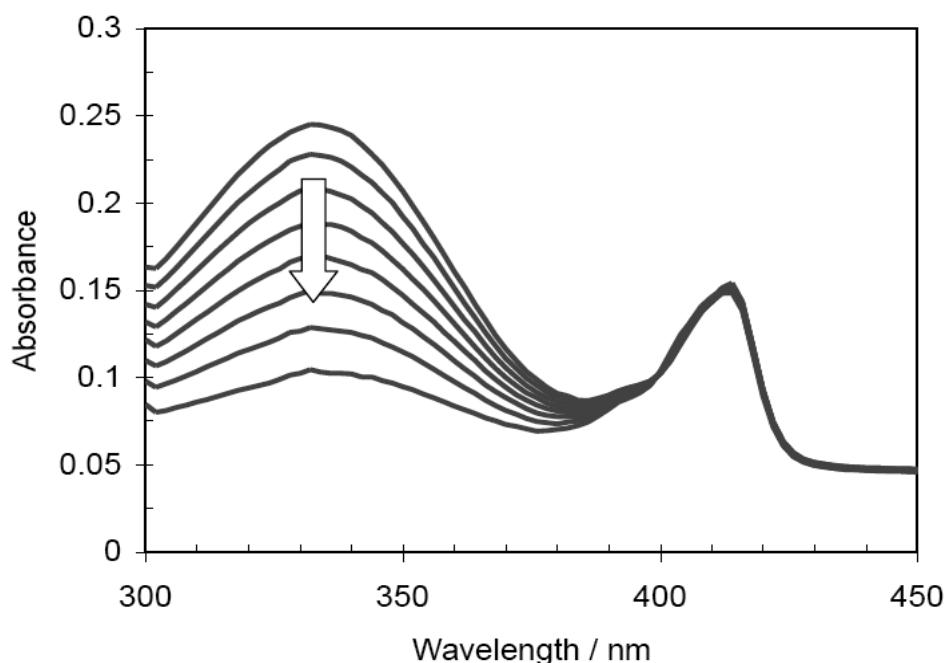
Figure 2.6 Leaching of *o*-NPOE from the film (thickness ~ 0.2 μm) under the continuous flow of chloride solution (1.0 x 10^{-3} M NaCl in 0.05 M phosphate buffer (pH 3.0), flow rate = 1.0 mL/min). Each spectrum was obtained every hour during the flow. The absorbance decrease with time at 332 nm is 0.02 /h, which corresponds to 11 % of the plasticizer loss during one hour.

2.3.2 Amine vapor sensor

The dimer-monomer equilibrium of In(III)[OEP] as an optical transduction mechanism for detection of amine vapor was investigated previously [1]. It was found that fully reversible sub-ppm detection of volatile primary amines can be achieved and that the response requires humidification of the analyte gas phase(> 60% R.H.). In order to apply this transduction scheme to the more practical and rapidly responding optical waveguide configuration, further characterization was required in terms of response time and lifetime. In addition, a closer investigation of the observed analyte hysteresis effect and the influence of humidity may yield solutions that minimize these effects.

2.3.2.1 Response time and hysteresis

The response mechanism for amine vapor sensing is summarized in the Fig. 2.1(b). Prior to use, the film with In(III)[OEP] and lipophilic borate is conditioned in the deionized water to form the dimeric form of the indium porphyrin. When the film is exposed in the gas phase containing amine species, the amine vapor partitions into the film, breaks the dimer, and generates In(III)[OEP]OH and In(III)[OEP]-amine in a reversible manner. Faster response was observed in the highly humidified gas carrier stream with higher flow rate. Fig. 2.7(a) shows the reversible response of In(III)[OEP]-doped optical sensing film using the optical waveguide scheme upon changing the gas phase concentration of methylamine between 0 ppm and 15 ppm (in the presence of >80% R.H.). The response time (t_{95}) for methylamine is less than 1 s, whereas the recovery of the optical signal to 0 ppm takes about 15 s.

Interestingly, the recovery time is further reduced by lowering the borate level in the film and pre-conditioning it in the high pH solution. The hysteresis effect is explained by protonation of the amine in the film. The protonation of amine converts the neutral amine to cationic form that is not able to efficiently leave the film into gas phase. That is, if the film does not easily allow protonation, the hysteresis effect may be reduced. So

hysteresis can be minimized by suppressing protonation of amines in the film. One way to decrease [H$^+$] in the film is to decrease borate level which is the counter anion for any ammonium cation formation. However, reducing the mol% of borate too much will also result in an initial decrease in the degree of dimerization and a subsequent decrease in spectral change in response to the gas phase amine species. Based on this rationale, a film with 45 mol% of borate was prepared on the waveguide and conditioned in 1 mM NaOH solution for a few minutes, prior to testing in the flowing gas phase. As shown in Fig. 2.7(b), this approach successfully decreases the recovery time. The t_{95} value for recovery with such films was measured to be in the order of 1 s for both concentrations tested (14 and 40 ppm). One possible explanation is that coextraction of NaOH into the film occurs during the conditioning and the amount of the co-extracted hydroxide ion is not enough to change dimer-monomer equilibrium significantly but adequate to suppress protonation of methylamine. However, the hysteresis is also a function of the exposure time. Longer exposure to the analyte can increase the recovery time depending on the nature of interaction between the analyte and the polymeric film.
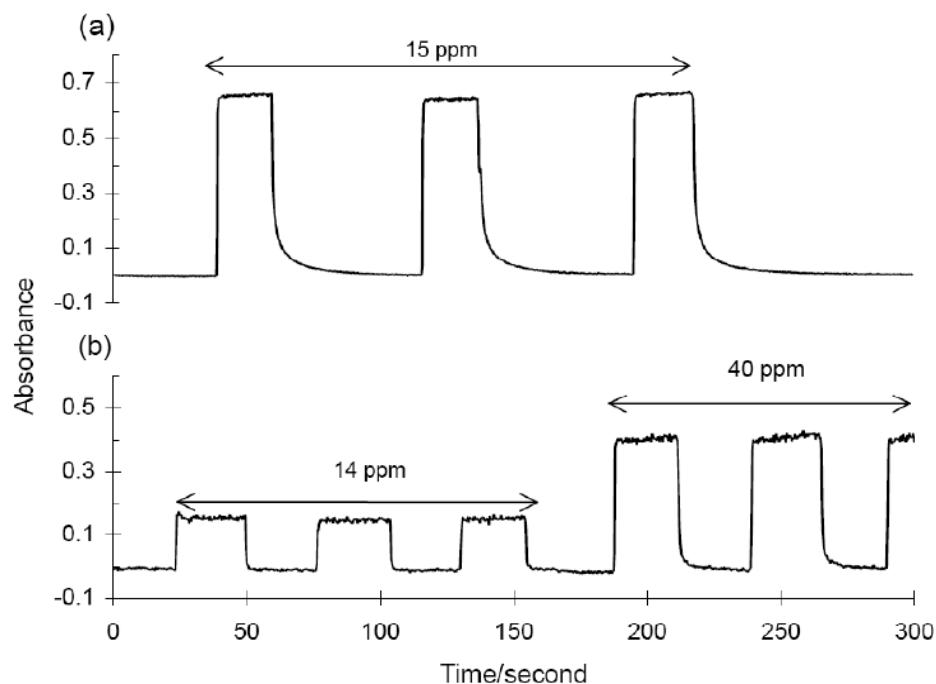
Figure 2.7 Response time for amine vapor sensor toward (a) 15 ppm methylamine using In(III)[OEP]OH/KTFPB (80 mol%)/*o*-NPOE/PVC film; (b) 14 ppm and 40 ppm methyl-amine response using In(III)[OEP]OH/KTFPB (45 mol%)/*o*-NPOE/PVC film.

37

2.3.2.2 Plasticizer loss

In case of aqueous chloride detection based on thin films, leaching of film components was a critical problem. In this regard, it was anticipated that gas phase detection with the same films would be much more stable than aqueous detection since the highly lipophilic sensor components are virtually non-volatile under ambient condition. However, as shown in Fig. 2.8(a), response to 40 ppm of methylamine is
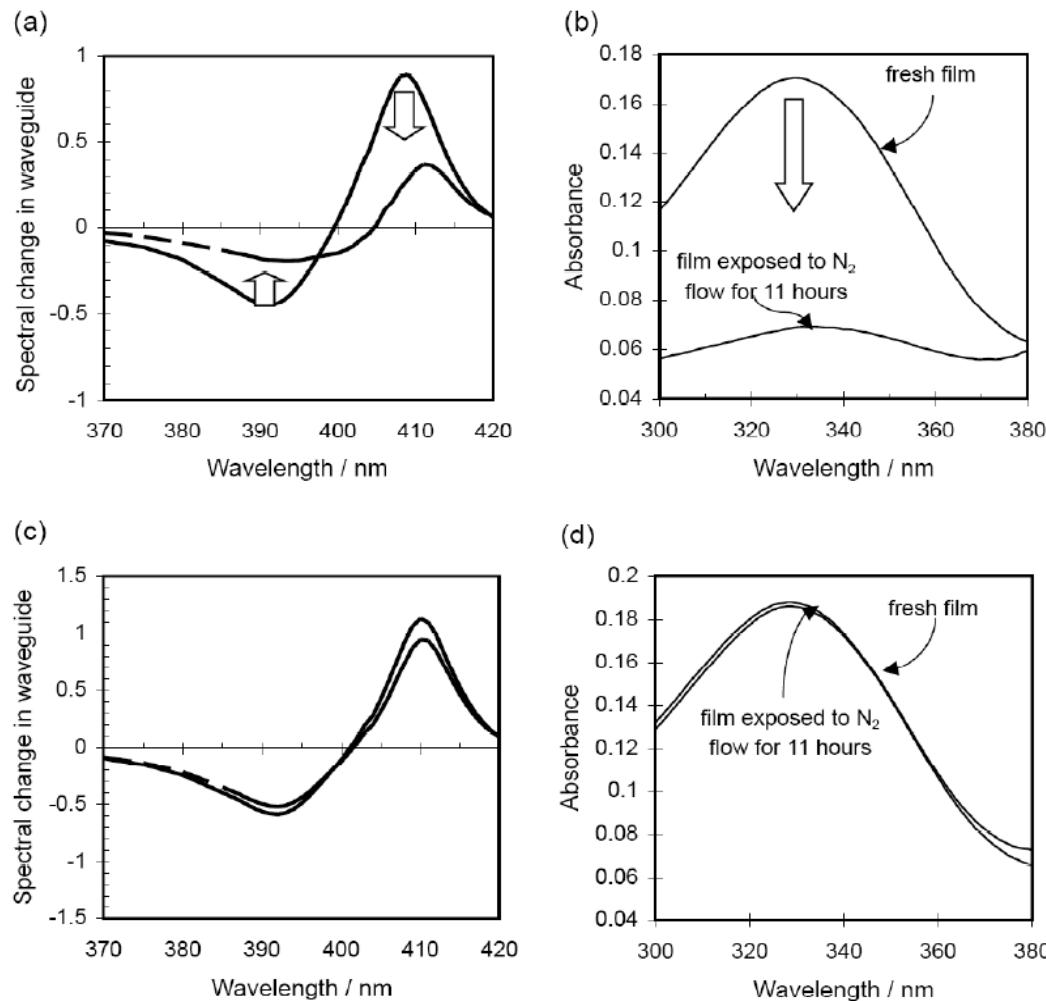
Figure 2.8 Spectra of In(III)[OEP] for 40 ppm methylamine response before and after 11 h-exposure to nitrogen stream in the waveguide with (a) the *o*-NPOE film; and (c) the ETH 8045 film. Absorbance spectra of plasticizers in (b) the *o*-NPOE film; and (d) the ETH 8045 film before and after the exposure of nitrogen stream. Thickness of all films is ca. 0.2 μm.

significantly reduced (decrease in intensity of monomeric band and increase in dimer band) after 11 h under a constant N_2 stream. The gradual decrease of absorbance of the plasticizer o-NPOE (λ_{max} = 332 nm) suggests loss of the plasticizer is responsible for this response decline (see Fig. 2.8(b)). Plasticizers typically have a high boiling point and thus low volatility (for example, b.p. of o-NPOE = 197-198 °C at 11 mmHg) so that the film acts as an organic phase for the sensor components for long periods of time. Although the loss of this solvent may be inevitable, the rate of loss should be slow enough so that the resultant response drop can be effectively handled by recalibration of the sensor periodically. Clearly, loss of o-NPOE from very thin films used in this work is exacerbated by the greatly reduced volume element of the films, and is not desirable for long-term applications. Therefore, further investigations were conducted to find a less volatile plasticizer.

Plasticizers that can help stabilize the dimeric form of In(III)[OEP] are found to be non-ester type plasticizer such as chloroparaffin, o-NPOE, ETH 8045, and DNPE. Indeed, films formulated with dioctyl adipate (DOA), dioctyl phthalate (DOP) and dioctyl sebacate (DOS) were found not to form appreciable levels of dimeric porphyrin species. ETH 8045 and DNPE were tested as alternate plasticizers for gas phase amine sensing based on their molecular weights (i.e., 411.58, 307.41 respectively), suggesting a low vapor pressure. Indeed, as shown in Fig. 2.8(c), a thin film prepared with ETH 8045 on the waveguide retained its response to 40 ppm of methylamine under 80% R.H. humidity after 11 h of continuous N_2 flow. As shown in Fig. 2.8(d), virtually no loss of ETH 8045 is confirmed during this time period. However, two drawbacks are observed with ETH 8045 film. First, due to the high viscosity of ETH 8045, the response time is increased: t_{95}(to 40 ppm) ~ 1 s and t_{95}(to 0 ppm) ~ 20 s. In addition, some photodecomposition of KTFPB is observed. Employment of DNPE instead of ETH 8045 proved to be an alternative to reduce photo-decomposition of KTFPB. However, unlike ETH 8045, DNPE facilitates methylamine uptake in an irreversible manner and thus the blank response always rises depending on the exposure time of methylamine and its concentration. This shift is reversed by reconditioning the film in the deionized water. Fig. 2.9 shows the response curves toward methylamine of In(III)[OEP]Cl/KTFPB(45

mol%)/PVC film with different plasticizers. The detection limit for methylamine is in the order of DNPE < ETH 8045 < *o*-NPOE which indicates that methylamine partitioning is favored in the reverse order. In summary, ETH 8045 is most suitable for the long-term use with controlled irradiation of light, and DNPE is appropriate for the long-term application if frequent reconditioning is possible.
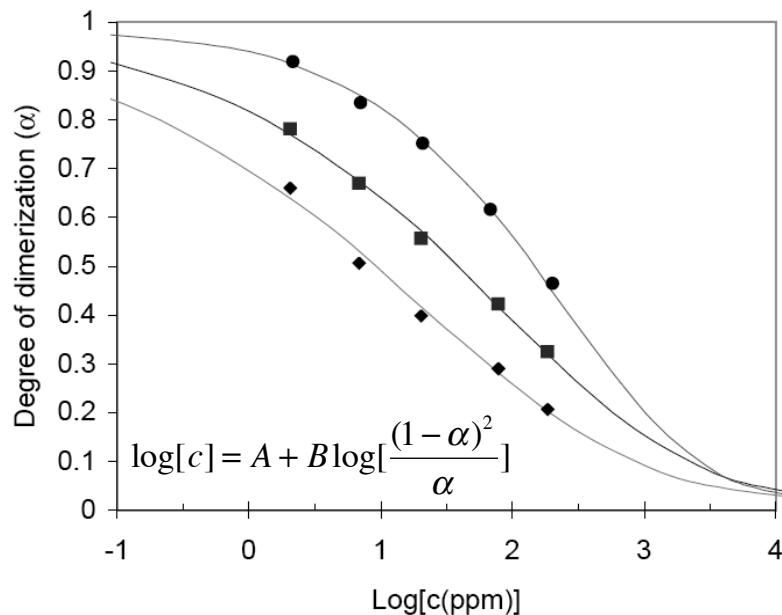
Figure 2.9 . Response curve to the methylamine vapor of the In(III)[OEP]-based sensor with different plasticizers: *o*-NPOE (●), ETH 8045 (■), DNPE (◆). The mathematical expression applied for the curve fitting is derived from the response function [1].

2.3.2.3 Humidity dependency

Optical sensors based on dimer-monomer equilibrium of the In(III)[OEP] species showed slightly different behaviors between the aqueous phase (for chloride detection) and the gas phase (for amine detection). The amine vapor sensor used in the previous work [1] exhibited a humidity response; dimerization is favored in a humidified gas phase. In this section, further examination of this humidity effect on the dimer-monomer equilibrium of metalloporphyrin in the amine vapor sensor is provided.

In general, water content in an organic phase affects the dielectric constant of the

40

medium and thus has a significant influence on interactions between ionic species; ion dissociation constants greatly depend on the dielectric constant of the medium especially when ionic species are generated from neutral species [35]. Since the plasticized thin film is believed to behave as a solvent phase for ionophores and ionic species, an ion-ion interaction in the plasticized film is also strongly dependent on the degree of hydration of the film. For example, the In(III)[OEP] dimer in the chloride sensor and in the amine vapor sensor is slowly broken into the monomers when films are exposed to a dry nitrogen gas phase (~ 0% R.H.). Monomers turn to the dimer again when the film is fully hydrated by soaking or partially hydrated by increasing humidity of the nitrogen gas phase. This can be explained by considering interaction between cationic porphyrins and anionic sites. In the dry environment, the anionic sites break the dimer as a result of the increased interaction between the cationic monomer species and anionic sites. However, when the film is fully hydrated by soaking in the deionized water, monomers turn to the dimer again since the hydrated organic phase now solvates ionic sites better than dry organic phase and thus weakens the interaction between the cationic metalloporphyrins and anionic sites.

It should be noted here that the degree of In(III)[OEP] dimerization in the fully hydrated film is strictly determined by the added borate level. When the amount of the lipophilic borate (TFPB$^-$) is 80 mol% of the metalloporphyrin, the effective anionic site concentration is about 85 mol% including the contribution from the endogenous anionic impurities within the PVC [2]. Under such a condition, the dimeric form of the metalloporphyrin (L$_2$OH$^+$) is only 15 mol% to the total concentration of metalloporphyrin (L$_{total}$) since the only available hydroxo-monomer (LOH) for dimerization is 15 mol%. After dimer formation, the remaining monomer is L$^+$ which is about 70 mol% of L$_{total}$.

As can be seen in Fig. 2.10(a), when such a film (80 mol% TFPB$^-$) is partially hydrated by humidifying the gas phase (10 ~ 80 % R.H.), the behavior of the dimer-monomer equilibrium shows humidity-dependant behavior. As humidity increases from 10% R.H. to 80% R.H., spectral change of the film indicates an increase of the dimer (L$_2$OH$^+$, 391 nm) and a decrease of one monomer band (L$^+$, 400-404 nm). This suggests

the following equilibrium is present:

$$2L^+ + R^- + H_2O \xrightleftharpoons[\text{dehumidify}]{\text{humidify}} L_2OH^+ + H^+R^-$$

(rxn 2.1)
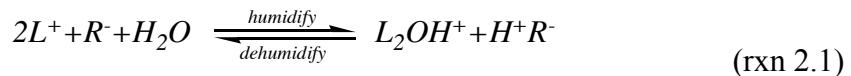
where R^- is lipophilic anionic sites (TFPB$^-$). This process can be described stepwise by the following two equations:

$$L^+ + R^- + H_2O \rightarrow LOH + H^+R^-$$

(rxn 2.2)

$$LOH + L^+ \rightarrow L_2OH^+$$

(rxn 2.3)
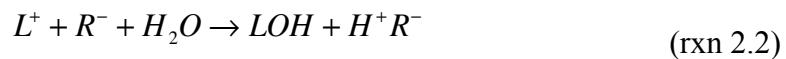
The rxn. 2.2 suggests that, in the partially hydrated films, ionic species are converted to neutral species more readily than in the fully hydrated film (in the aqueous phase), so that L^+ and R^- can react with water to give neutral species (i.e., LOH is formed and H^+ is
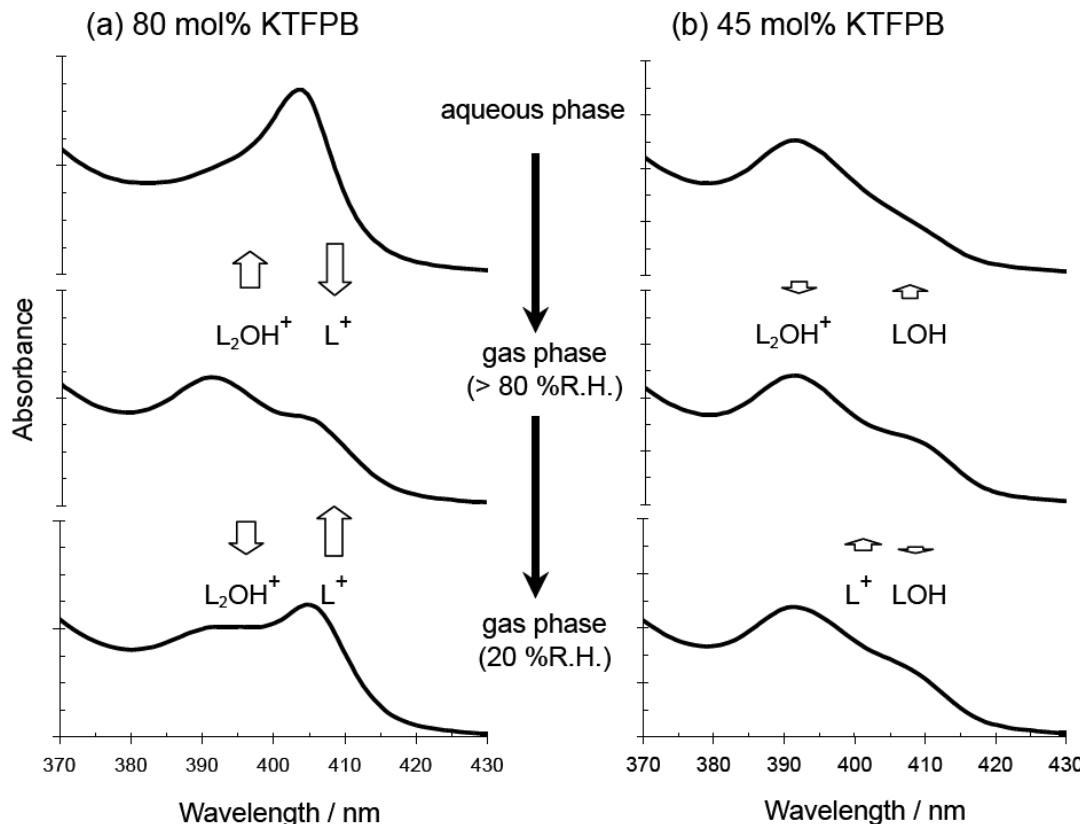
Figure 2.10 Spectral change after contacting with aqueous phase and then to humidified gas phase (>80% R.H.) following exposure to 20% R.H. gas phase. Film compositions are In(III)[OEP]/o-NPOE/PVC with (a) 80 mol% KTFPB and (b) 45 mol% KTFPB.

42

counter-balanced by R$^-$). However, as can be seen in equilibrium rxn 2.3, the remaining R$^-$ does not strongly interact with L$_2$OH$^+$ which still allows dimerization. Therefore, the partially hydrated films show humidity response by the reaction between L$^+$, R$^-$ and water whereas the fully hydrated films show enhanced solvation of L$^+$ and R$^-$ and thus reaction with water is not observed.

Fig. 2.10(b) shows that the humidity effect can be minimized by using films containing 45 mol% borate (so overall anionic sites is 50 mol%). Since LOH and L$^+$ are at a 1:1 ratio in these film, when LOH and L$^+$ form a dimer (L$_2$OH$^+$), there will be no residual monomeric species. When this film is exposed to a gas phase of 80% R.H., no significant change in dimerization is observed due to absence of L$^+$ species in the film; rxn 2.2 is not observable since L$^+$ is not available. Therefore, the degree of dimerization is maintained in the gas phase until the gas phase is fully dried (< 10% R.H.).

2.4 Conclusions

Planar waveguide type optical sensors based on a dimer-monomer equilibrium of In(III)[OEP] in an ultra-thin solvent polymeric film (0.2-0.3 μm) is demonstrated and examined in terms of response time, lifetime and role of humidity (for gas phase sensing). For aqueous chloride ion detection, response times are rapid enough to be employed for use as an optical detector in an FIA system. However, leaching of membrane components is a critical issue that must be overcome to ensure more stable sensor response over longer time periods. Use of more lipophilic version of In(III) porphyrin will likely help overcome this current limitation. The rapid detection of gas phase amine is more feasible with this sensor; response times are fast (~ 1 s) and lifetime/stability can be enhanced by using a less volatile plasticizer to prepare the ultrathin films. A close look at the mechanism of amine vapor response has provided an approach to suppress the analyte hysteresis effect and reduce recovery times by optimizing the amount of anionic sites. In addition, by optimizing the level of anionic sites added, the effect of humidity on the optical response of the sensor can be greatly reduced. These assessments will provide useful approaches for practical applications (i.e., FIA, HPLC and GC) of waveguide type

optical sensors based on polymeric thin films containing In(III)[OEP] and potentially other metalloporphyrin species.

2.5 References

[1] W. Qin, P. Parzuchowski, W. Zhang, M.E. Meyerhoff, Anal. Chem. 75 (2003) 332.

[2] W. Zhang, E. Rozniecka, E. Malinowska, P. Parzuchowski, M.E. Meyerhoff, Anal. Chem. 74 (2002) 4548.

[3] E. Malinowska, J. Niedziolka, E. Rozniecka, M.E. Meyerhoff, J. Electroanal. Chem. 514 (2001) 109.

[4] E.D. Steinle, S. Amemiya, P. Bühlmann, M.E. Meyerhoff, Anal. Chem. 72 (2000) 5766.

[5] P.G. Parzuchowski, J.W. Kampf, E. Rozniecka, Y. Kondratenko, E. Malinowska, M.E. Meyerhoff, Inorg. Chim. Acta 355 (2003) 302.

[6] I.H.A. Badr, M.E. Meyerhoff, Anal. Chem. 77 (2005) 6719.

[7] I.H.A. Badr, M.E. Meyerhoff, J. Am. Chem. Soc. 127 (2005) 5318.

[8] E.D. Steinle, U. Schaller, M.E. Meyerhoff, Anal. Sci. 14 (1998) 79.

[9] E. Malinowska, J. Niedziolka, M.E. Meyerhoff, Anal. Chim. Acta 432 (2001) 67.

[10] L. Gorski, E. Malinowska, P. Parzuchowski, W. Zhang, M.E. Meyerhoff, Electroanalysis 15 (2003) 1229.

[11] E. Malinowska, L. Gorski, M.E. Meyerhoff, Anal. Chim. Acta 468 (2002) 133.

[12] L. Gorski, E. Malinowska, Anal. Chim. Acta 540 (2005) 159.

[13] L. Gorski, M.E. Meyerhoff, E. Malinowska, Talanta 63 (2004) 101.

[14] Y. Qin, E. Bakker, Anal. Chem. 76 (2004) 4379.

[15] M. Gouterman, D. Holten, E. Lieberman, Chem. Phys. 25 (1977) 139.

[16] K. Seiler, W. Simon, Anal. Chim. Acta 266 (1992) 73.

[17] E. Bakker, W. Simon, Anal. Chem. 64 (1992) 1805.

[18] W.E. Morf, K. Seiler, B. Lehmann, C. Behringer, K. Hartman, W. Simon, Pure Appl. Chem. 61 (1989) 1613.

[19] O.S. Wolfbeis, Anal. Chem. 72 (2000) 81.

[20] O.S. Wolfbeis, Anal. Chem. 74 (2002) 2663.

[21] O.S. Wolfbeis, Anal. Chem. 76 (2004) 3269.

[22] C.R. Lavers, K. Itoh, S.C. Wu, M. Murabayashi, I. Mauchline, G. Stewart, T. Stout, Sens. Actuators B 69 (2000) 85.

[23] B. Kovacs, G. Nagy, R. Dombi, K. Toth, Biosens. Bioelectron. 18 (2003) 111.

[24] K. Toth, G. Nagy, B. Thi Thu Lan, J. Jeney, S.J. Choquette, Anal. Chim. Acta 353 (1997) 1.

[25] H. Hisamoto, K.-H. Kim, Y. Manabe, K. Sasaki, H. Minamitani, K. Suzuki, Anal. Chim. Acta 342 (1997) 31.

[26] U.E. Spichiger, D. Freiner, M. Lerchi, E. Bakker, R. Dohner, W. Simon, Proc. SPIE 1796 (1993) 371.

[27] U.E. Spichiger, D. Citterio, M. Bott, Proc. SPIE 2508 (1995) 179.

[28] A.M. Goodman, Appl. Opt. 17 (1978) 2779.

[29] Z. Li, X. Li, M. Rothmaier, D.J. Harrison, Anal. Chem. 68 (1996) 1726.

[30] Z. Li, X. Li, S. Petrovic, D.J. Harrison, Anal. Chem. 68 (1996) 1717.

[31] K. Stulik, Anal. Chim. Acta 273 (1993) 435.

[32] S. Picioreanu, I. Poels, J. Frank, J.C. Van Dam, G.W.K. Van Dedem, L.J. Nagels, Anal. Chem. 72 (2000) 2029.

[33] U. Schaller, E. Bakker, U.E. Spichiger, E. Pretsch, Anal. Chem. 66 (1994) 391.

[34] S. Peper, M. Telting-Diaz, P. Almond, T. Albrecht-Schmitt, E. Bakker, Anal. Chem. 74 (2002) 1327.

[35] U. Muinasmaa, C. Rafols, E. Bosch, M. Roses, Anal. Chim. Acta 340 (1997) 133.

Chapter 3

Optical and Electrochemical Fluoride Selective Sensors Based on Dimer-Monomer Equilibrium of Scandium(III) Octaethylporphyrin.

3.1   Introduction

Fluoride measurements are receiving continuous attention from sensor research communities due to the clinical importance of fluoride levels in drinking water [1-4] and potential applications in enzyme-coupled sensors for detecting a wide range of substrates that liberate hydrogen peroxide in the presence of selective oxidase enzymes (the peroxide generated can oxidize fluorophenol compounds in the presence of peroxidase enzyme to liberate free fluoride ion [5]). Fluoride ion can also be liberated enzymatically or by inorganic catalysts from toxic fluorophosphate species, including the nerve gases such as soman and sarin [6, 7]. Although the most useful fluoride ion selective sensor is based on a LaF_3 crystal (solid-state ion-selective electrode) [8], development of very inexpensive fluoride selective devices is of interest, especially using liquid polymeric membrane/film configurations to create potentiometric or optical devices [9, 10]. However, the very negative Gibbs free energy of hydration of fluoride ion (-366.5 kcal/ mol) makes the fluoride one of the most difficult anions to be solvated within the organic polymeric phase of such sensors. In order to compensate for this unfavorable partitioning, a fluoride selective ionophore in the organic phase must exhibit exceptionally strong yet reversible binding with fluoride ion.

Recently, a number of new ionophores have been suggested for detection of fluoride, either potentiometrically or optically, using polymer membranes/films doped with lipophilic metal ion-ligand complexes. Initially, gallium(III) porphyrins were found to exhibit non-Hofmeister selectivity patterns when used as ionophores in polymeric

membrane electrodes, with potentiometric fluoride response significantly improved [11]. Subsequently, various zirconium(IV) porphyrins were found to also exhibit greatly enhanced selectivity toward fluoride when employed to prepare membrane electrodes [12]. These ionophores have been thoroughly studied in terms of response mechanisms, optimized polymeric matrices as well as fundamental studies of ligation and dimerization reactions using mass spectrometry [13-16]. Beyond porphyrin complexes, Schiff-base complexes of Ga(III) or Zr(IV) have also demonstrated potentially useful selectivity for fluoride when employed as ionophores to construct polymer membrane electrodes [17, 18].

The most selective ionophores reported to date for detection of fluoride are aluminum(III) porphyrins [19, 20]. Aluminum(III) octaethylporphyrin (Al(III)OEP) was found to provide unmatched selectivity for fluoride over all other anions when used in an optode configuration to quantify fluoride in the range of $10^{-7} \sim 10^{-3}$ M. The polymer film used in this earlier work included a pH chromoionophore along with the Al(III) porphyrin, and optical detection was based on a co-extraction principle [21]. Use of Al(III) porphyrins in polymeric films to create highly selective potentiometric fluoride sensors has also been reported, with the optimal potentiometric response being achieved using a sterically hindered picket-fence-type Al(III)-tetraphenylporphyrin structure [22]. Al(III)-salophenes as well as other porphyrin structures have also been examined for creating optical and electrochemical fluoride sensors [23, 24].

It is important to understand how metalloporphyrins of group IIIA metal ions exhibit their selective ligation with given anions. Although In(III)-porphyrins exhibit good selectivity for chloride sensing [25, 26], and sensors based on Ga(III)-porphyrins exhibit much improved fluoride response, Al(III)-porphyrin ionophores exhibit unrivaled selectivity for fluoride in both optical and potentiometric transduction modes. This trend is consistent with the hard-soft acid-base convention [27]; if hardness of the central metal ion increases (i.e., $Al^{3+} > Ga^{3+} > In^{3+}$), its porphyrin complex exhibits higher selectivity for fluoride, since fluoride is a hard base. This idea is further supported by the fact that high-valent transition metal ion (hard acid) complexes, such as zirconium(IV) porphyrins,

have also been shown to be useful for developing fluoride-selective sensors [12, 14].

It is known that scandium(III) exhibits similar complexation chemistry as Al(III). For example, among the group IIIB cations in the periodic table, the coordination number of Sc(III) is same as Al(III) (i.e., ≤ 6) and less than that of other group IIIB cations (i.e., > 6) [28]. In addition, Sc(III) can form the cryolite phase, Na_3ScF_6, which is the chemical equivalent of the naturally occurring cryolite Na_3AlF_6 [29]. This fact suggests that Sc(III) complexes may behave like Al(III) complexes in terms of their interaction with fluoride. In this chapter, the chemistry of Sc(III) octaethylporphyrin (Sc(III)OEP) in plasticized polymeric films is examined in an effort to devise optical and electrochemical fluoride selective sensors. It will be shown that very high selectivity for fluoride over other inorganic anions can be achieved based on formation of a unique difluoro-bridged dimer when fluoride is present in solutions that contact polymeric films doped with Sc(III)OEP.

3.2   Experimental

3.2.1   Reagents

Hydroxo(2,3,7,8,12,13,17,18-octaethylporphyrinato) scandium(III) (Sc(III)OEP-OH) and hydroxo(5,10,15,20-tetraphenylporphyrinato) scandium(III) (Sc(III)TPP-OH) were prepared according to previous literature reports [30, 31]. 4',5'-Dibromofluorescein octadecyl ester (ETH 7075), tridodecylmethylammonium chloride (TDMACl), potassium tetrakis(*p*-chlorophenyl)borate (KTpClPB), potassium tetrakis(3,5-bis[trifluoromethyl]-phenyl)borate (KTFPB), high molecular weight poly(vinyl chloride) (PVC), di(tridecyl) adipate (DTDA) *o*-nitrophenyl octyl ether (*o*-NPOE), and bis(2-ethylhexyl) sebacate (DOS) were used as received from Fluka (Ronkonkoma, NY). Tetrahydrofuran (THF) was from Sigma-Aldrich (St. Louis, MO) and distilled before use. Glycine was obtained from Fisher Scientific (Cincinnati, OH). Acids (phosphoric acid and hydrofluoric acid (35 wt. % in water)), sodium salts of anions (bromide, chloride, nitrate, perchlorate, phosphate monobasic, salicylate, and thiocyanate), and trans-1,2-diaminocyclohexane-N,N,N',N'-tetraacetic acid (CDMA) were obtained from Sigma-Aldrich.

3.2.2 Film preparation

Optical film cocktails were prepared by dissolving Sc(III)OEP-OH (1.0 mg), ETH 7075 (100 mol% relative to Sc(III)OEP-OH), a given plasticizer (66 mg), and PVC (33 mg) in 5 mL THF. The films used in the transmission mode were manually cast using a pipette on a glass slide (ca. 50 mm x 9 mm x 1 mm) or on a silica glass slide (77 mm x 25 mm x 1 mm; Chemglass, Vineland, NJ). The films used for the waveguide experiments were spin-coated on the silica glass slide, using a spin coating device (model SGS-G3-8; Cookson Electronics, Providence, RI): 150 µL of cocktail was loaded on the substrate and spun at 1000 rpm for 20 s. The film was dried overnight and used within 1 ~ 3 days. The film should be kept in the dark to minimize any loss by photo-decomposition.

Ion-selective membranes for electrochemical sensor fabrication were prepared by casting the membrane cocktail in a glass o-ring (i.d. = 22 mm) affixed on the glass slides (75 mm x 50 mm x 1 mm). The composition of membrane cocktails were Sc(III)OEP-OH (2.0 mg), ionic additives (either TDMACl or KTpClPB), plasticizer (either DOS or o-NPOE, 132 mg), PVC (66 mg), and THF (2 mL). The membrane was dried overnight in the dark, and a 8 mm-diameter disk was cut to prepare an electrode. The electrode was conditioned in the buffer (0.05 M gly-phosphate, pH 3.0) for 8 h before any experiments.

3.2.3 Optical measurements

Optical studies of the dimer-monomer chemistry of Sc(III)OEP were performed in the transmission mode. In this arrangement, a UV-Vis spectrophotometer (model Lambda 35; Perkin-Elmer, Boston, MA) was employed with a polymer film-coated glass slip in the quartz cuvette [25] or with a flowcell made of the fused silica glass coated with the optical sensing film, a teflon gasket (0.18 mm thickness), and another fused silica glass slide with inlet and outlet holes. Continuous flow of buffer (1 mL/min) was achieved via a peristaltic pump (Miniplus-3; Gilson, Middleton, WI).

Optical response for fluoride sensing was assessed by determining the degree of

deprotonation (α) of the ETH 7075 chromoionophore or the degree of dimerization of Sc(III)OEP in the polymer sensing film. According to the coextraction principle of bulk optodes [21], when an analyte anion in the aqueous phase is introduced into the organic phase and tightly binds with an ionophore, a cation is transferred into the organic phase at the same time to maintain charge neutrality in both phases. When ETH 7075, a proton-binding chromoionophore, is doped in the organic phase, it is the proton that partitions into the film along with anions. Therefore, the degree of anion transfer can be monitored by looking at protonation (1-α) (or deprotonation (α)) of the ETH 7075, and the degree of protonation (or deprotonation) is correlated to the activity of analyte anion in the aqueous phase. Since Sc(III)OEP employed as the ionophore also changes its Soret band by binding with fluoride, absorbances of ETH 7075 and dimeric Sc(III)OEP have been measured simultaneously to evaluate the degree of deprotonation (α) and dimerization, respectively.

Optical anion sensors based on the coextraction mechanism generally achieve better detection limit by decreasing pH since the anionic response depends on the product of the concentration of anion and the concentration of protons in the aqueous phase. In this work, all the measurements were done at pH 3.0 where about 60% of fluoride exists as HF (pKa = 3.17) and the content of fluoride is described in terms of total concentration of fluoride, which is the sum of anionic fluoride and neutral hydrogen fluoride in the aqueous phase.

While selectivity was studied in the same transmission mode, reversibility, response time measurements, and flow injection analysis (FIA) of several samples containing fluoride were carried out using a waveguide optical sensing configuration [32]. The same flow-cell used in the transmission mode was fixed horizontally with two light-coupling prisms placed on the waveguide (a fused silica glass slide spin-coated with the fluoride sensing polymer film on one side). The light from a deuterium-tungsten lamp (DT-1000; Ocean Optics, Dunedin, FL) was guided into one prism by an optical fiber connected with a collimating lens at the end. The light coming out from the second prism was collected into another optical fiber by a collimating lens. A CCD detector (USB 2000;

Ocean optics) was connected to the optical fiber and the spectrum was digitized from 200 to 800 nm. In the FIA arrangement, a 50 µL injection loop was used and the cell volume was ca. 40 µL. The optical response at 550 nm was recorded simultaneously every 0.5 seconds. See chapter 2 for more details regarding the optical waveguide based sensor configuration.

For most experiments, a 0.05 M glycine-phosphate buffer (pH 3.0) was used as the background electrolyte. This buffer was prepared by adjusting the pH of a 0.05 M glycine solution with phosphoric acid. For FIA experiments for commercial mouth wash samples, a total ionic strength adjustor buffer was prepared from 0.5 M glycine, 1 M NaCl, and 2.9 mM CDMA with the pH adjusted to 3.1 by adding phosphoric acid. Anion solutions were prepared by dissolving corresponding sodium salts in the same buffer. A stock fluoride solution (1 M) was prepared by dilution of hydrofluoric acid solution with the buffer and the pH was adjusted to ca. 3 by addition of sodium hydroxide. For selectivity experiments, 50 mL of buffer was pumped into the flow-cell and its outlet was introduced back into the buffer reservoir. The concentration was adjusted by adding increasing volumes of the test anion salt solution to the reservoir. For response time measurements, a two-way flow configuration with a switch valve [32] was employed in order to minimize the concentration gradient between the two concentrations that were being tested.

Ion-selective electrodes based on Sc(III)OEP-doped plasticized membranes were prepared using electrode bodies (Oesch Sensor Technology, Sargans, Switzerland). The galvanic cell employed in this work consisted of: Ag/AgCl(s), KCl(4 M)(aq)/LOAc(1 M)(aq)/sample solution/membrane/internal solution, AgCl(s)/Ag. Potential responses of sensors were measured by a high impedence voltmeter (VF-4, World Precision Instruments) connected to a personal computer running Labview software (version 7.0, National Instruments). The internal solution was prepared by dissolving NaCl (10 mM) and NaF (10 mM) in the gly-phosphate buffer (0.05 M, pH 3.0). All the EMF responses are correlated to activities of anions which are calculated based on the two-parameter Debye-Hückel method [39]. In this calculation, ionic strength of buffer was approximated

by considering the net charge of the zwitterion species.

3.2.4 X-ray crystallography

The single crystal of the bis(μ-fluoro) Sc(III)OEP dimer was prepared by dissolving Sc(III)OEP-OH (5 mg) in dichloromethane (5 mL) and equilibrating with 2 M fluoride solution (ca. pH 3) several times. The organic phase was then dried with sodium sulfate and filtered. Hexanes were carefully added to the filtrate and then this dichloromethane/ hexanes solution was left partially open to air for a couple of days in the dark as crystals were formed at 22 °C.

A crystal of dimensions 0.36 x 0.34 x 0.04 mm was mounted on a standard Bruker SMART CCD-based X-ray diffractometer equipped with a LT-2 low temperature device and normal focus Mo-target X-ray tube (λ = 0.71073 A) operated at 2000 W power (50 kV, 40 mA). The X-ray intensities were measured at 123(2) K; the detector was placed at a distance 4.969 cm from the crystal. A total of 2525 frames were collected with a scan width of 0.5° in ω and phi with an exposure time of 30 s/frame. The integration of the data yielded a total of 23732 reflections to a maximum 2θ value of 49.64° of which 5309 were independent and 3834 were greater than 2σ(I). The final cell constants were based on the xyz centroids of 4623 reflections above 10σ(I). Analysis of the data showed negligible decay during data collection; the data were processed with SADABS and corrected for absorption.   The structure was solved and refined with the Bruker SHELXTL (version 6.12) software package, using the space group P1bar with Z = 1 for the formula $C_{72}H_{88}N_8Sc_2$. All non-hydrogen atoms were refined anisotropically with the hydrogen atoms placed in idealized positions. The molecule lies on an inversion center in the crystal lattice. The fluoride bridging atoms are disordered over two positions and were refined with aprtial occupancy atoms constrained to sum to one. Full matrix least-squares refinement based on F2 converged at R1 = 0.0730 and wR2 = 0.2347 [based on I > 2sigma(I)], R1 = 0.1050 and wR2 = 0.2500 for all data [33].

3.3   Results and Discussion

3.3.1   Bis(μ-hydroxide) dimer and bis(μ-fluoro) dimer of Sc(III)OEP

Metalloporphyrins can be utilized not only as anion-selective ionophores but also as chromophores that exhibit optical changes upon binding of target anions. One of the best examples reported in the literature is an optical chloride sensor based on a dimer-monomer equilibrium of indium(III) porphyrin where a hydroxo-bridged dimer of In(III)OEP is broken into corresponding monomeric species as chloride replaces hydroxide as an axial ligand of the metalloporphyrin. This dimer-monomer equilibrium results in a simultaneous optical shift of the Soret absorption band [25]. Scandium(III) porphyrins are also known to form dimers that exhibit a hypsochromic shift of the Soret band from monomeric scandium(III) porphyrins. Gouterman et al. [30] reported the X-ray structure of the μ-oxo-dimer of Sc(III)OEP and observed a blue shift of the Soret band for this dimer species (vs. monomer). Arnold et al. [31] argued that the bis(μ-hydroxide) dimer of Sc(III)OEP (see Fig. 3.1(a)) could be observed, depending on the degree of hydration during crystal growth. However, there have been no report on the study of dimer-monomer chemistry of Sc(III)OEP as a (chromo)ionophore for sensing purposes. In this chapter, the dimer-monomer equilibrium of Sc(III)OEP is utilized for the detection of fluoride using organic polymer phases doped with this metalloporphyrin.
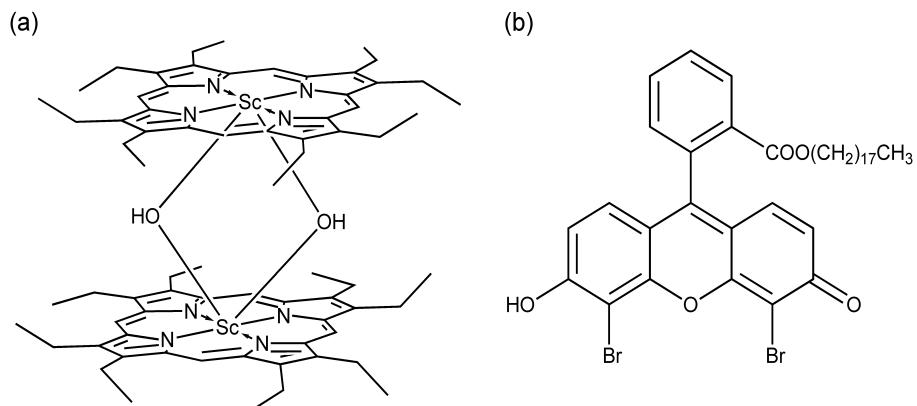
Figure 3.1 Structures of μ-hydroxo-dimer of Sc(III)OEP (a) and ETH 7075 (b).

When Sc(III)OEP(OH) is incorporated within a plasticized film, a similar UV-Vis spectral change is observed. The dimeric band is observed within a plasticized polymeric film before contact with solutions containing fluoride, and this species is believed to be the bis(μ-hydroxide) dimer (Fig. 3.1(a)) since the organic phase in contact with aqueous phase (no fluoride) is saturated with water. The formation of the bis(μ-hydroxide) dimer of Sc(III)OEP does not require any ionic sites in the organic phase since it is a neutral species. This is in contrast to Ga(III)OEP and In(III)OEP, where dimerization results in positively charged μ-hydroxo-bridged dimers only in the presence of anionic additives (e.g., tetraphenylborate derivatives) within the organic phase [34]. Hence, the degree of dimerization will be a function of the initial concentration of Sc(III)OEP-OH in the organic polymer film phase if there are no ligands present other than OH$^-$. Indeed, when Sc(III)OEP-OH alone is doped within plasticized (*o*-NPOE as a plasticizer) PVC films at high concentrations (3 wt%, 50 mmol/kg), the Soret band is at 393 nm (see Fig. 2(a)) and, at lower concentrations (0.7 wt%, 12 mmol/kg), λ_{max} of the Soret band is 408 nm. Since it is known that the corresponding dimer and monomer species in chloroform exhibit Soret bands at 390 nm and 405 nm, respectively [30], it is reasonable to assign the 393 nm band observed in the PVC film as a dimer and the 408 nm band as originating from a monomer.
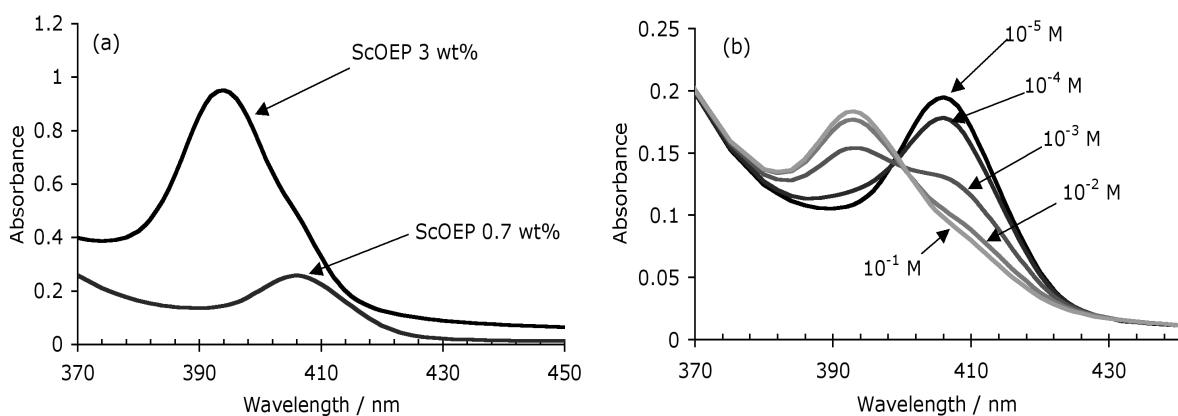
Figure 3.2 UV-Vis spectra of Sc(III)OEP in plasticized PVC films. (a) Shift of the Soret band of films containing Sc(III)OEP-OH (3 wt% or 0.7 wt%)/*o*-NPOE (66 mg)/PVC (33 mg) when films are conditioned in the blank buffer. (b) Shift of the Soret band of a film (Sc(III)OEP-OH (1 wt%)/*o*-NPOE(66 wt%)/PVC(33 wt%) contacting various concentration of fluoride in 0.05 M gly-phosphate buffer (pH 3.0).

When similar PVC films (Sc(III)OEP-OH(1 wt%)/o-NPOE(66 wt%)/PVC(33 wt%)) are exposed to fluoride ion in the bathing solution (pH 3.0 buffer), as the fluoride concentration is increased, the absorbance at 393 nm increases and the absorbance at 408 nm decreases (see Fig. 3.2(b)). Since the band at 393 nm in Fig. 3.2(a) is believed to originate from a dimeric structure, the data shown in Fig. 3.2(b) suggest that fluoride binding may initiate the conversion of monomeric porphyrin to the dimeric porphyrin within the polymeric film, even when the porphyrin is present at concentrations where only minimal bis(μ-hydroxide) dimers form spontaneously in the absence of fluoride.

To prove that fluoride can promote the formation of a dimer Sc(III)OEP species, an organic phase solution of dichloromethane containing 1 mg/mL of Sc(III)OEP-OH was equilibrated with an aqueous phase of 2 M fluoride solution at pH 3.0. The organic phase was separated, dried with sodium sulfate, and filtered. Hexane was added into the clear and dark red filtrate. This hexane-dichloromethane mixture was left in the dark and allowed to slowly evaporate, which led to formation of crystals. Single crystal X-ray diffraction analysis of these crystals yielded the dimer structure shown in Fig. 3.3. The structure shows the N_4 planes (consisting of four nitrogen atoms in each porphyrin) are parallel to each other and slightly off center, and clearly bridged via two fluoride ions. These structural features are quite similar to the reported bis(μ-hydroxide) dimer [31].
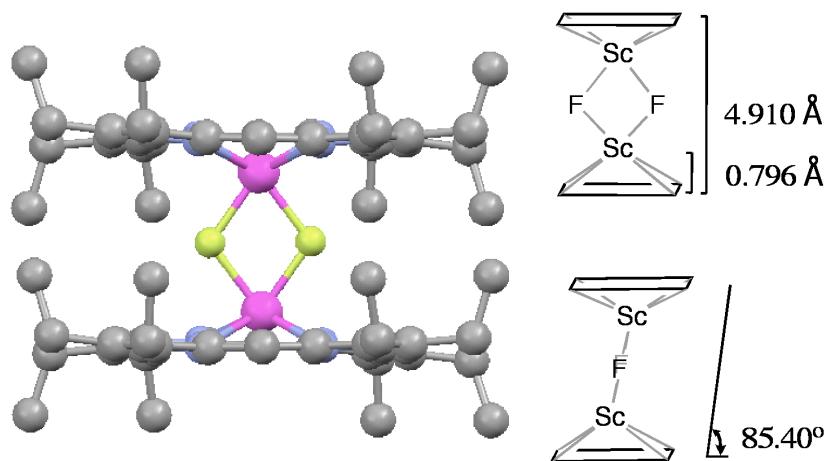
Figure 3.3 X-ray crystal structure of [Sc(III)OEP]$_2$(μ-F)$_2$.

The structural parameters are summarized in Table 1. The only difference is that the bis(μ-fluoro) dimer has slightly shorter bond lengths between the Sc(III) and fluorides, a larger F-Sc-F angle, and a smaller Sc-F-Sc angle compared to the bis(μ-hydroxide) dimer species. As a result, the distance between two N4 planes of bis(μ-fluoro) dimer is 4.910 Å, which is 0.15 Å shorter than that of bis(μ-hydroxide) dimer (5.06 Å). These dimeric structures are fairly distinctive from μ-hydroxo-dimeric structures of Ga(III)OEP and In(III)OEP [34], which have previously been utilized as ionophores. The most prominent difference of the Sc(III)OEP-dimers from the μ-hydroxo-dimers is orientation of the two porphine ring planes (Table 1). That is, ring planes of Sc(III)OEP dimers are essentially parallel with only a small torsion angle (2.09°), while those of In(III)OEP dimers are tilted with a torsion angle of 22.85°.

Table 3.1 Comparison of structural parameters of various metalloporphyrin dimer species.

	$[Sc(III)OEP]_2$ $(\mu\text{-}F)_2$ [33]	$[Sc(III)OEP]_2$ $(\mu\text{-}OH)_2$ [31]	$[Ga(III)OEP]_2$ $(\mu\text{-}OH)^+$ [34]	$[In(III)OEP]_2$ $(\mu\text{-}OH)^+$ [34]
		Distance (Å)		
Metal to N4-plane	0.796	0.84	0.225	0.42
Metal to N	2.188	2.203	2.033	2.136
Metal to O/F	2.046	2.078	1.945	2.119
N4-plane to N4-plane	4.910	5.06	3.43[a]	3.76[a]
		Angle (°)		
Dihedral[b]	0.00		15	23
Torsion[c]	2.09		22.23	22.85
Metal-O/F-Metal	108.96	109.90	151.96	114.45
O/F-Metal-O/F	71.04	70.12		

[a] Closest distance between two carbons in two porphyrin macrocycles [33].
[b] The angle between the two porphyrin mean planes.
[c] Average N-M-M′-N′ torsion angle.

Even with these configurational variations, similar hypsochromic shifts of the Soret band are observed for bis(μ-fluoro) dimer species of Sc(III)OEP as observed for the μ-hydroxo dimers of In(III)OEP and Ga(III)OEP. These blue shifts can be explained conceptually by exciton coupling theory [35]. When two dyes are placed in parallel, an energy level of an excited state splits into two energy levels; the lower level is with two transition dipole moments aligned in a opposite direction, which is optically inactive, and the higher level is the one with the two dipole moments in a same direction and, therefore, optically active. The energy gap between these two levels is varied by the distance and the relative orientation between the two dyes.

Considering the fact that most axial anion ligation reactions with monomeric metalloporphyrins do not cause a significant shift in the Soret band by more than 5 nm, and that the crystal structure obtained in the presence of fluoride is the bis(μ-fluoro) dimer, it is likely that the optical fluoride response of Sc(III)OEP observed in the polymeric films, as shown in Fig. 3.2(b), can be attributed to dimer formation in the organic phase induced by the presence of fluoride in the aqueous solution. The reaction can be expressed by the following equilibrium:

$$LOH + F^-_{(aq)} \rightleftharpoons 1/2\ L_2F_2 + OH^-_{(aq)} \qquad \text{(rxn 3.1)}$$
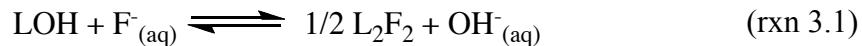
where L denotes the Sc(III)OEP species in the polymer film. Species in the aqueous phase are denoted with the subscript (aq) and species in the film are denoted without any subscript. In principle, the direct dimerization reaction based on the presence of fluoride in the aqueous phase can be utilized to devise a highly selective fluoride sensor. However, such an approach to obtain a practical optical sensor for fluoride has certain limitations. Indeed, the bis(μ-fluoro) dimer is not optically distinguishable from the bis(μ-hydroxide) dimer, and some small amount of the bis(μ-hydroxide) dimer can form in the polymer film, depending on the initial concentration of Sc(III)OEP used to cast the film. In addition, it is not easy to fully assess the sensor selectivity pattern by using polymer films doped with only the Sc(III)OEP species since the monomer absorption bands can shift somewhat in location, depending on which anions are present as counter-

anions within the polymer (based on anion exchange of initial hydroxide ligand with sample phase anions). Therefore, to further evaluate the use of Sc(III)OEP as an ionophore for optical fluoride sensing, a lipophilic pH chromoionophore, ETH 7075 (see Fig. 1b) , was also added to the polymeric film (at 100 mol% of Sc(III)OEP level) to prevent any initial formation of the bis(μ-hydroxide) dimer and to determine selectivity patterns by monitoring intensity of the absorbance band corresponding to the protonated form of the ETH 7075 species (i.e., based on co-extraction of protons along with fluoride ion).

3.3.2 Optical fluoride sensor

All experiments to evaluate the more practical fluoride sensing films (with Sc(III)OEP and ETH 7075 together in the polymeric film) were carried out in a flowing system (~ 1 mL/min) using either a spectrophotometer for selectivity determinations, or a waveguide configuration for reversibility and response time studies. Each anion response was obtained in a 0.05 M Gly-phosphate (pH 3.0) buffer, and the optical signal was measured as the degree of protonation (1-α) of ETH 7075 in the polymer film (see Experimental Section). It should be noted that, while only the absorbance changes of the ETH 7075 dye are used for sensing purposes, the Soret band of the Sc(III)OEP species also shifts to a lower wavelength (393 nm) when fluoride is extracted into the films, indicating that the dimeric porphyrin species still forms in the presence of the added ETH 7075 species (see below, Fig. 3.6(a)).

3.3.2.1 Selectivity

As shown in Fig. 3.4, the Sc(III)OEP/ETH7075-based films yield favorable optical response toward both fluoride and salicylate when (1-α) is plotted as a function of anion concentration equilibrated with the films (in the flowing solutions). Responses to all other anions are far less, even for highly lipophilic anions such as ClO_4^-, SCN^-, and NO_3^-. This selectivity pattern (i.e., Sal^-, $F^- \gg ClO_4^-$, SCN^-, $NO_3^- > Br^-$, Cl^-) deviates significantly from the classical Hofmeister selectivity series [36]. The hardness of fluoride as a base

suggests that hard acids have higher affinity for fluoride than soft acids. Previous success in using Al(III) porphyrin and salen complexes [19, 20, 22, 23] as well as zirconium(IV) complexes [12-14, 17] as ionophores to devise fluoride selective sensors (electrochemical and optical) is consistent with this "hard-soft acid-base" concept. Sc(III) porphyrins should, therefore, be good candidates for devising fluoride sensors and the selectivity pattern illustrated in Fig. 3.4, clearly supports this prospect.
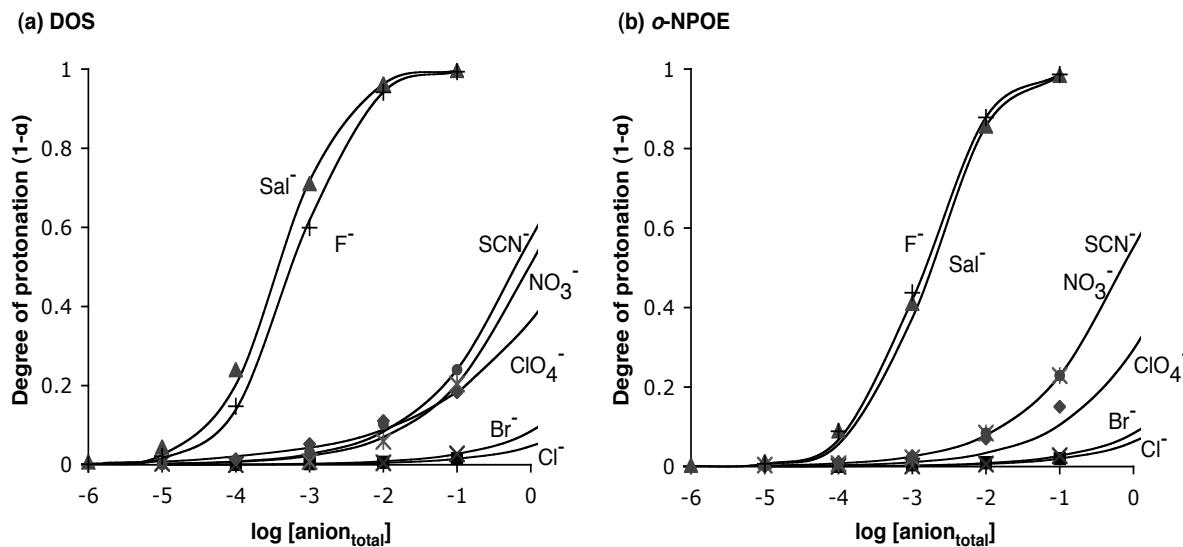
Figure 3.4 Optical responses of polymer films to various anions in pH 3.0 buffer. The compositions of optical sensing films are Sc(III)OEP (1 wt%)/ETH 7075 (100 mol%)/ plasticizer (DOS (a) or _o_-NPOE (b)) (66 wt%)/PVC (33 wt%). Degree of protonation is determined by absorbance change at 550 nm.

It is known that the ligation properties of metal-ligand complexes are dependent on the surrounding solvation environment of the interacting species within the organic polymeric phase. Hence, the nature of the plasticizer (e.g., dielectric constant) can also play a significant role in altering the strength of interaction between the Sc(III)OEP ionophore and fluoride, as well as other anions. Therefore, the response and selectivity of the optical fluoride sensor was examined using two different plasticizers, _o_-NPOE (ε = 21) and DOS (ε = 2.4) [37]. As shown in Fig. 3.4a, the films prepared with DOS exhibits slightly better selectivity over most lipophilic anions (ClO_4^-, SCN^-, NO_3^-) than films prepared with _o_-NPOE, while selectivity for salicylate shifts only slightly (less selective)

(see also Table 3.2). At the same time, the detection limit for fluoride in using DOS as the plasticizer is lower than when o-NPOE is employed. This behavior can be explained based on the dielectric constant of plasticizers tested. In general, the higher dielectric constant of o-NPOE should support greater affinity toward fluoride, and thus better response for fluoride is expected when using this plasticizer. However, fluoride is not the only species that is solvated by the membrane solvent. Sc(III)OEP and ETH 7075 are also dissolved in the "organic liquid" film. Given the highly symmetric structure of the bis(μ-fluoro) dimer species, it is expected that this dimer would have lower polarity than Sc(III)OEP monomers. Thus, it is likely that the bis(μ-fluoro) dimer is more stable in the low dielectric constant medium than the ligated monomer. Hence, lower detection limits and improved selectivity over most lipophilic anions (ClO_4^-, SCN^-, NO_3^-) using the DOS plasticized film may be attributed to the lower polarity of the bis(μ-fluoro) dimer.

Table 3.2 Optical selectivity coefficients and detection limits for fluoride as determined from data shown in Fig. 3.4.

Selectivity ($\log k_{opt}F,Y$)			
DOS		o-NPOE	
Sal$^-$	0.2	F$^-$	0
F$^-$	0	Sal$^-$	-0.1
SCN$^-$	-3.0	SCN$^-$	-2.7
NO$_3^-$	-3.2	ClO$_4^-$	-3.1
ClO$_4^-$	-3.8	NO$_3^-$	-3.5
Br$^-$	-5.0	Br$^-$	-4.7
Cl$^-$	-5.5	Cl$^-$	-4.9
Detection range for F$^-$			
$3.4 \times 10^{-5} \sim 1.1 \times 10^{-2}$ M		$7.7 \times 10^{-5} \sim 2.5 \times 10^{-2}$ M	

The anion selectivity of the Sc(III)OEP/ETH 7075 doped films can be estimated more quantitatively by comparing the concentrations of anions required to achieve $\alpha =$ 0.5. The complete response functions of the anions for which relatively small optical responses are observed can be projected by extrapolating curves if the exact response function is known. The response function varies depending on the specific equilibrium

that takes place for each anion with the Sc(III)OEP species and chromoionophore in the polymer phase. For the fluoride response, the following equilibrium is expected:

$$L^+ + C^- + H^+_{(aq)} + F^-_{(aq)} \xrightleftharpoons{K_F} 1/2\ L_2F_2 + CH \qquad \text{(rxn. 3.2)}$$
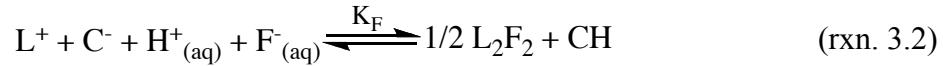
When total concentration of the porphyrin and the chromoionophore is identical, the corresponding response function is given by:

$$[Y^-]_{(aq)} = \left(\frac{1}{\sqrt{2L_T}\,K_F[H^+]_{(aq)}} \right) \frac{(1-\alpha)^{3/2}}{\alpha^2} \qquad \text{(eqn. 3.1)}$$

where α is degree of deprotonation, K_F is equilibrium constant, and L_T is total concentration of ionophore.

However, as can be seen in the Fig. 3.5, the experimental data fits best with the function:

$$[F^-]_{(aq)} \propto \frac{(1-\alpha)}{\alpha} \qquad \text{(eqn. 3.2)}$$

One of the possible equilibria that yields eqn. 3.2 is:

$$LC + H^+_{(aq)} + F^-_{(aq)} \xrightleftharpoons{K_F} 1/2\ L_2F_2CH + 1/2\ CH \qquad \text{(rxn. 3.3)}$$
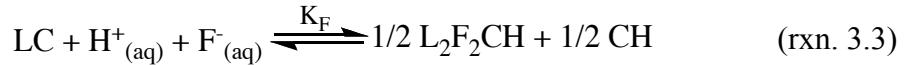
This equilibrium suggests not only an interaction between the Sc(III)OEP (L^+) and the chromoionophore (C^-) (e.g., strong $\pi-\pi$ type interaction, as suggested for ETH 7075 and Al(III)OEP [19]), but also a certain degree of affinity between the dimeric porphyrin and the protonated ETH 7075 in the film. Further effort to identify such complexes formed in the plasticized film is ongoing. Therefore, rxn. 3.3 should remain as a hypothetical equilibrium at this point.

The response curve for salicylate follows eqn. 3.2, which suggests the following equilibrium:

$$LC + H^+_{(aq)} + Sal^-_{(aq)} \xrightleftharpoons{} LSal\ CH \qquad \text{(rxn. 3.4)}$$

However, for most inorganic interferent anions tested (see Fig. 3.4), the response function fits well with the form:

$$[Y^-]_{(aq)} \propto \frac{(1-\alpha)^2}{\alpha} \qquad \text{(eqn. 3.3)}$$

and eqn. 3.3 suggests the following equilibrium reaction:

$$LC + H^+_{(aq)} + Y^-_{(aq)} \rightleftharpoons LY + CH \qquad \text{(rxn. 3.5)}$$

To quantify the selectivity coefficient from different response functions, the concentration of anions that yield $\alpha = 0.5$ are compared. Table 3.2 summarizes the optical selectivity coefficients for anions relative to fluoride based on the absorbance change of ETH 7075 at 550 nm. As can be seen in Table 3.2, the Sc(III)OEP/ETH 7075-doped film exhibits the best response toward fluoride and salicylate (nearly equal), but extremely high selectivity over all other anions tested. It also reports the detection limits for each type of film, as defined by the limiting sensitivity (a slope 1/5 of the maximum) of the response function. As suggested above, slightly improved detection limits are obtained using DOS, the lower polarity plasticizer.
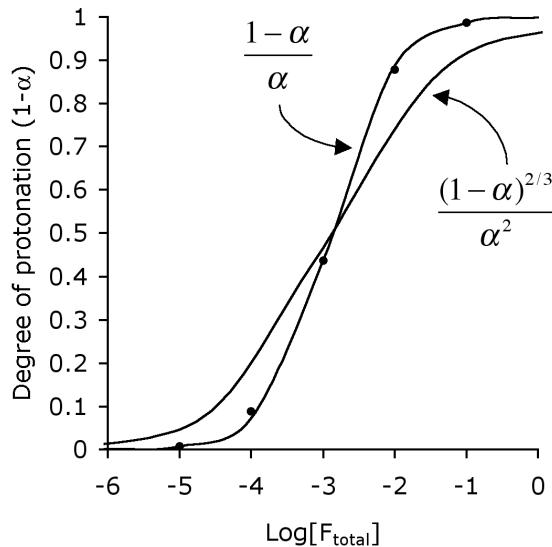
Figure 3.5 Response curve for fluoride of the film (Sc(III)OEP-OH/ETH 7075/o-NPOE/ PVC) and theoretical curves based on the response mechanisms (rxn. 3.2 and rxn. 3.3).

It should be pointed out that if the absorbance of the dimer band at 393 nm is also monitored, only fluoride binding yields an observable optical change. As can be seen in Fig. 3.6, fluoride response increases absorbance at 393 nm which corresponds to a

dimeric Sc(III)OEP complex, whereas salicylate increases 408 nm which corresponds to a monomeric Sc(III)OEP complex. Considering that most anions except for fluoride and hydroxide form monomeric complexes and that deprotonated ETH 7075 prevents hydroxo-dimer formation, the absorbance change at 393 nm is evidence of fluoride in the sample phase. Therefore, by monitoring fluoride-specific response (393 nm) and non-specific anionic response (550 nm) simultaneously, selectivity for fluoride could potentially be further improved.
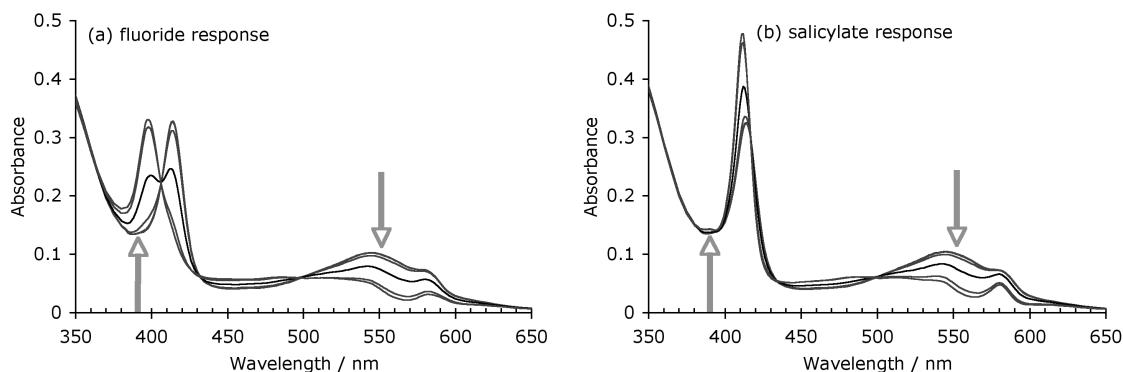
Figure 3.6 UV-Vis spectra of the film composed of Sc(III)OEP/ETH 7075/o-NPOE/PVC contacting various increasing concentrations of fluoride (a) and salicylate (b).

3.3.2.2 Reversibility, response time, and lifetime

Rapid and fully reversible optical response toward fluoride of both the DOS and NPOE plasticized Sc(III)OEP/ETH 7075-doped PVC films are clearly shown in Fig. 3.7 (monitoring at λ = 550 nm, the λ_{max} of the deprotonated ETH 7075 species). This figure illustrates response between two fluoride levels; $[F_{total}]_{(aq)}$ = 10^{-2} M ($\alpha \sim 0.2$) and $[F_{total}]_{(aq)}$ = 10^{-4} M ($\alpha \sim 0.8$) in a flow system (flow rate 1 mL/min) using a waveguide based optical sensor configuration. For the o-NPOE plasticized film, the t_{90} response times (time required to reach 90% of full equilibrium) were measured as $\sim$ 6 sec and $\sim$ 4 sec when changing from blank buffer to 10^{-4} M fluoride and 10^{-2} M fluoride, respectively. The t_{90} values of the reverse optical response were measured as $\sim$ 6 sec and $\sim$ 9 sec in going from 10^{-4} M and 10^{-2} M to the blank buffer, respectively. Response times for the DOS

63

plasticized fluoride sensing films are 20 ~ 40 % longer than the corresponding o-NPOE plasticized films, owing to the higher viscosity of DOS [38]. Compared to previously reported Al(III)OEP/ETH 7075-doped films [19, 20], the Sc(III)OEP/ETH 7075 system exhibits a higher detection limit but faster response times. This suggests that Sc(III)OEP-F binding is not as strong as Al(III)OEP-F, and that reversible ligation of fluoride to Sc(III)OEP is kinetically more facile, making them more suitable as detection systems for flow-injection type measurements.
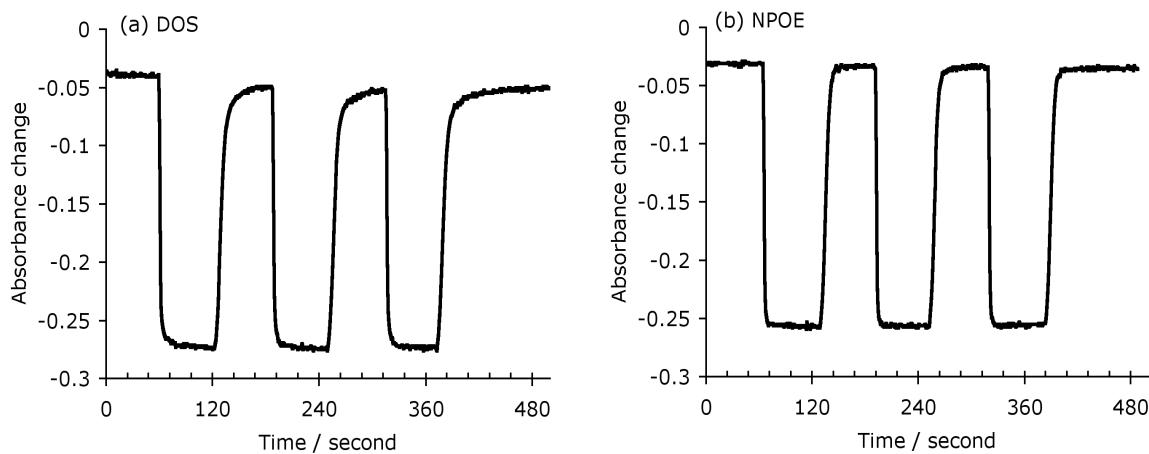
Figure 3.7 Optical responses of films composed of Sc(III)OEP/ETH 7075/DOS (a) or o-NPOE (b)/PVC at 550 nm between two concentrations of fluoride (0.01 M, 0.0001 M).

The lifetime of the Sc(III)OEP/ETH 7075-doped films is limited by leaching of active compounds and photo-bleaching of optically active species. Over a few hours of continuous flow-through measurements, loss of Sc(III)OEP from the film is observed. Based on the absorbance changes of Sc(III)OEP and ETH 7075, loss of Sc(III)OEP is about 13%/h and loss of ETH 7075 is about 4%/h. However, such loss is anticipated using the waveguide configuration, where extremely thin polymeric films are employed (< ca. 0.5 μm) to achieve fast response times with a flow-through arrangement [32]. If thicker films were employed, at the expense of response time, greater stability would be achieved. The optical drift that occurs due to continuous loss of active species from the sensing film can be corrected for by frequent monitoring of background absorbances at the detection wavelengths during FIA experiments.

64

Another important effect that limits the operational lifetime of the sensors based on ScOEP/ETH 7075-doped films is photo-bleaching of the Sc(III)OEP species. When the film is exposed to the ambient light, Sc(III)OEP slowly decomposes and loses its optical properties. Such photo-degradation occurs over a 2-3 day period, and results in loss of the Soret band and Q-bands, which are characteristic absorption bands of metalloporphyrins. This can be prevented by storing films in the dark before use. Given the extremely low cost of the polymeric sensing films, changing flow through detectors after a given period of use can overcome this photobleaching issue, as well as loss of active components by continuous use in the flow-injection analysis mode.

3.3.2.3 Preliminary applications

Commercial samples of mouth wash were tested with the FIA configuration. Each of the samples was diluted 10 times with total ionic strength adjustor buffer (0.5 M Glycine-phosphate buffer, pH 3.1 with 1 M NaCl and 2.9 mM CDMA) before measurement. Potentiometric measurements using LaF_3 electrode were done with same samples as well. For example, one sample with fluoride (PhosFlur, Colgate, $[F_{total}]$ = 0.01112 M (n = 3, standard deviation (s) = 0.00004, measured by LaF_3 electrode) yielded both absorbance changes at 393 nm and 550 nm and $[F_{total}]$ was measured to be 0.0114 M (n =6, s = 0.0002) based on the absorbance change at 550 nm. Another sample without fluoride (biotene, Laclede,Inc) showed absorbance change only in 550 nm, indicating fluoride level is less than the lower detection limit. However, in the other sample (ACT, Johnson & Johnson, [Ftotal] = 0.013 M by LaF_3 electrode), absorbance change at dimer band is too high compared to the change of ETH 7075 band. It has been confirmed that lipophilic cationic species such as cetylpyridinium chloride (anti-septic reagent) were responsible for this observation; not only protons but also lipophilic cations facilitated fluoride coextraction into the film and the coextraction of fluoride with lipophilic cations must have increased the level of bis(μ-fluoro) dimeric band. Currently, further studies are underway to resolve this lipophilic cation interference effect.

3.3.3 Fluoride-selective electrode

The promising results for optical sensors based on Sc(III)OEP for fluoride detection have led to the study of ion-selective electrodes based on Sc(III) porphyrins. Both Sc(III)OEP and Sc(III)TPP were examined as ionophores in plasticized PVC membranes. A membrane doped with Sc(III)OEP exhibits a stable and a reproducible response to anions, while a membrane with Sc(III)TPP exhibits unstable responses during an experiment. Instability of the Sc(III)TPP-doped membrane can be ascribed to the fast photobleaching of Sc(III)TPP under ambient conditions. Therefore, a fluoride-selective electrode based on Sc(III)OEP in a plasticized PVC film is characterized here in terms of selectivity, reversibility, lifetime, and response mechanism. Binding constants of Sc(III)OEP with various anions in the plasticized film are also discussed.

3.3.3.1 Selectivity

Fig. 3.8 illustrates the selectivity change as ionic sites are varied in the plasticized film doped with Sc(III)OEP. Increasing anionic sites improves the potentiometric selectivity coefficient for fluoride and it suggests a charged carrier mechanism where the following equilibrium determines the free ion concentration of F^- in the membrane:

$$L^+ + F^- \rightleftharpoons LF \qquad\qquad \text{(rxn. 3.6)}$$
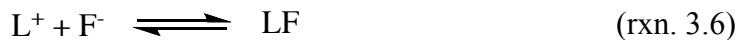
At the optimized condition (i.e., 40 mol% of KTFPB), the calibration curves for anions tested are shown in Fig. 3.9. The selectivity sequence is $F^- \sim Sal^- \gg SCN^- > Cl^-$, Br^-, NO_3^-, ClO_4^-. This pattern is clearly the same as the selectivity pattern observed in the optical sensors based on Sc(III)OEP and ETH 7075 as shown in Fig. 3.4. The response slope is slightly sub-Nerntian (51.9 mV/decade (o-NPOE) and 56.5 mV/decade (DOS)) and the
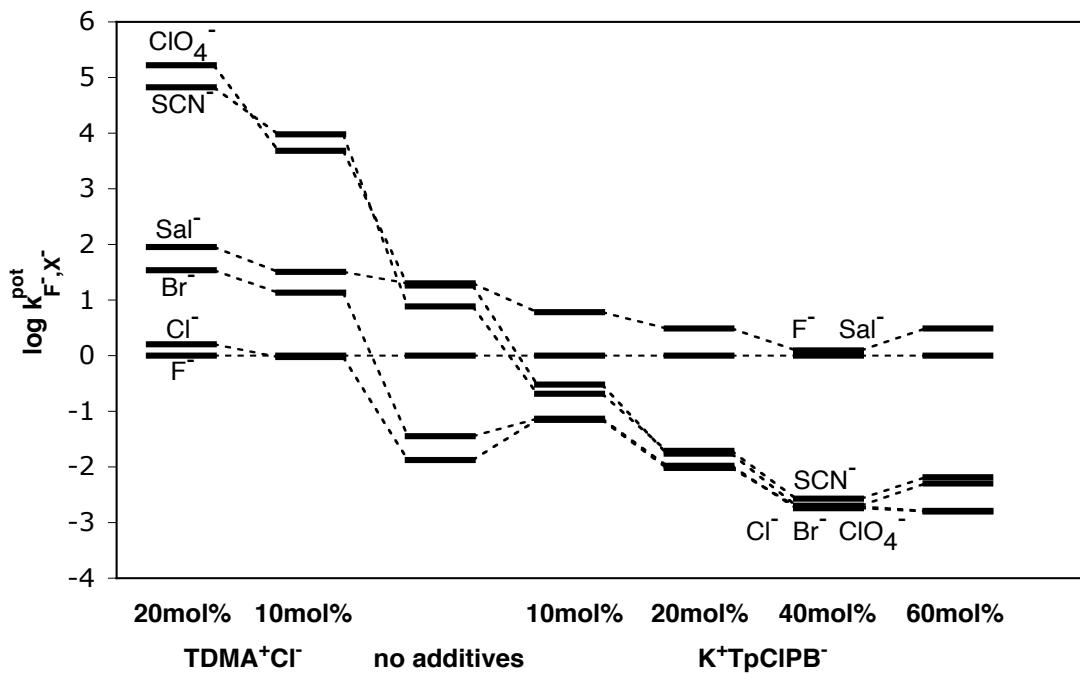
Figure 3.8 Potentiometric selectivity coefficient changes for various anions (relative to fluoride) with varying amount of ionic additives in the polymer membrane (Sc(III)OEP-OH (1 mg)/ TDMACl or KTpClPB/o-NPOE (66 mg)/PVC (33 mg)).
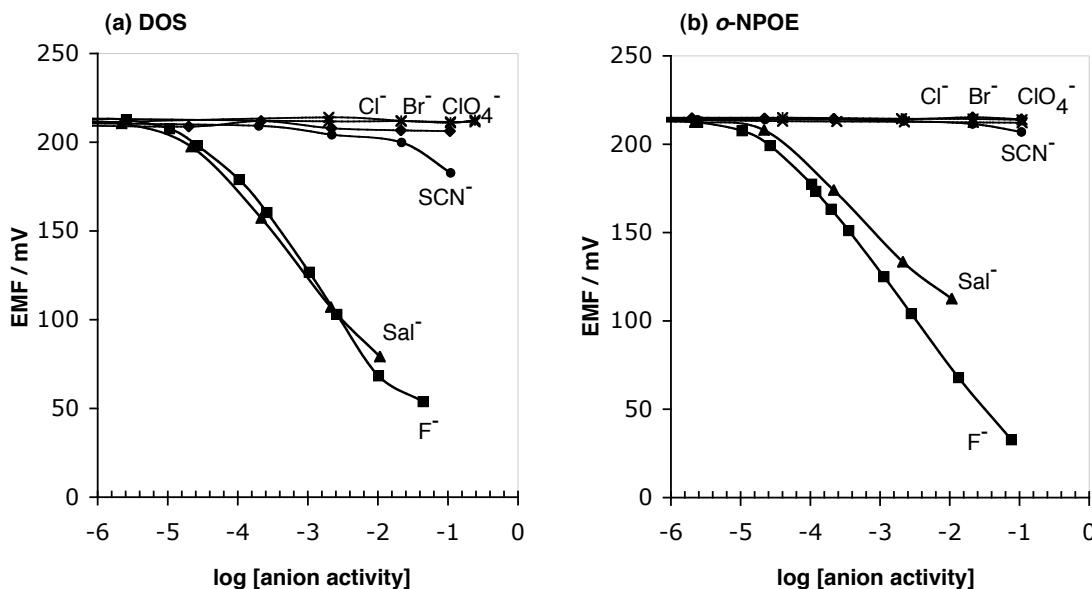
Figure 3.9 Response curves of fluoride-selective electrodes based on Sc(III)OEP containing 40 mol% KTFPB in plasticized (DOS (a) and o-NPOE (b)) PVC membranes.

detection limit for fluoride is about 1.9×10^{-5} M (*o*-NPOE) and 2.6×10^{-5} M (DOS). Activities of anions at pH 3.0 are correlated with EMF responses in Fig. 3.9 and are depicted with respect to the logarithmic scale of anionic activities at pH 3.0, which are calculated based on the two-parameter Debye-Hückel approximation [39].

Dimer-monomer equilibria are known to initiate so-called super-Nernstian response in the fluoride sensors based on Ga(III) porphyrins, Zr(IV) porphyrins, and the chloride sensor based on In(III) porphyrins [11, 12, 40]. At a first glance, it seems to be inconsistent that Sc(III)OEP does not exhibit super-Nernstian response even though it forms a dimer in the given membrane composition. It should be noted that the super-Nernstian responses observed with films is the consequence of increasing concentration of the charged carrier (L^+) in rxn. 3.7 when the dimer is broken into monomers [40]:

$$L_2OH^+ + \ X^-_{(aq)} \ \rightleftharpoons \ LX + L^+ + OH^-_{(aq)} \qquad \text{(rxn. 3.7)}$$
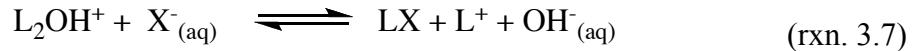
Fig. 3.10 shows the Soret band shift upon fluoride responses of the film containing Sc(III)OEP and 40 mol% of KTFPB. Blue shift of the Soret band suggests dimer formation by fluoride. Therefore, fluoride forms the dimeric structure rather than breaking the dimer:

$$LOH + \ F^-_{(aq)} \ \rightleftharpoons \ 1/2 \ L_2(\mu\text{-F})_2 + OH^-_{(aq)} \qquad \text{(rxn. 3.8)}$$
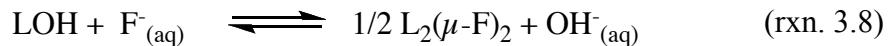
Since dimer itself is a neutral species in rxn. 3.8, this equilibrium does not alter the concentration of the charged carrier, $[L^+]$, in the film, which is fixed by the concentration of anionic sites. In conclusion, when neutral dimers are involved in the response mechanism, dimer-monomer equilibria do not change the concentration of charged species, and thus super-Nernstian response will not be observed.
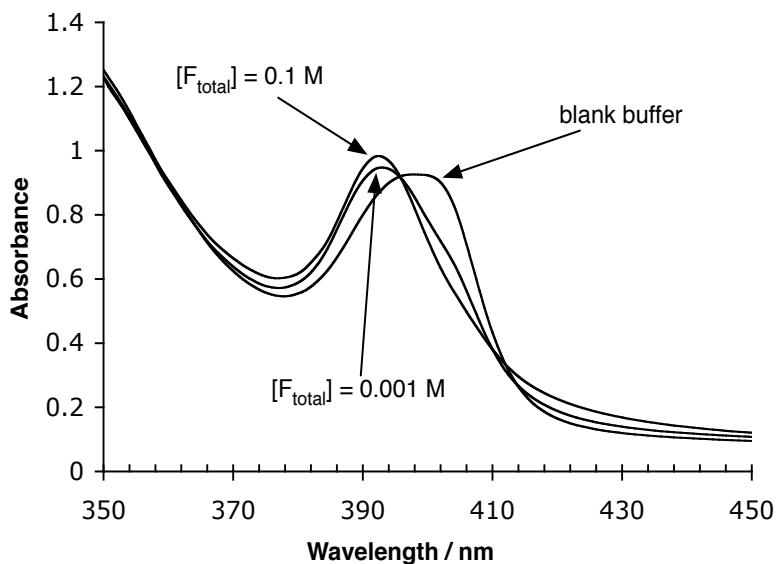
Figure 3.10 UV-Vis spectra of the film (Sc(III)OEP/KTpClPB (40 mol%)/o-NPOE/PVC) upon fluoride responses. In the presence of fluoride, a bis-μ-fluoro-dimer (390 nm) is observed.

3.3.3.2 Reversibility and Lifetime

Reversibility tests (Fig. 3.11) clearly indicates fast and reproducible EMF response toward fluoride based on electrodes made with the film ScOEP/KTFPB (40 mol%)/plasticizer (either o-NPOE or DOS)/PVC. The response to higher F$^-$ concentrations or lower concentrations requires about 10 sec to stabilize. The observed fast recovery time further supports the argument discussed previously that formation of the bis(μ-fluoride)dimer does not affect the response time whereas positively charged dimer exhibits much slower recovery time upon the response to analyte anion [40]. The experiment for assessing the lifetime (Fig. 3.12) of the film (Sc(III)OEP-OH/KTFPB (40 mol%)/o-NPOE/PVC) indicates that loss of Sc(III)OEP would be the main cause of response deterioration when the film is stored in the 0.05 M gly-phosphate buffer (pH 3.0). The electrodes are kept in the dark except for the moment when the fluoride responses are measured under ambient conditions. Decreasing membrane dielectric constant (employing plasticizer with lower dielectric constant) seems to minimize the deterioration of responses over time (Fig. 3.12(a)).
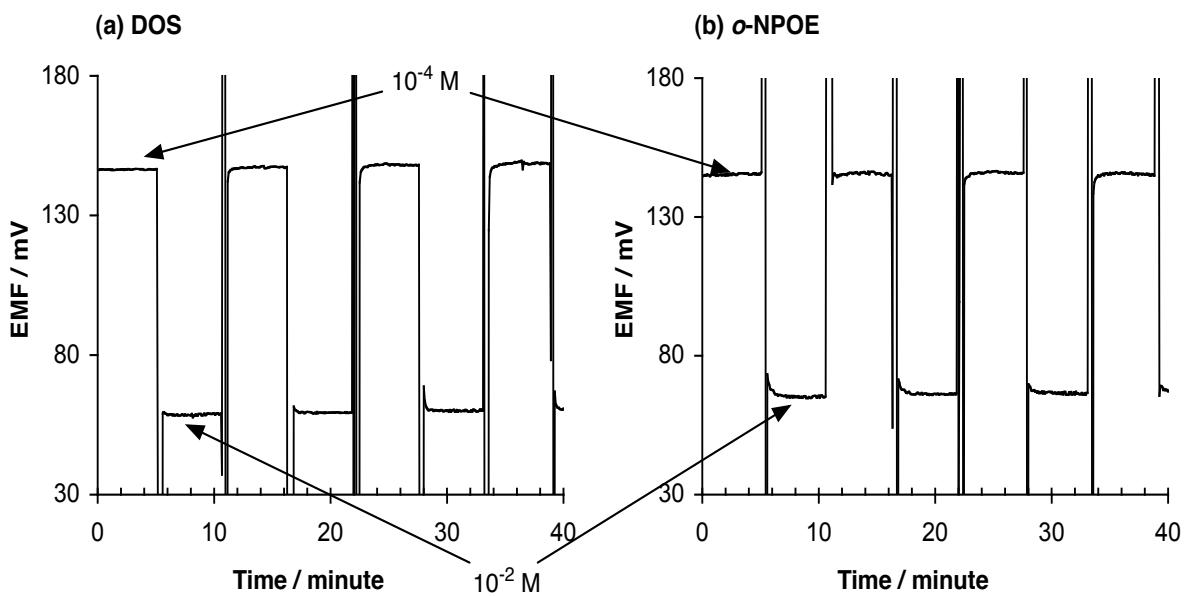
Figure 3.11 EMF responses of fluoride-selective electrodes using a film composed of Sc(III)OEP/KTpClPB (40 mol%)/DOS (a) or *o*-NPOE (b)/PVC between 0.01M and 0.0001 M fluoride solutions.
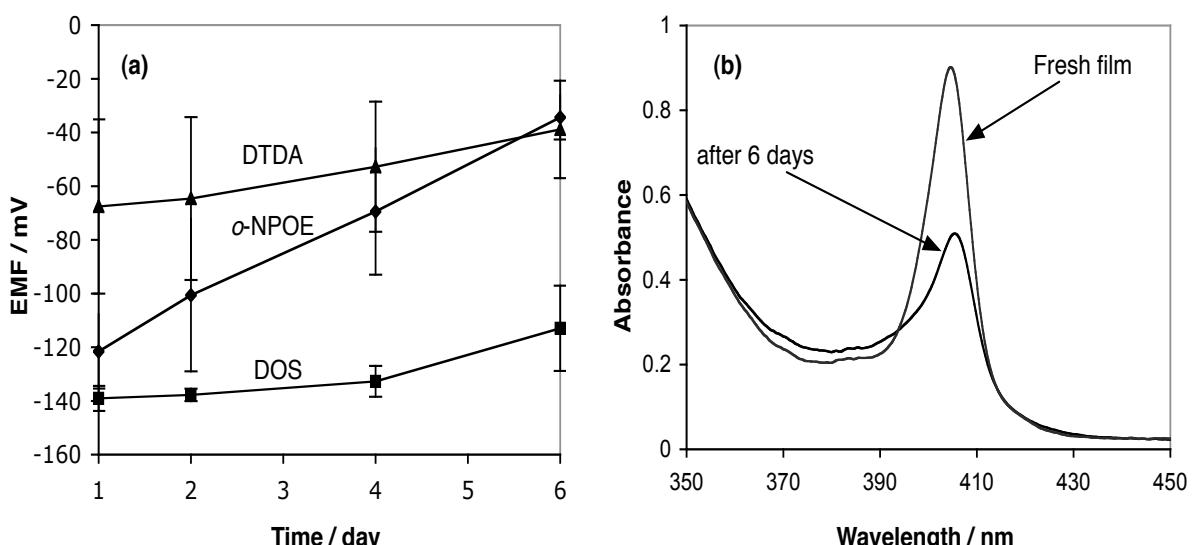
Figure 3.12 (a) Change in EMF response to 0.01 M fluoride over time with films (Sc(III)OEP/KTFPB (40 mol%)/plasticizer (DTDA or o-NPOE or DOS)/PVC). (b) UV-Vis spectra of the PVC film plasticized with o-NPOE before and after lifetime experiment.

3.3.3.3 Binding Constants

The sandwich membrane method [41, 42] was employed to measure the binding constants of the anions with Sc(III)OEP in the plasticized PVC film contacting the aqueous phase (Table 3.3). Since the selectivity of the membrane doped with Sc(III)OEP is given by:

$$k_{F^-,anion} = \frac{p_{anion}}{p_{F^-}} \times \frac{K_{anion}}{K_{F^-}} = \left(\begin{array}{c} \text{selectivity} \\ \text{by membrane} \end{array} \right) \times \left(\begin{array}{c} \text{selectivity} \\ \text{by ionophore} \end{array} \right) \qquad \text{(eqn. 3.4)}$$

the observed selectivity of the membrane can be described in terms of the membrane selectivity (i.e., Hofmeister selectivity series) and the ionophore selectivity (i.e., the relative binding constant). In Fig. 3.13, the first column on the left is selectivity coefficients of a film doped only with TDMACl, which reflects the Hofmeister selectivity series. The second column illustrates the ratio of binding constants of anions to the binding constant of fluoride determined by the sandwich membrane method. By combining the first and second column, the third column is generated as an estimated selectivity coefficient. The last column on the right illustrates the experimentally observed potentiometric selectivity coefficients. The estimated selectivity pattern and the observed selectivity pattern matches well except for the salicylate.

The strong response to salicylate in Fig. 3.9 indicates some degree of interaction between Sc(III)OEP and salicylate. Considering the lipophilicity of salicylate, the extraction of salicylate into the membrane is much more favorable than the extraction of fluoride. However, the negligible response for another lipophilic anion, perchlorate, suggests lipophilicity is not the only reason for the strong response to salicylate. The carboxylic acid in the salicylate can bind with the central metal ion in the porphyrin and a possible π-π interaction between a benzene group in salicylate and the porphyrin ring can contribute simultaneously to this binding [43]. Therefore, the formation of a complex between Sc(III)OEP and salicylate is very plausible. Even though the measured binding constant from the sandwich method in pH 3.0 buffer did not indicate this strong Sc(III)OEP-salicylate interaction, experimental difficulties of measuring partially proto-

nated species at pH 3.0 can explain the underestimated binding constant. For example, the diffusion of salicylic acid (protonated form) through the membrane may have interfered and altered the potential at the interface of the internal solution and the membrane, leading to underestimation of the binding constant for salicylate and Sc(III)OEP as measured by the sandwich membrane approach.

Table 3.3 Binding constants of Sc(III)OEP with various anions at pH 3.0 as determined by measuring voltage across sandwich of membranes (Sc(III)OEP-OH (1.0 mg)/KTpClPB (40 mol%)/*o*-NPOE (66 mg)/PVC (33 mg) and TDMACl (0.4 mg)/*o*-NPOE (66 mg)/PVC (33mg)).

anion	$\log(\beta)$
F^-	12.8
Cl^-	9.26
NO_3^-	7.31
SCN^-	5.76
Salicylate	5.71
ClO_4^-	4.6
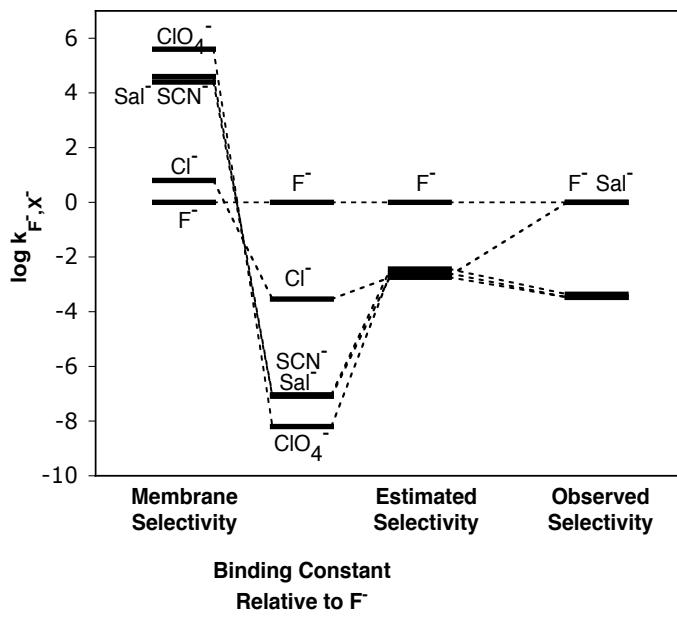
Figure 3.13 Comparison between estimated and experimentally observed potentiometric selectivity coefficients. Estimated coefficients are calculated based on the membrane selectivities and binding constants.

3.4   Conclusions

New fluoride-selective optical and electrochemical sensors based on using a Sc(III)OEP ionophore have been described. Fundamental studies of the dimer-monomer chemistry of the Sc(III)OEP species within the plasticized films suggest that this species forms a difluoro-bridged dimer when the film is bathed in sample solutions containing fluoride ion. Addition of a chromoionophore (ETH 7075) to the films helps stabilize the response, and provides an alternate wavelength to monitor optical fluoride response. Based on this dimer-monomer equilibrium, optical and electrochemical fluoride sensors have been evaluated in terms of selectivity, reversibility, response time, and lifetime. The lower detection limits of the optimized sensors for fluoride are about $10^{-4.5}$ M for both optical and electrochemical sensors. The selectivity for fluoride over ClO_4^-, SCN^-, NO_3^- Br^-, Cl^- is quite high. Only salicylate is a major interference. Fully reversible and fast response of the sensing film enables the optical configuration to be employed as an optical fluoride selective detector in an FIA system. The binding constants with Sc(III)OEP and various anions have been measured by the sandwich membrane method, and results indicate a high binding constant for fluoride ($\beta_{Sc(III)OEP-F} = 10^{12.8}$). These studies suggest that films doped with Sc(III)OEP may provide an alternative to previously reported Al(III)-porphyrins and salens for the preparation of efficient fluoride selective optical and potentiometric sensors.

3.5   Acknowledgement

3.6   References

[1] Ripa, L.W., Journal Of Public Health Dentistry 53 (1993) 17.

[2] Mcdonagh, M.S.; P.F. Whiting; P.M. Wilson; A.J. Sutton; I. Chestnutt; J. Cooper; K. Misso; M. Bradley; E. Treasure; J. Kleijnen, British Medical Journal 321 (2000) 855.

[3] Harrison, P.T.C., J. Fluorine Chem. 126 (2005) 1448.

[4] Ayoob, S.; A.K. Gupta, Critical Reviews In Environmental Science And Technology 36 (2006) 433.

[5] Cowell, D.C.; A.A. Dowman; J.D. Newman; R. Pirzad; C. Rantle, Biosensors & Bioelectronics 7 (1992) 27.

[6] Simonian, A.L.; J.K. Grimsley; A.W. Flounders; J.S. Schoeniger; T.C. Cheng; J.J. Defrank; J.R. Wild, Anal. Chim. Acta 442 (2001) 15.

[7] Viveros, L.; S. Paliwal; D. Mccrae; J. Wild; A. Simonian, Sensors And Actuators B-Chemical 115 (2006) 150.

[8] Frant, M.S.; J.W. Ross, Science 154 (1966) 1553.

[9] Bakker, E.; P. Buhlmann; E. Pretsch, Chemical Reviews 97 (1997) 3083.

[10] Buhlmann, P.; E. Pretsch; E. Bakker, Chemical Reviews 98 (1998) 1593.

[11] Steinle, E.D.; U. Schaller; M.E. Meyerhoff, Anal. Sci. 14 (1998) 79.

[12] Malinowska, E.; L. Gorski; M.E. Meyerhoff, Anal. Chim. Acta 468 (2002) 133.

[13] Gorski, L.; M.E. Meyerhoff; E. Malinowska, Talanta 63 (2004) 101.

[14] Gorski, L.; E. Malinowska, Anal. Chim. Acta 540 (2005) 159.

[15] Witowska-Jarosz, J.; L. Gorski; E. Malinowska; M. Jarosz, Journal Of Mass Spectrometry 37 (2002) 1236.

[16] Witowska-Jarosz, J.; L. Gorski; E. Malinowska; M. Jarosz, Journal Of Mass Spectrometry 38 (2003) 1265.

[17] Gorski, L.; A. Saniewska; P. Parzuchowski; M.E. Meyerhoff; E. Malinowska, Anal. Chim. Acta 551 (2005) 37.

[18] Mitchell-Koch, J.T.; E. Malinowska; M.E. Meyerhoff, Electroanalysis 17 (2005) 1347.

[19] Badr, I.H.A.; M.E. Meyerhoff, Anal. Chem. 77 (2005) 6719.

[20] Badr, I.H.A.; M.E. Meyerhoff, J. Am. Chem. Soc. 127 (2005) 5318.

[21] Seiler, K.; W. Simon, Anal. Chim. Acta 266 (1992) 73.

[22] Mitchell-Koch, J.T.; M. Pietrzak; E. Malinowska; M.E. Meyerhoff, Electroanalysis 18 (2006) 551.

[23] Badr, I.H.A.; M.E. Meyerhoff, Anal. Chim. Acta 553 (2005) 169.

[24] Badr, I.H.A., Anal. Chim. Acta 570 (2006) 176.

[25] Zhang, W.; E. Rozniecka; E. Malinowska; P. Parzuchowski; M.E. Meyerhoff, Anal. Chem. 74 (2002) 4548.

[26] Qin, Y.; E. Bakker, Anal. Chem. 76 (2004) 4379.

[27] Pearson, R.G., J. Am. Chem. Soc. 85 (1963) 3533.

[28] Cotton, F.A., G. Wilkinson, Advanced Inorganic Chemistry, Advanced Inorganic Chemistry, third ed., Interscience, New York, 1972, 1070.

[29] Dahlke, P.; D. Babel, Zeitschrift Fur Anorganische Und Allgemeine Chemie 620 (1994) 1686.

[30] Gouterman, M.; D. Holten; E. Lieberman, Chem. Phys. 25 (1977) 139.

[31] Arnold, J.; C.G. Hoffman; D.Y. Dawson; F.J. Hollander, Organometallics 12 (1993) 3645.

[32] Kang, Y.; M.E. Meyerhoff, Anal. Chim. Acta 565 (2006) 1.

[33] Crystallographic data for $[Sc(III)OEP]_2 (\mu\text{-}F)_2$: $C_{72}H_{88}F_2N_8Sc_2$, M = 1193.42 gmol^{-1}, orange plate, size 0.36 x 0.34 x 0.04 mm^3, triclinic, space group P-1, a = 10.940(4) Å, b = 13.072(5) Å, c = 13.303(5) Å, α = 117.987(5)°, β = 99.495(6)°, γ= 103.240(6)°, V = 1551.0(10) Å^3, Z = 1, T = 123(2) K, ϱ_{calcd} = 1.278 Mg/m^3, μ = 0.275 mm^{-1}, 23 732 reflections, 1.80° ≤ θ ≤ 24.82°, 5309 independent reflections, R_{int} = 0.0780, 3834 reflections with I ≥ 2σ(I), 397 parameters, R1 = 0.1050, wR2 = 0.2500 (all data), GOF = 1.097, Crystallographic data can be obtained free of charge as CCDC 645795 from the Cambridge Crystallographic Data Centre via www.ccdc.cam.ac.uk/data_request/cif or 12 Union Road, Cambridge CB2 1EZ, U.K.

[34] Ab, P.G.P.; J.W. Kampf; E. Rozniecka; Y. Kondratenko; E. Malinowska; M.E. Meyerhoff, Inorg. Chim. Acta 355 (2003) 302.

[35] Kasha, M., Radiat. Res. 20 (1963) 55.

[36] Hofmeister, F., Arch. Exp. Pathol. Pharmakol. 24 (1888) 247.

[37] Eugster, R.; T. Rosatzin; B. Rusterholz; B. Aebersold; U. Pedrazza; D. Ruegg; A. Schmid; U.E. Spichiger; W. Simon, Anal. Chim. Acta 289 (1994) 1.

[38] Oesch, U.; W. Simon, Anal. Chem. 52 (1980) 692.

[39] Meier, P., Anal. Chim. Acta 136 (1982) 363.

[40] Steinle, E.D.; S. Amemiya; P. Buhlmann; M.E. Meyerhoff, Anal. Chem. 72 (2000) 5766.

[41] Mi, Y.; E. Bakker, ELECTROCHEMICAL AND SOLID STATE LETTERS 3 (2000) 159.

[42] Qin, Y.; E. Bakker, Talanta 58 (2002) 909.

[43] Hawley, J.; N. Bampos; R. Abraham; J. Sanders, CHEMICAL COMMUNICA-TIONS (1998) 661.

Chapter 4

Anion Selective Sensors Based on Indium(III) Texaphyrin

4.1   Introduction

The measurement of anions that are important in the clinical, environmental, and industrial areas has gained great interest among the sensor community, and developing more selective and reliable anion recognition agents is a growing avenue of research [1]. Various classes of host molecules are being developed based on coulombic dipolar interactions, hydrogen bonding or metal-ligand interactions. A number of those metal-ligand interactions have been successfully applied for the detection of various inorganic and organic anions [2-6]. As described in Chapter 1, metalloporphyrins have been studied extensively as ionophores in ion-selective electrodes where the ionophores are dissolved in the hydrophobic solvent polymeric membrane [7, 8]. This approach has been extremely useful in designing selective anion sensors with moderate chemical manipulations of their structures such as choosing an appropriate metal ion within the core or attaching peripheral groups to the porphyrin structures [9, 10].

Since 1988, potentiometric and optical sensors based on metalloporphyrins have been utilized for the detection of fluoride, chloride, thiocyanate, nitrite, salicylate and other organic anions. Metal cations that have been incorporated into porphyrin cores have included Sc(III), Zr(IV), Cr(III), Mn(III), Fe(III), Co(III), Mo(V), Ru(II), Al(III), Ga(III), In(III), Tl(III), Sn(IV), and Lu(III) (see Chapter 1). Metal cations that are not listed would suffer from insufficient selectivity patterns, or irreversible metal-anion interactions that do not allow reproducible electrochemical or optical responses, or fail to form stable complexes with given metal cations. The issues of unstable formation of metal ion

complexes are caused by the weak interaction betwen the metal cation of the four nitrogens in the core of the porphyrin due to either the nature of metal cations or an over-sized ionic radius of the metal cation which fails to afford appropriate spacial distance and configuration relative to the nitrogen atoms in the porphyrin. For example, cations of zirconium, hafnium and lanthanides easily form a sandwich structure where two porphyrinoids are bound to a large metal cation and block any anion access to the central metal cation [11-13]. Therefore, to explore a metal cation that cannot form a stable complex to the porphyrin, one can employ an expanded porphyrin as a possible ligand to bind the metal cation in a stable form within a plasticized polymeric film.

Expanded porphyrins such as sapphyrins (see Fig. 4.1) have been reported to trap an anion in the core through hydrogen bonding [14-16]. Fluoride, phosphate, and carboxylic acids are bound to protonated pyrroles in the core of the highly conjugated planar structure. Those interactions have been utilized for the separation of nucleotides, oligonucleotides, and amino acids by using columns packed with silica gel possessing immobilized sapphyrin derivatives [17]. Potentiometric sensors based on plasticized PVC membranes doped with the expanded porphyrins such as sapphyrin, rubiryn, and triphenylrosarin have been also reported [18, 19]. While these expanded porphyrins have exhibited selective responses for 3,5-dinitrobenzoate over other organic acids, the sapphyrin-doped ion-selective membrane exhibited an improved fluoride response over chloride and bromide. Currently, anion recognition by heterosapphyrins, texaphyrins and other cyclic and linear polypyrroles is also being studied [20-23].

However, a metal ion-anion interaction has not yet been exploited as an anion ionophore using expanded porphyrins. Among those expanded porphyrins, texaphyrins (see Fig. 4.1) are reported to form stable metallocomplexes that are not hydrolyzed in the presence of acid or water [24]. Metallotexaphyrin exhibits very similar optical and structural properties as metalloporphyrins; the highly conjugated planar structure containing five nitrogens in the core exhibits a porphyrin-like absorbance spectrum that is red-shifted from the porphyrin bands including a strong Soret band at 450 nm and Q-bands around 650 nm ~ 750 nm. A texaphyrin has one proton and the charge of the
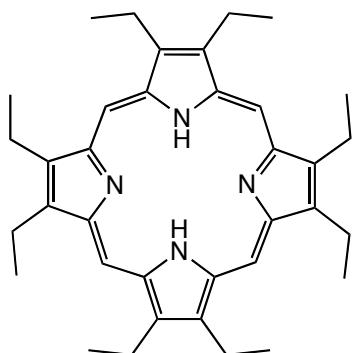
Porphyrin
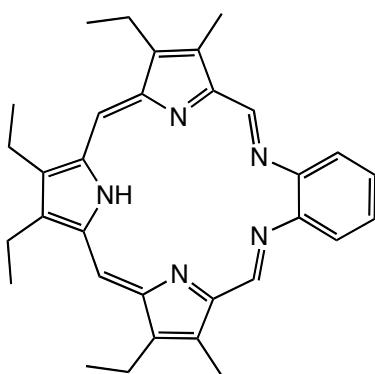
Texaphyrin
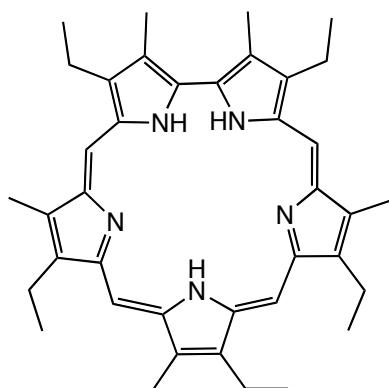
Sapphyrin
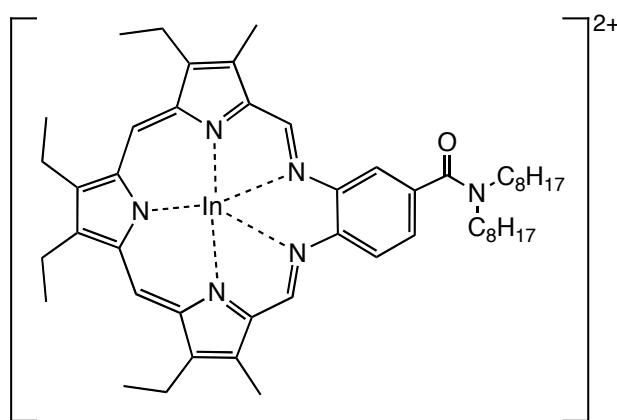
Lipophilized indium(III) texaphyrin

Figure 4.1 Porphyrin and expanded porphyrins employed as anion recognitions. The lipophilized indium(III) texaphyrin which is studied in this chapter is shown as well.

deprotonated form is -1, whereas the porphyrin contains two protons and has a charge of -2. Texaphyrins form stable metal ion complexes with relatively large metal cations such as low oxidation state transition metals (i.e., Mn(II), Fe(II)), In(III), and lanthanides(III)); otherwise the complex will be easily demetallated either by the trace amount of acid or in water [24].

In this chapter, an In(III) texaphyrin will be examined as a potential anion ionophore in plasticized PVC films using both optical and electrochemical transduction modes. An appropriate structural change will be made in order to improve the

lipophilicity of In(III) texaphyrin. Optical monitoring of anionic response provides information about ligand chemistries and any conformational changes of the In(III) texaphyrin. The potentiometric selectivity pattern of membranes formulated with In(III) texaphyrin will be compared to that of In(III) porphyrin to assess how this expended ligand affects the metal ion-anion binding properties in the plasticized PVC film when a porphyrin is switched to a texaphyrin.

4.2   Experimental

4.2.1   Reagents

All reagents and solvents were used as received without further purification except for tetrahydrofuran (THF) which was distilled by refluxing bulk THF with sodium and benzophenone prior to use. The chromoionophore VI (ETH 7075), *o*-nitrophenyloctylether (*o*-NPOE), potassium tetrakis(*p*-chlorophenyl) borate (KTpClPB), and poly(vinyl chloride) (PVC) were from Fluka (Ronkonkoma, NY). Glycine, o-phosphoric acid, and sodium salts of anions tested were purchased from Aldrich.

4.2.2   Preparation of lipophilized In(III) texaphyrin

All the syntheses were performed as described in the literature [25-33]. Most of the vacuum sources were employed from an aspirator that creates vacuum by running tap-water. When high vacuum was required, a vacuum pump (Emerson Model C63CXGZP-4780, St. Louis, MO) was used with a liquid nitrogen trap or a dry ice/acetone trap. For characterization of compounds, UV/Vis spectra, mass spectra, and 1H NMR spectra were obtained using a Perkin-Elmer Lambda-35 spectrophotometer, a Varian 400 MHz spectrometer, and MALDI-TOF mass spectrometer (Micromass Tof-Spec-2E), respectively. For the fast identification of crude reaction mixtures of

polypyrroles, texaphyrins, and metallotexaphyrins, obtaining MALDI mass spectra using dithranol as a matrix was the most efficient way.

Preparation of Mn(II) texaphyrin. Mn(II) Texaphyrin (**12**, for the numbers of compounds, see scheme 4.1, 3.2, and 3.3 in the section 4.3.1) was prepared as a test synthesis because Mn(II) texaphyrin is well characterized in terms of synthesis, stability in solution, and its optical and electrochemical properties [32, 34]. Most of reactions were straightforward. However, decarboxylation of terpyrrole diacid (**5**) in the literature [28] was not reproducible and later modified [33]. Understanding the side reaction (see section 4.3.1) led to an optimized method for the conversion of terpyrrole diacid (**5**) to terpyrrole dialdehyde (**7**) as follows: 250 mg of diacid (**5**) was added in trifluoroacetic acid (0.5 mL) that liberates CO_2 immediately. The mixture was stirred for 2 min at rt. then the flask was cooled in the ice-salt bath for 3~4 min. Pre-cooled orthoformate (0.5 mL) was added very slowly for 5 min then stirred for another 5 min in the cold bath. The ice-water (25 mL) was added slowly for 3~5 min and stirred for 5 min. The resulting solid was filtered, washed with water, and then dissolved quickly in the warm ethanol (4 mL). The mixture was stirred while 30 % ammonia (10 mL) was added dropwise. The water phase was introduced slowly. The resulting solid was filtered and purified by recrystallization (ethanol/dichloromethane) to yields 180 mg of dialdehyde (**7**) (77 %). ^{1}H NMR (CDCl$_3$, CDCl$_3$ as reference): δ 1.02 (t, 6H, pyrr-CH$_2$C*H$_3$*), 1.09 (t, 6H, pyrr-CH$_2$C*H$_3$*), 2.17 (s, 6H, unassigned), 2.22 (s, 6H, pyrr-C*H$_3$*), 2.41 (m, 8H, pyrr-C*H$_2$*CH$_3$), 3.83 (s, 4H, pyrr-C*H$_2$*-pyrr), 8.62 (br, 1H, N*H*), 9.21 (s, 2H, CO*H*), 9.60 (br, 2H, N*H*).

N,N-dioctyl 3,4-diaminobenzamide (9). 3,4-Diaminobenzoic acid (2 g), N-hydroxybenzotriazole (HOBt, 1.89 g), and 4-dimethylaminopyridine (DMAP, 320 mg) were added in the solvent (50 mL, DMF : THF = 1:1). N,N'-dicyclohexylcarbodiimide (DCC, 2.8 g) was then added and stirred for 3 h. Dioctylamine (3.6 g) and triethylamine (Et$_3$N, 400 μL) were then added and the reaction mixture was stirred for an additional 24 h. The solvent was removed and the product was purifed by column (silica gel) using a gradient solvent from hexane to ethyl acetate yielding 3.7 g (75 %) of (**9**). MALDI-TOF m/z 376.2 (**9**H$^+$), 751.4 ((**9**)$_2$H$^+$).

Lipophilized sp³-texaphyrin (11). A round bottom flask containing toluene (100 mL) and ethanol (20 mL) was bubbled with nitrogen for 3 h. The terpyrrole dialdehyde (**7**, 100 mg) and diamine (**9,** 107 mg) were added to the flask with HCl (12 M, 0.05 mL). The mixture was refluxed for 3 h at 85 ºC. After cooling, the mixture was washed with 1 M K_2CO_3 solution once and then distilled water twice using a separatory funnel. The organic layer was dried with K_2CO_3 and then filtered. The solvent was removed under high vacuum at 30 ºC. Due to difficulties in purifying the oily product, the crude product was directly used in the following step.

Lipophilized In(III) texaphyrin (13). Indium(III) chloride (220 mg), triethylamine (230 µL), and lipophilized sp³-texaphyrin (ca. 150 mg) were mixed in the methanol (75 mL). The solution was stirred in air at r.t. overnight. The solvent was removed and the crude mixture was redissolved in dichloromethane and then washed with water. A solvent gradient column (silica gel) was carried out with dichloromethane/methanol (0 % ~ 20 %). Recrystallization in dichloromethane/heptane yielded 121 mg (ca. 65 %) of (**13**). ^{1}H NMR (CDCl₃, CDCl₃ as reference): δ 0.8-1.5 (30H, alkyl chain), 1.7 (6H, pyrr-CH₂C*H₃*), 3.0 (6H, pyrr-C*H₃*), 3.2 (4H, NC*H₂*), 3.6 (8H, pyrr-C*H₂*CH₃), 8.3 (H, Ph-H), 9.6 (4H, C=C*H*), 11.5 (2H, *H*C=N). UV/vis (CHCl₃) [$\lambda_{max, \; nm}$ (log ε)]: 336.4 (3.7), 438.1 (4.1), 703.4 (3.2), 768.5 (3.7). MALDI-TOF m/z 870.4 (**13•⁺**), 905.4 (**13-Cl⁺**).

4.2.3 Preparation of ion-selective membranes

The film used in the leaching test was prepared by dissolving Mn(II) texaphyrin (1 mg), o-NPOE (66 mg), and PVC (33 mg) in THF (5 mL), which was cast on a glass slide (9 mm x 50 mm x 1 mm) and dried. Film cocktails for optical sensors were prepared by dissolving the lipophilized In(III) texaphyrin (**13**, 1 mg), ETH 7075 (100 mol% or 200 mol%), o-NPOE (66 mg), PVC (33 mg) in THF (5 mL). The film cocktail (20 µL) was cast on a glass slide (9 mm x 50 mm x 1 mm) and dried overnight before use. Membrane cocktails for electrochemical sensor membranes were prepared by dissolving the lipophilized In(III) texaphyrin (**13**, 2 mg), KTpClPB (0 mol% to 140 mol%), o-NPOE

(132 mg), and PVC (66 mg) in THF (4 mL). The cocktails were swirled overnight and then cast in a glass O-ring (i.d. = 22 mm), affixed on a glass slide (50 mm x 75 mm x 1 mm). Films were kept in the dark until used.

4.2.4   Optical and electrochemical measurements

All the optical measurements were performed using a UV-Vis spectrophotometer (model Lambda 35; Perkin-Elmer, Boston, MA). A glass strip coated with a polymeric film was placed into a quartz cuvette containing a sample solution. The sample solutions were prepared by dissolving the sodium salt of a given anion in a 0.05 M glycine-phosphate buffer (pH 3.0). For the leaching test, absorbances of the plasticized PVC film with Mn(II) texaphyrin on the glass slide were monitored when it was immersed in the buffer and when it was removed. For anionic responses of films doped with In(III) texaphyrin (**13**), the film was conditioned in the buffer with each concentration of anions for 5 to 10 min before absorbances were recorded.

Electrodes with membranes containing the lipophilized In(III) texaphyrin (8 mm diameter disk) were prepared using standard ISE electrode bodies (Oesch Sensor Technology, Sargans, Switzerland). The galvanic cell employed in this work consisted of: Ag/ AgCl(s), KCl(4 M)(aq)/LOAc(1 M)(aq)/sample solution/membrane/internal solution, AgCl(s)/Ag. Potential responses of sensors were measured by a high impedence voltmeter (VF-4, World Precision Instruments) connected to a personal computer running Labview software (version 7.0, National Instruments). The internal solution for the assembled electrodes was prepared by dissolving NaCl (10 mM) and NaF (10 mM) in the gly-phosphate buffer (0.05 M, pH 3.0) and sample solutions were prepared from a sodium salt of an anion dissolved in the gly-phosphate buffer.

4.3   Results and discussion

4.3.1   Preparation of lipophilized indium(III) texaphyrin

The synthetic pathways to prepare metallotexaphyrins are illustrated in Schemes 4.1, 4.2, and 4.3 with citations to the original work. In this section, syntheses to prepare the lipophlized In(III) texaphyrin are briefly discussed. The preparation of texaphyrin was initiated by preparing appropriate pyrroles: 3,4-diethylpyrrole (**3**) and benzyl 5-ace-toxymethyl-4-ethyl-3-methylpyrrole-2-carboxylate (**4**) by following scheme 4.1. Those pyrroles were converted to a terpyrrole dialdehyde(**7**) by scheme 4.2 and then cyclized through diaminobenzene. The resulting cyclic compound is not a fully conjugated species and is sometimes termed sp^3-texaphyrin (scheme 4.3). It can be further oxidized to form a fully conjugated metal-free texaphyrin ligand [35] or it can be oxidized during metalla-tion to yield a metallotexaphyrin (scheme 4.3) [32, 36]. An additional pendant group can be attached by employing an appropriate diamine species. In this work, in order to im-prove lipophilicity of the metallotexaphyrins, dioctyl amide was prepared by employing compound **9** in the cyclization step.

Among these synthetic steps, one step requires particular attention in order to per-form a successful synthesis. In scheme 4.3, decarboxylation of terpyrrole (**5**) was carried out in trifluoroacetic acid at room temperature [28]. The first attempt of this step resulted in a mixture of unidentified pyrroles. Meanwhile, rearrangement of dipyrroles under acidic condition has been reported [37] and the mixtures shown in the mass spectra were consistent with fragmentation and rearrangement. Further efforts revealed that de-carboxylation under given conditions would reach full conversion within a few minutes [38] but after ca. 10 min, the fragmentation and rearrangement reaction [37] can not be

Scheme 4.1

Scheme 4.2

Scheme 4.3 [32]

8 R = H
9 R = CON(C$_8$H$_{17}$)$_2$

7

10 R = H
11 R = CON(C$_8$H$_{17}$)$_2$
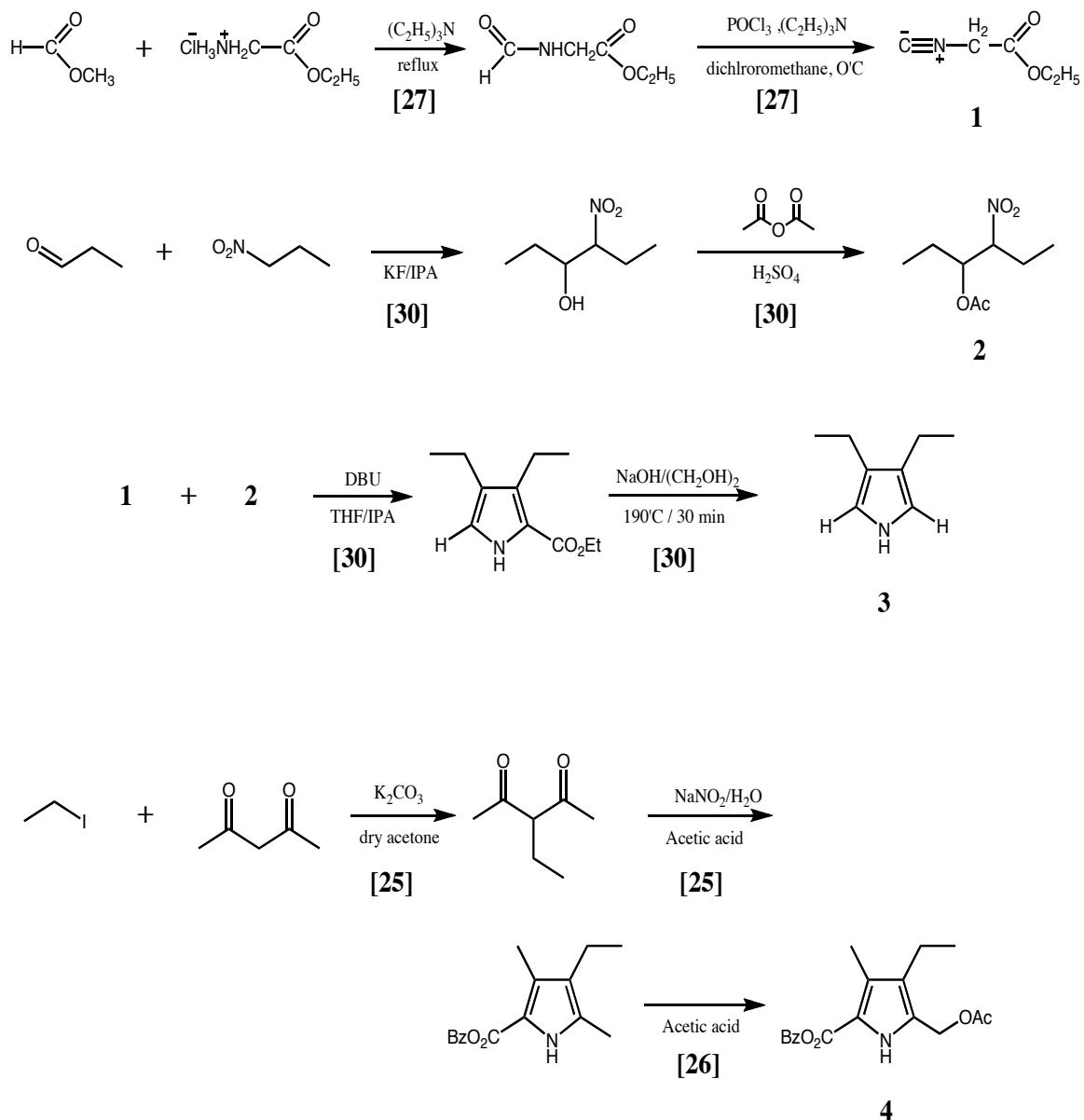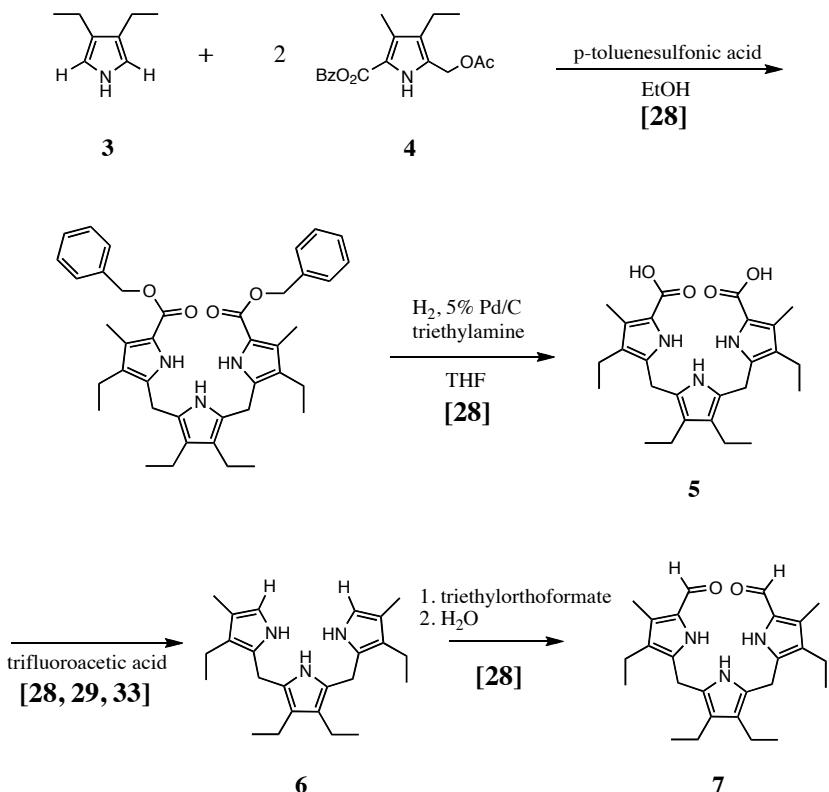
12 R = H, M = Mn(II); n = 1
13 R = CON(C$_8$H$_{17}$)$_2$, M = In(III); n = 2
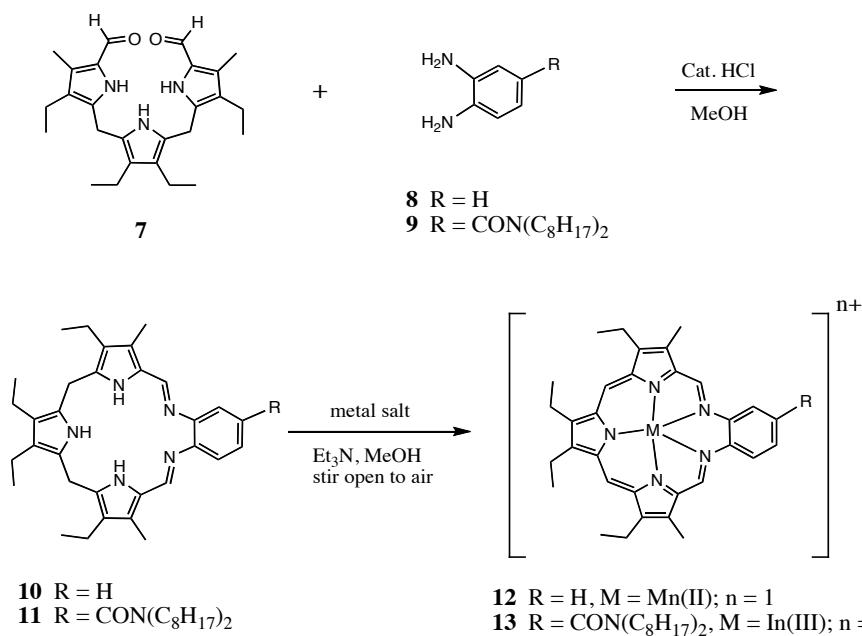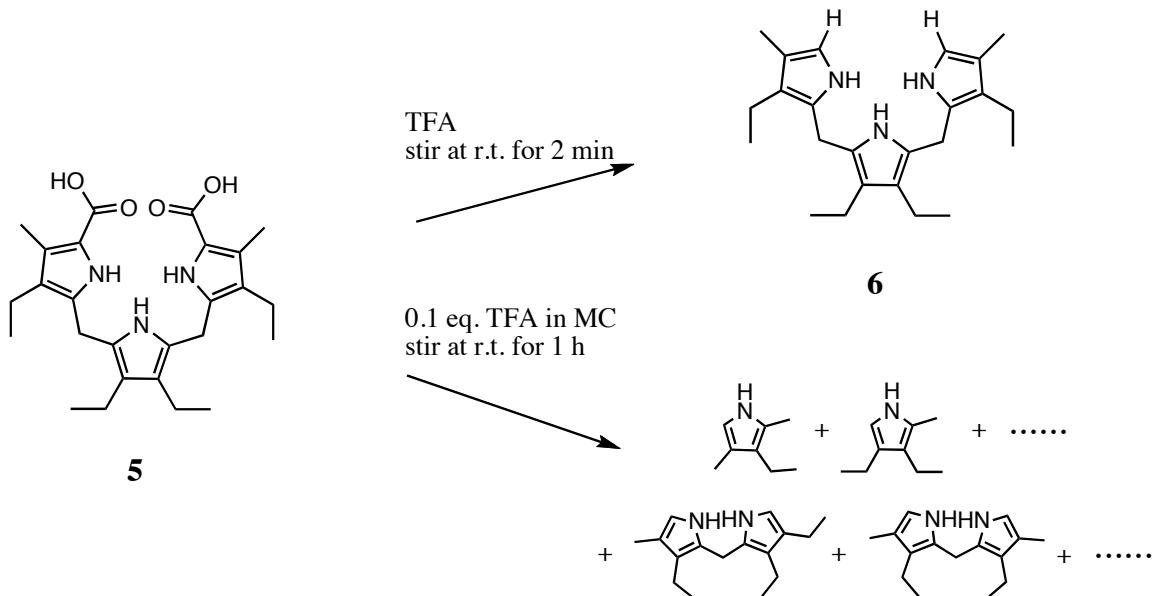
Figure 4.2 Reaction pathways from dicarboxylic acid (5) that can take place under acidic conditions.

ignored. Therefore, this step should be carried out within three to four min and then the next step should begin as quickly as possible (see Fig. 4.2).

The first metallotexaphyrin tested in a plasticized PVC film was Mn(II) texaphyrin, primarily to assess stability of a model metallotexaphyrin within a polymer film. Mn(II) texaphyrin was prepared as described previously [34]. Fig. 4.3 shows the absorbance spectrum of an Mn(II)-doped plasticized PVC film on the glass slide contacting an aqueous phase and an absorbance spectrum of the same film after aqueous phase is removed. Absorbance loss of the Soret band and Q-bands clearly indicates the Mn(II) texaphyrin has been washed out by the aqueous phase. This experiment suggests that the solubility of Mn(II) texaphyrin in the aqueous phase is low but is not low enough. Therefore, lipophilization of ligand was attempted in order to prevent leaching of metallotexaphyrins from plasticized PVC films.
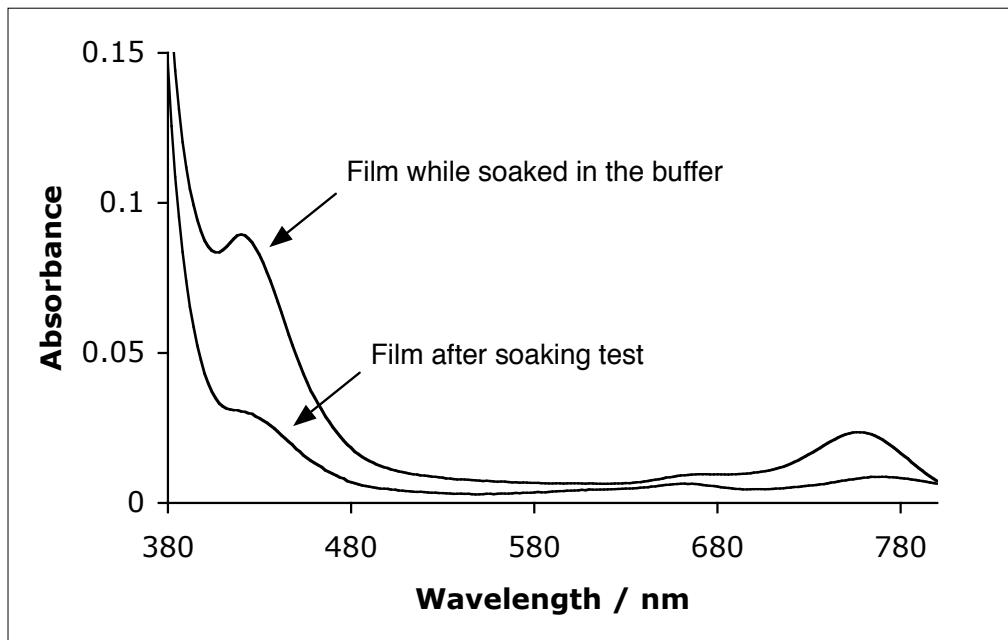
Figure 4.3 Optical spectra of the film (Mn(II) texaphyrin (1 wt%)/o-NPOE (66 wt%)/PVC (33 wt%) soaked in the buffer and taken out of the buffer. The reduction of absorbance indicates loss of Mn(II) texaphyrin into the aqueous phase.

Lipophilization of texaphyrin was carried out by using dioctyl diaminobenzamide (**9**) which was obtained from direct amidation of diaminobenzoic acid with dioctyl amine without any protection of amines in the benzene ring. Maintaining the reaction mixture basic by adding triethylamine seemed to allow dioctyl amine to compete against diamines in the benzene to react with the ester. This yielded a reasonable amount of product after purification. The dioctyl diaminobenzamide was reacted with dialdehyde (**7**) to form a sp^3-texaphyrin (**11**), which was followed by metallation and oxidation, which yielded the lipophilized In(III) texaphyrin (**13**).

4.3.2   Optical sensor study

An optical sensor based on the plasticized film doped with an ionophore and a chromoionophore is especially useful in investigating the response mechanism quantitatively by directly monitoring the concentration change of the protonated or deprotonated

chromoionophore involved in the response process. In this section, optical studies were performed in order to understand the ligand chemistry with anions and any involved conformational change of In(III) texaphyrin in the plasticized film. The optical film doped with lipophilized In(III) texaphyrin (**13**) and chromoionophore VI (ETH 7075) in the plasticized film was assessed as an optical thiocyanate sensor. All the optical measurements of the film were done in a quartz cuvette containing an appropriate aqueous solution and the glass slide coated with the film and equilibrated for 10 min before recording the spectra.

4.3.2.1 Dimer-monomer equilibrium of In(III) texaphyrin

UV/Vis absorbance spectra of the plasticized In(III) texaphyrin in the o-NPOE/ PVC film show a great similarity to In(III) porphyrins. A strong 450 nm band corresponds to the Soret band and absorption bands around 700 nm correspond to the Q-bands. It is quite intriguing to see that, in the presence of fluoride, the Soret band shifts about 40 nm to the blue region. This observation is exactly same as the spectral change of Sc(III) porphyrin that forms a bis-μ-fluoro-dimer in the plasticized film contacting fluoride solution. By varying non-ligatible anionic sites in the film, it can be rationalized what charge of the metal complex most stabilizes the dimer in the film. As can be seen in Fig. 4.4(a), the amount of the dimeric form is maximized at 50 mol% of KTpClPB. Therefore, the possible dimeric form is either a bis-μ-fluoro-dimer or mono-μ-fluoro-dimer (Fig. 4.4(b)). Since no crystallographic data is yet available, it is not clear whether a complex of In(III) texaphyrin forms cis-ligands or trans-ligands.

(a)

(b)

bis-μ-fluoro-dimer   mono-μ-fluoro-dimer
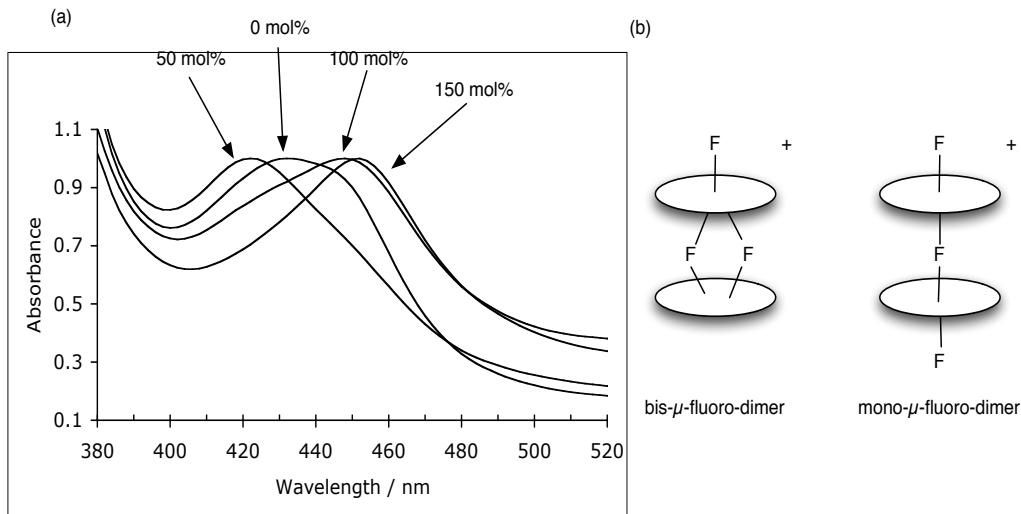
Figure 4.4 (a) Soret band shift of In(III) texaphyrin-doped film containing various amounts of anionic sites upon exposure to fluoride (0.001 M in 0.05M gly-phosphate buffer (pH 3.0). Note that 50 mol% of KTpClPB in the film maximizes the dimeric form and increasing anionic content over 50 mol% breaks the dimer. (b) Possible dimeric forms of In(III) texaphyrin via a fluoride bridge.

4.3.2.2 Optical thiocyanate sensor

For demonstration as an optical sensor, ETH 7075 (chromoionophore VI) was added with In(III) texaphyrin into the o-NPOE/PVC film. Since the net charge of non-ligated In(III) texaphyrin is +2, two ligation sites are available for the anion response. The first ligation would exhibit a harder interaction than the second ligation according to the hard-soft acid-base convention [39]. Therefore, in order to see the responses from the first ligation and the second ligation, an appropriate amount of anionic sites or acidic dye can be doped into the film. For example, when 100 mol% of ETH 7075 is incorporated with lipophilized In(III) texaphyrin (**13**), a possible response equilibrium would be:

$$LX^+ + C^- + H^+_{(aq)} + X^-_{(aq)} \rightleftharpoons LX_2 + CH \qquad \text{(rxn 4.1)}$$
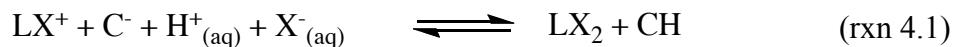
where LX^+ and LX_2 are In(III) texaphyrins with one and two X^- ligands, respectively. C^- and CH are deprotonated and protonated ETH 7075, repectively. Species in the aqueous

phase are denoted with (aq) and species in the film are denoted without any subscript. When 200 mol% of ETH 7075 is doped in the film, the following equilibrium may occur:

$$L^{2+} + 2C^- + H^+_{(aq)} + X^-_{(aq)} \rightleftharpoons LX^+ + CH + C^- \qquad \text{(rxn 4.2)}$$

where L^{2+} indicates In(III) texaphyrin without any analyte ligand. The resulting LX^+ and the remaining C^- can further respond to anion X^- by rxn 4.1. However, the film containing 200 mol% of ETH 7075 was not deprotonated fully, indicating L^{2+} was not formed by the conditioning process. Therefore, while LX^+ is formed by coextraction during conditioning, L^{2+} is not formed due to the strong metal-ligand interaction with the first ligand:

$$LX_2 + CH \longrightarrow LX^+ + C^- + H^+_{(aq)} + X^-_{(aq)} \qquad \text{(rxn 4.3)}$$

$$LX^+ + CH \xrightarrow{\quad//\quad} L^{2+} + C^- + H^+_{(aq)} + X^-_{(aq)} \qquad \text{(rxn 4.4)}$$
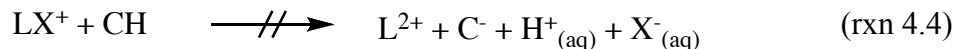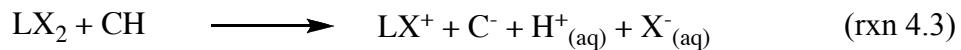
The film with 100 mol% KTpClPB and 100 mol% ETH 7075 did not show any stoichiometric indication of L^{2+} (data not shown). Therefore, it can be concluded that the first metal ion-anion interaction is too strong to be removed by counter anions or anionic ETH 7075, and only the second ligation can be utilized for optical sensing.
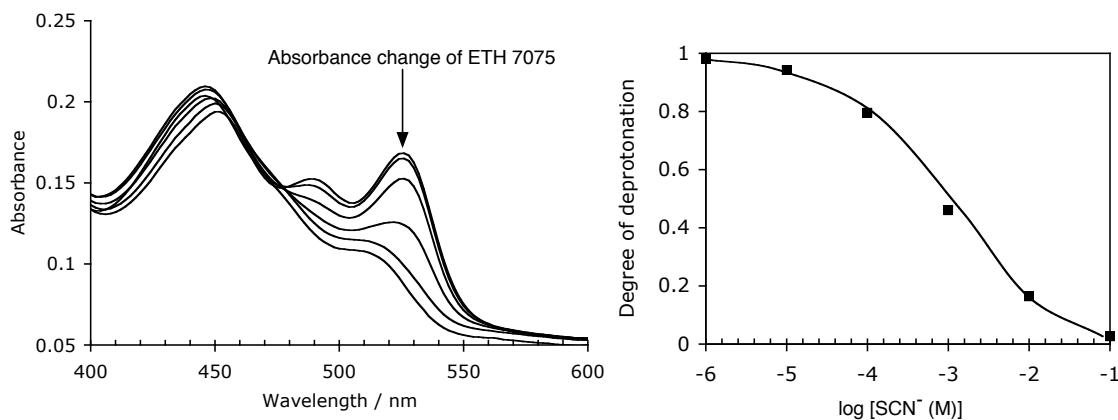
Figure 4.5 Optical response of the film (In(III) texaphyrin (1 mg)/ ETH 7075 (100 mol%)/ o-NPOE (66 mg)/ PVC (33 mg)) in the presence of SCN⁻ in the gly-phosphate buffer.

An optical sensors based on lipophilized In(III) texaphyrin (**13**) is demonstrated with the film containing 100 mol% ETH 7075/o-NPOE/PVC. Responses to anions is via co-extraction and anion ligation as a second ligand (rxn 4.1). The selectivity coefficients found in this configuration are SCN⁻ (0.0) > Salicylate (-0.7) > F⁻ (-2.2) > Br⁻ (-2.3) > Cl⁻ (-2.4) > ClO$_4^-$ (-3.0) > NO$_3^-$ (-3.4) where numbers in the parenthesis indicates logarithmic optical selectivity coefficients for thiocyanate. It is obvious that the presence of In(III) texaphyrin in the plasticized film significantly perturbs the Hofmeister selectivity pattern. Considering that In(III) porphyrin has been utilized as an optical chloride sensor when it was doped with dichlorofluorescein octadecyl ester (DCFOE) in a plasticized PVC film [40], thiocyanate-selectivity of In(III) texaphyrin suggests that In(III) texaphyrin with one ligand (LX⁺) behaves as a softer acid than In(III) porphyrin (L⁺) without any ligand.

4.3.3 Electrochemical sensor studies with films doped with lipophilic In(III) texaphyrin

In order to evaluate In(III) texaphyrin as an anion-selective ionophore for potentiometric sensing, ion-selective electrodes based on the plasticized PVC film doped with lipophilized In(III) texaphyrin (**13**) and various amounts of anionic sites (i.e., KTpClPB) were prepared. Depending on the molar ratio of anionic sites to the In(III) texaphyrin in the membrane, the concentration of anions in the membrane can be maintained by different processes. For example, when less than 100 mol% of anionic sites are present in the membrane, the following equilibrium will determine the concentration of free anion X⁻ in the highly plasticized membrane:

$$LX^+ + X^- \rightleftharpoons LX_2, \text{ when } R^- < 100 \text{ mol\%} \qquad \text{(rxn 4.5)}$$
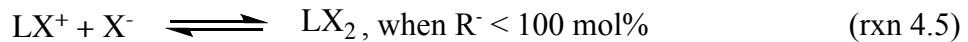
where R⁻ is denoted for anionic sites (i.e., TpClPB⁻). When the anionic sites are more than 100 mol%, L²⁺ rather than LX⁺ will be the ionophore that will bind with anion X⁻:

$$L^{2+} + X^- \rightleftharpoons LX^+, \text{ when } R^- > 100 \text{ mol\%} \qquad \text{(rxn 4.6)}$$
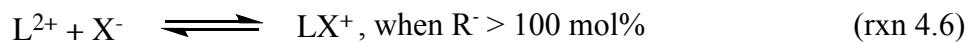
However, this process (rxn 4.6) does not effectively take place in the given system according to the result of the optical study. Meanwhile, the presence of fluoride is suggested to trigger dimerization based on the blue shift of the Soret band. Considering the dimer-monomer equilibrium in the presence of fluoride, the following process is more likely to occur:

$$LF_2 + LF^+ \rightleftharpoons L_2F_3^+ \quad (50 \text{ mol}\% < R^- < 100 \text{ mol}\%) \qquad \text{(rxn 4.7)}$$

In this equilibrium, free anion X^- in the membrane primarily binds LX^+ and the resulting LX_2 dimerizes with LX^+, which is abundant in the film when the borate level is between 50 mol% and 100 mol%. Therefore, varying the molar ratio of anionic sites to In(III) texaphyrin would change the selectivity pattern in the potentiometric configuration.

Fig. 4.6 shows the measured potentiometric selectivity change with varying amounts of anionic sites in the plasticized membrane. The experimental result shows that the sensor responds for SCN$^-$ when low levels of borate are present and to both SCN$^-$ and
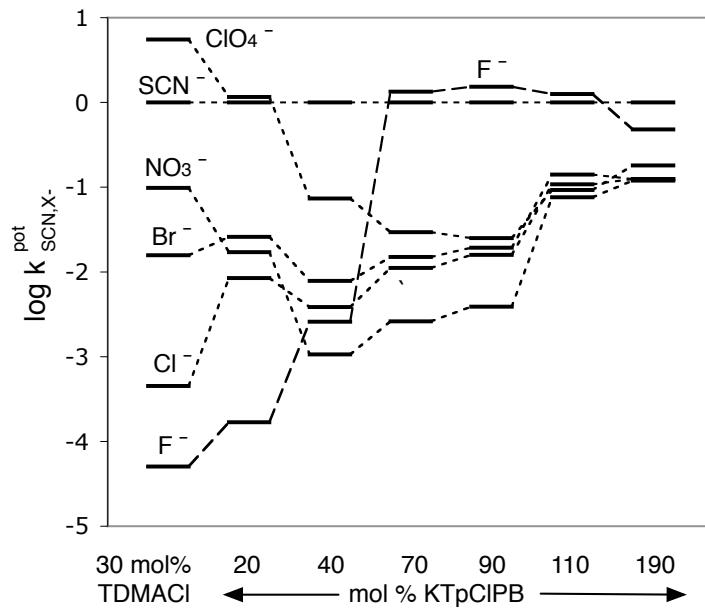
Figure 4.6 Selectivity change by varying ionic additives in the membrane. Film compositions are In(III) texaphyrin (1 mg)/ionic additives/o-NPOE (66 mg)/PVC (33 mg). Note that fluoride response is greatly improved when anionic sites are more than 50 mol%.

F⁻ when higher levels of borate are added. A borate level greater than 20 mol% enhances the response for SCN⁻ over other anions. As discussed previously, at this mol% of anionic sites, rxn 4.5 governs the membrane response. Therefore, response for SCN⁻ is based on the second axial ligation of the In(III) texaphyrin. It is noticeable that the potentiometric response for fluoride is greatly enhanced when the film is doped with more than 50 mol% of anionic sites. Apparently, dimerization plays an important role in this observation. At less than 50 mol% of anionic sites, in the presence of fluoride, In(III) texaphyrins would exist in the form of $L_2F_3^+$ and LF_2 since LF^+ will dimerize as soon as it interacts with LF_2 in the membrane phase. Therefore, LF^+, which would be the ionophore for F⁻ as the second ligand, would be at an ineffective concentration in the membrane. However, when anionic sites are more than 50 mol%, the primary species of In(III) texaphyrin found in the membrane would be LF^+ and $L_2F_3^+$. This rationale is further supported by the observation that the recovery time (the time required to reach the base-line signal when the film is moved from high concentration of fluoride to the blank solution) is about 10 ~ 20 min. The slow recovery time indicates that the anionic response causes an additional equilibrium (i.e., dimer-monomer equilibrium) within the bulk membrane and the electrochemical signal is not stabilized until the membrane reaches full equilibrium.

When over 100 mol% of borate is present in the film, overall responses are greatly deteriorated: slopes are lower than 25 mV/decade. As discussed previously, removing the two ligands is not likely to happen by adding more anionic sites in the membrane. At this high level of borate, anionic sites now function as cation exchangers and cationic responses now interfere leading to anionic responses that are all sub-Nernstian.

One of the reasons for choosing indium(III) as a central metal in the texaphyrin is to compare the effect of a texaphyrin vs. porphyrin as the ligand for In(III) and to determine how the ligand changes the behavior of ISEs using these different In(III) complexes. The anionic selectivities of potentiometric sensors based on In(III)OEP, Ga(III)OEP and In(III) texaphyrin are summarized in Fig. 4.7 [41, 42]. All of the ionophores listed in

the figure experience a severe interference from SCN⁻. However, In(III)OEP exhibits significant chloride response whereas Ga(III)OEP shows greatly improved fluoride response. Therefore, In(III) texaphyrin behaves more like Ga(III) porphyrin rather than the In(III) porphyrin. Considering that Ga(III) is a harder metal than In(III), switching from porphyrin to texaphyrin would make the metal ion harder as an anion binding site.
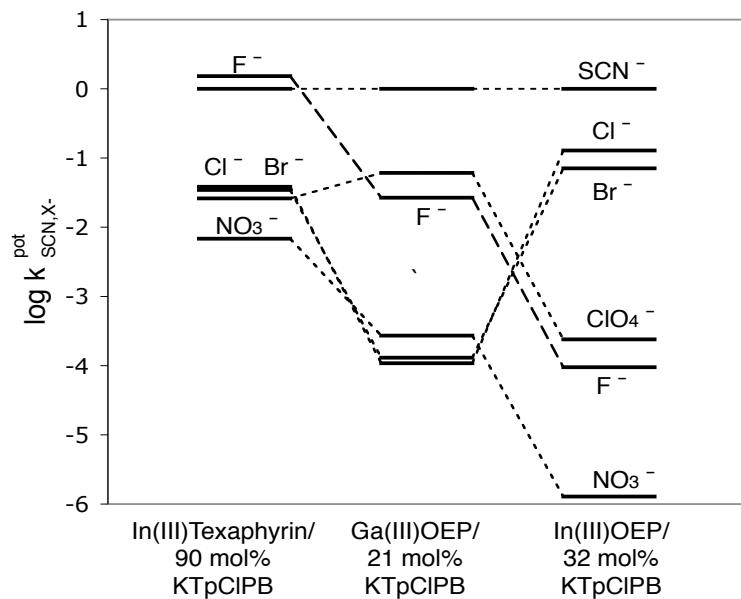
Figure 4.7 Comparison of selectivity patterns with In(III) texaphyrin, Ga(III) porphyrin, and In(III) porphyrin.

4.4   Conclusions

A metallotexaphyrin has been studied for the first time as an ionophore for preparing anion selective optical and electrochemical sensors based on plasticized PVC films. In(III) texaphyrin has been chosen to understand how a texaphyrin as a ligand is different from a porphyrin with respect to the anion recognition behavior. Optical sensors based on the plasticized PVC film doped with the lipophilized In(III) texaphyrin (**13**) and chromoionophore VI (ETH 7075) exhibit a strong SCN⁻ response over other anions. Potentiometric sensors prepared using In(III) texaphyrin and varying amounts of lipophilic borate site yield SCN⁻ and F⁻ selectivity depending on the amount of anionic sites. The selectivity pattern observed in the high borate ratio (over 50 mol%) is comparable with that

95

observed in the Ga(III) porphyrin-based ion-selective electrode. Therefore, it appears that the texaphyrin as a ligand can make the central metal cation harder than the metal cation in the porphyrin ring. Results from this study suggest the possibility of using metallotexaphyrins as anion receptors that can make use of metal cations with larger ionic radii and thus the possibility of achieving novel selectivity patterns significantly distinctive from that of both the Hofmeister series and that achieved using metalloporphyrins as membrane ionophores.

4.5   References

[1] Schmidtchen, F.P.; M. Berger, Chem. Rev. 97 (1997) 1609.

[2] Holliday, B.; C. Mirkin, Angew. Chem. Int. Ed. 40 (2001) 2022.

[3] Gale, P., Coord. Chem. Rev. 240 (2003) 191.

[4] O'neil, E.; B. Smith, Coord. Chem. Rev. 250 (2006) 3068.

[5] Filby, M.; J. Steed, Coord. Chem. Rev. 250 (2006) 3200.

[6] Arnendola, V.; M. Bonizzoni; D. Esteban-Gomez; L. Fabbrizzi; M. Licchelli; F. Sancenon; A. Taglietti, Coord. Chem. Rev. 250 (2006) 1451.

[7] Meyerhoff, M.E.; D.M. Pranitis; N.A. Chaniotakis, Advances in Instrumentation 42 (1987) 469.

[8] Biesaga, M.; K. Pyrzynska; M. Trojanowicz, Talanta 51 (2000) 209.

[9] Qin, Y.; E. Bakker, Anal. Chem. 76 (2004) 4379.

[10] Mitchell-Koch, J.T.; M. Pietrzak; E. Malinowska; M.E. Meyerhoff, Electroanalysis 18 (2006) 551.

[11] Duchowski, J.; D. Bocian, Inorg. Chem. 29 (1990) 4158.

[12] Kim, K.; W.S. Lee; H.J. Kim; S.H. Cho; G. Girolami; P.A. Gorlin; K. Suslick, Inorg. Chem. 30 (1991) 2652.

[13] Buchler, J.; A. Decian; S. Elschner; J. Fischer; P. Hammerschmitt; R. Weiss, Chem. Ber. Recl. 125 (1992) 107.

[14] Nishimoto, J.; T. Yamada; M. Tabata, Anal. Chim. Acta 428 (2001) 201.

[15] Sessler, J.; S. Camiolo; P. Gale, Coord. Chem. Rev. 240 (2003) 17.

[16] Gorden, A.; J. Davis; J. Sessler; V. Kral; D. Keogh; N. Schroeder, Supramol. Chem. 16 (2004) 91.

[17] Sessler, J.; J. Genge; V. Kral; B.L. Iverson, Supramol. Chem. 8 (1996) 45.

[18] Lin, X.M.; K. Umezawa; K. Tohda; H. Furuta; J. Sessler; Y. Umezawa, Anal. Sci. 14 (1998) 99.

[19] Umezawa, K.; K. Tohda; X.M. Lin; J. Sessler; Y. Umezawa, Anal. Chim. Acta 426 (2001) 19.

[20] Sessler, J.; W.S. Cho; S. Dudek; L. Hicks; V. Lynch; M. Huggins, J. Porphyrins Phthalocyanines 7 (2003) 97.

[21] Kumar, M.; T. Chandrashekar, J. Inclusion Phenom. Macrocyclic Chem. 35 (1999) 553.

[22] Sessler, J.; J. Davis, Acc. Chem. Res. 34 (2001) 989.

[23] Sessler, J.; D. Seidel, Angew. Chem. Int. Ed. 42 (2003) 5134.

[24] Mody, T.; J. Sessler, J. Porphyrins Phthalocyanines 5 (2001) 134.

[25] Johnson, A.W.; E. Markham; R. Price; K.B. Shaw, Journal of Chemical Society (1958) 4254.

[26] Johnson, A.W.; I.T. Kay; E. Markham; R. Price; K.B. Shaw, Journal of Chemical Society (1959) 3416.

[27] Hartman, G.D.; L.M. Weinstock, Org. Synth. 59 (1979) 18.

[28] Sessler, J.; M. Johnson; V. Lynch, J. Org. Chem. 52 (1987) 4394.

[29] Alhazimi, H.; A. Jackson; D. Knight; T. Lash, J. Chem. Soc., Perkin Trans. 1 (1987) 265.

[30] Sessler, J.L.; A. Mozaffari; M.R. Johnson, Org. Synth. 70 (1992) 68.

[31] Sessler, J.; G. Hemmi; T. Mody; T. Murai; A. Burrell; S. Young, Acc. Chem. Res. 27 (1994) 43.

[32] Hannah, S.; V. Lynch; D. Guldi; N. Gerasimchuk; C. Macdonald; D. Magda; J. Sessler, J. Am. Chem. Soc. 124 (2002) 8416.

[33] Sessler, J.; T. Mody; G. Hemmi; V. Lynch, Inorg. Chem. 32 (1993) 3175.

[34] Shimanovich, R.; S. Hannah; V. Lynch; N. Gerasimchuk; T. Mody; D. Magda; J. Sessler; J. Groves, J. Am. Chem. Soc. 123 (2001) 3613.

[35] Hannah, S.; V. Lynch; N. Gerasimchuk; D. Magda; J. Sessler, Org. Lett. 3 (2001) 3911.

[36] Mody, T.; L. Fu; J. Sessler, Prog. Inorg. Chem. 49 (2001) 551.

[37] Jackson, A.; W. Lertwanawatana; R. Pandey; K. Rao, J. Chem. Soc., Perkin Trans. 1 (1989) 374.

[38] Dunn, G.; G. Lee, Can. J. Chem. 49 (1971) 1032.

[39] Pearson, R.G., J. Am. Chem. Soc. 85 (1963) 3533.

[40] Wang, E.; C. Romero; D. Santiago; V. Syntilas, Anal. Chim. Acta 433 (2001) 89.

[41] Steinle, E.D.; U. Schaller; M.E. Meyerhoff, Anal. Sci. 14 (1998) 79.

[42] Zhang, W.; E. Rozniecka; E. Malinowska; P. Parzuchowski; M.E. Meyerhoff, Anal. Chem. 74 (2002) 4548.

Chapter 5

Modulation of Dimer-Monomer Equilibrium of Ga(III) Porphyrins for the Detection of Fluoride

5.1 Introduction

Developing recognition molecules for anions that are important in biological and environmental systems has been one of the most active areas in recent sensor research effort [1-4]. Among anions, fluoride has created the most debate regarding its effect on public health when fluoride is administered in the drinking water [5-8]. To date, quick and easy detection of fluoride has relied on the classical LaF_3 solid state electrode [9]. Even though ion-selective electrodes (ISEs) based on polymeric membranes doped with ionophores have been successfully applied for many important ions [10, 11], detection of fluoride with this configuration has been a great challenge since polymeric membranes do not favor the partitioning of fluoride, an anion with a very negative hydration energy [12].

Recent studies of anion-selective electrodes based on metalloporphyrins as anion ionophores have suggested that highly selective detection of fluoride in water may be possible. Ion-selective polymeric membrane electrodes based on Ga(III) porphyrins have exhibited much improved fluoride response comparable to the response to SCN⁻ and sali-cylate [13]. Zr(IV) porphyrins [14, 15], Al(III) porphyrins [16-18], and Sc(III) porphyrins [19] have also been studied as fluoride ionophores. Membranes doped with Zr(IV) por-phyrins have shown improved fluoride selectivity over other anions but its complicated ligand chemistry has made it difficult to modulate the response mechanism. Ion-selective sensors based on Al(III) porphyrins have exhibited unmatched selectivity for fluoride

even over lipophilic anions (i.e., SCN$^-$), but a concomitant conformational change (i.e., dimer-monomer equilibrium) in the membrane causes slow response times for potentiometric measurements.

In general, a search for a better ionophore is usually done by varying the central metal ion without changing the ligand structure. If preliminary results with a given central metal cation in the ligand are promising, further optimization is done by attaching appropriate side groups to the ligand or by incorporating lipophilic additives in the polymeric matrix. When the ionophore undergoes a conformational change like a dimer-monomer equilibrium, this process can be manipulated in order to improve the selectivity or lower the detection limit. However, since this dimer-monomer equilibrium is understood in electrochemical sensors [20], only an optical chloride sensor based on In(III) porphyrins has actively utilized this process as a transduction mechanism [21, 22]. Conventionally, the dimer-monomer equilibrium is the main cause of the slow responses of the anion-selective electrodes based on metalloporphyrin ionophores and thus should be suppressed for optimal response properties of ISEs [23, 24].

In this chapter, approaches to take advantage of a dimer-monomer equilibrium of metalloporphyrins are investigated. For this purpose, Ga(III) porphyrins are chosen as model compounds for the fluoride detection. Sensors based on Ga(III) porphyrins suffer from severe SCN$^-$ interference and their detection limit is not low enough to measure the fluoride in the drinking water. It is shown here that Ga(III) porphyrins can form not only a hydroxo-dimer but also a fluoro-bridged dimer. By understanding and modulating the dimer-monomer process of Ga(III) porphyrins, efforts to improve the sensor response for fluoride may be possible.

5.2 Experimental

5.2.1 Reagents

All the reagents were used as received without further purification. Tetrahydrofuran (THF) was distilled by refluxing bulk THF with sodium and benzophenone. *o*-Nitrophenyloctylether (*o*-NPOE), potassium tetrakis(3,5-bis(trifluoromethyl)phenyl) borate (KTFPB), potassium tetrakis(p-chlorophenyl) borate (KTpClPB), and poly(vinyl chloride) (PVC) were from Fluka (Ronkonkoma, NY). 2,3,7,8,12,13,17,18-Octaethyl-21H,23H-porphyrin (H$_2$OEP) was purchased from Frontier Scientific (Logan, UT). Glycine, o-phosphoric acid, and sodium salts of anions tested were purchased from Aldrich. Dinonylnaphthalene sulfonate (DNNS) was a gift from King Industries (Norwalk, CT). All the aqueous solution tested in this work were glycine-phosphate buffer (glycine 0.05 M, pH 3.0 adjusted by addition of phosphoric acid).

5.2.2 Preparation of di(metalloporphyrins)

All the reagents and solvents employed in syntheses were used as received. For characterization of compounds, UV/Vis spectra, mass spectra, and 1H NMR spectra were obtained using a Perkin-Elmer Lambda-35 spectrophotometer, a Varian 400 MHz spectrometer, and MALDI-TOF mass spectrometer (Micromass TofSpec-2E), respectively. For a MALDI-TOF mass spectrum, dithranol was used as a matrix.

Preparation of Ga(III) octaethylporphyrin (Ga(III)OEP), Ga(III) tetraphenylporphyrin (Ga(III)TPP), and diporphyrins. Ga(III)OEP, Ga(III)TPP [25], and diporphyrins with various links [26] were prepared as described in the literature.

[GaTPP-OH]$_2$-C$_4$H$_8$ (2). Diporphyrin **1** (114 mg, see Scheme 5.1), Ga(III)acac$_3$ (320 mg), NaOAc·(H$_2$O)$_3$ (4.7 g), and glacial acetic acid (90 mL) were placed into a reaction vessel. The mixture was refluxed for 4 h while the reaction was monitored by UV-Vis spectrophotometer. The mixture was cooled and poured into the water (75 mL), which

was filtered, washed with water/methanol (5 ~ 10 %) and dried in the oven (110 ºC). The resulting solid was dissolved in chloroform and washed with 1 M NaOH solution by using a separatory funnel. The organic layer was dried with Na_2SO_4. The product was further purified by gradient column using silica gel with dichloromethane/methanol (0 % to 10 %), yielding 109 mg (85 %) of complex **2**. MALDI-TOF m/z 1676.1 (**2**+dithranol).

[GaTPP-OH]$_2$-*o*-xylene (4a). Diporphyrin **3a** (100 mg), Ga(III)acac$_3$ (270 mg), NaOAc·(H$_2$O)$_3$ (4 g), and acetic acid (75 mL) were added in the round bottom flask. The product obtained was 80 mg (71 %) of complex **4a**. MALDI-TOF m/z 1725.2 (**4a**+dithranol).

[GaTPP-OH]$_2$-*m*-xylene (4b). Diporphyrin **3b** (100 mg), Ga(III)acac$_3$ (270 mg), NaOAc·(H$_2$O)$_3$ (4 g), glacial acetic acid (75 mL), and chlorobenzene (75 mL) were added in the flask and refluxed for 12 h. The reaction mixture was washed with 1 M NaOH solution (2~3 times) then with water using a separatory funnel. Chloroform was used as the solvent. The organic layer was taken and dried in vacuum. The solid was further purified by a gradient column using silica gel with dichloromethane/methanol (0 % to 10 %), yielding 84 mg (75 %) of complex **4b**. MALDI-TOF m/z 1725.2 (**4b**+dithranol).

[GaTPP-OH]$_2$-*p*-xylene (4c). Diporphyrin **3c** (90 mg), Ga(III)acac$_3$ (240 mg), NaOAc·(H$_2$O)$_3$ (3.6 g), glacial acetic acid (66 mL), and chlorobenzene (66 mL) were aded in the flask and refluxed for 2 h. After purification, the product was 98 mg (97 %) of complex **4c**. MALDI-TOF m/z 1725.2 (**4c**+dithranol).

5.2.3   Preparation of optical films and ion-selective membranes

The optical sensing films were prepared by dissolving Ga(III)OEP-OH (1 mg), anionic sites (either KTFPB or DNNS), o-NPOE (66 mg), and PVC (33 mg) in THF (5 mL), and spin-coating the sensing films on a glass slide (75 mm x 25 mm x 1 mm) using a spin coater (model SCS-G3-8, Cookson Electronics). Membrane cocktails for electrochemical sensors were prepared by dissolving Ga(III)TPP-OH (2 mg), KTpClPB (20

Scheme 5.1

1

2

3
a o-xylene; b m-xylene; c p-xylene

4
a o-xylene; b m-xylene; c p-xylene
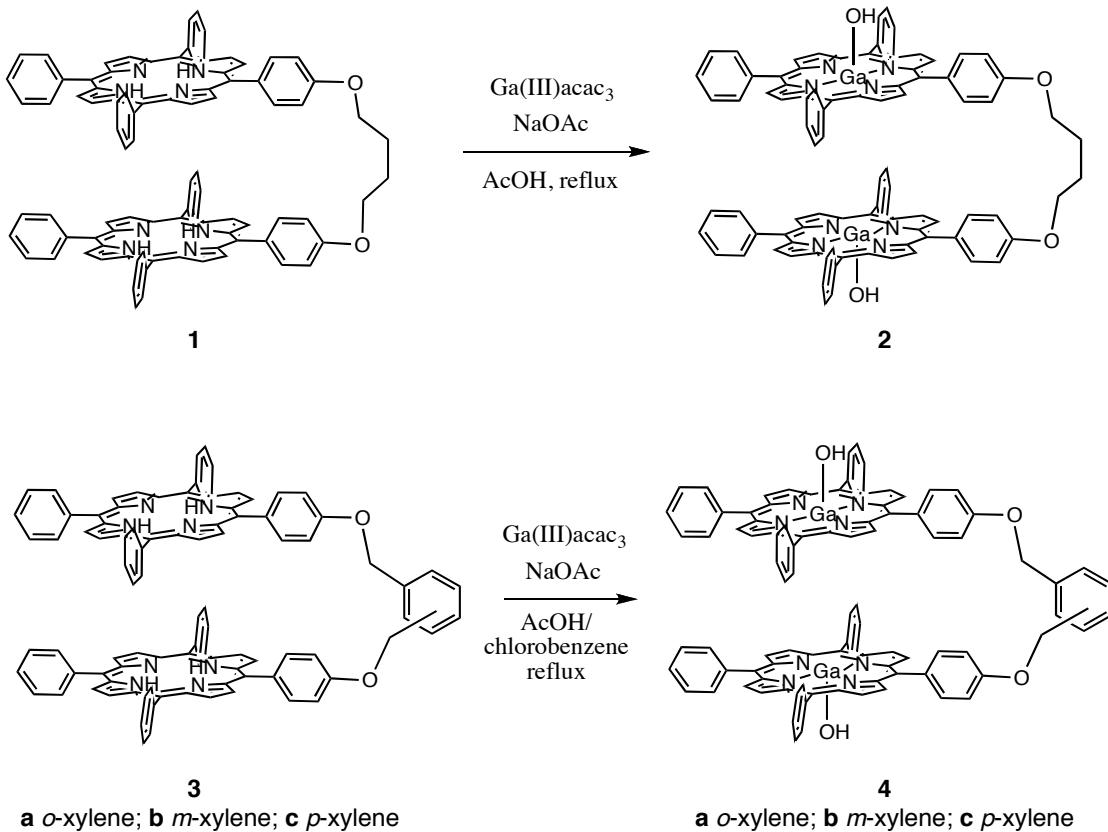
mol% ~ 80 mol%), o-NPOE (132 mg), and PVC (66 mg) in THF (4 mL) or Ga(III) dipor-phyrin (2.2 mg), KTpClPB (40 mol% ~ 160 mol%), o-NPOE (132 mg), and PVC (66 mg) in THF (4 mL). The cocktails were swirled overnight and cast in a glass O-ring (i.d. = 22 mm), affixed on the glass slide (50 mm x 75 mm x 1 mm). Films were kept in the dark overnight before use.

5.2.4 Optical and electrochemical measurements

All the optical measurements were performed using a UV-Vis spectrophotometer (model Lambda 35; Perkin-Elmer, Boston, MA). A glass slide coated with a polymeric film was equipped with a flow cell where the optical sensor slide, teflon gasket (0.18 mm thick), and another glass slide with inlet and outlet holes were held together by clips. A sample solution was introduced by a peristaltic pump. A circular flow of buffer solution

(50 mL) by the pump was maintained and varying amounts of anion stock solution were added to change the concentration of the anion in the flowing buffer solution for the measurement.

Ion-selective electrodes with membranes based on Ga(III)TPP or Ga(III) diporphyrins (8 mm diameter disk) were prepared using electrode bodies (Oesch Sensor Technology, Sargans, Switzerland). The galvanic cell employed in this work consisted of: Ag/ AgCl$_{(s)}$, KCl(4 M)$_{(aq)}$/LOAc(1 M)$_{(aq)}$/sample solution/membrane/internal solution, AgCl$_{(s)}$/ Ag. EMF responses were monitored by a high impedence voltmeter (VF-4, World Precision Instruments) connected to a personal computer running Labview software (version 7.0, National Instruments). The internal solution was NaCl (10 mM)/ NaF (10 mM) in the gly-phosphate buffer (0.05 M, pH 3.0).

5.3 Results and discussion

5.3.1 Dimer-monomer equilibrium of gallium(III) porphyrin

Ga(III) Porphyrins have been studied as ionophores in the potentiometic configurations [13]. The selectivity pattern has been reported as Salicylate > SCN$^-$ > ClO$_4^-$ > F$^-$ > NO$_2^-$ > I$^-$ > NO$_3^-$ > Cl$^-$ > Br$^-$, where the response for fluoride is greatly improved compared to conventional Hofmeister selectivity pattern. An optical shift of the Soret band exhibits In(III)OEP-like behavior. Indeed, with the appropriate amount of anionic sites, a blue shift of the Soret band is observed in the buffer solution without any analyte present. Crystallographic data and an optical study have confirmed that the blue-shift of the Soret band originates from a Ga(III) porphyrin-based dimeric structure [25, 27, 28]. Therefore, an optical fluoride sensor based on dimer-monomer mechanism can be examined. A preliminary result shows that the presence of fluoride in the aqueous phase decreases the dimeric band (384 nm) and increases the monomeric band (400 nm) as can be seen in Fig. 5.1.
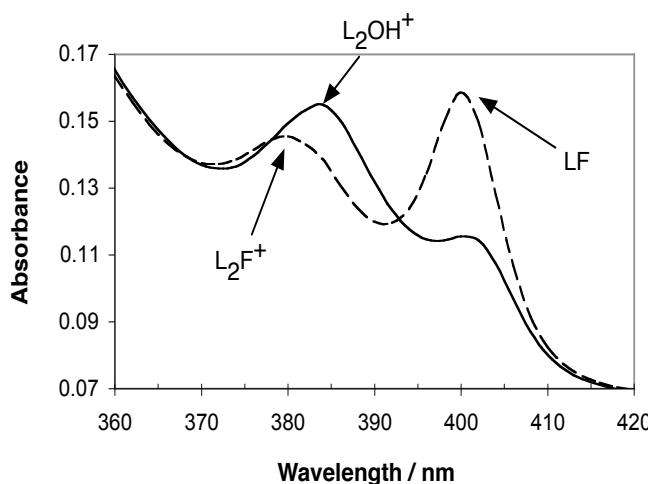
Figure 5.1 Spectral change of the film (Ga(III)OEP-OH (1 mg)/KTFPB (45 mol%)/o-NPOE (66 mg)/PVC (33 mg)) before and after contacting 0.1 M fluoride solution at pH 3.0. In the buffer without fluoride (solid line), the hydroxo-dimer (384 nm) is the major form of the Ga(III)OEP. In 0.1 M fluoride solution (broken line), the fluoro-dimer (380 nm) and fluorinated monomer (400 nm) are the major forms.

However, the full response for fluoride does not turn all the dimeric band to monomeric bands. Increasing the concentration of fluoride in the buffer solution results in two bands observed at 380 nm and 400 nm, possibly the dimeric band and monomeric band, respectively. Further studies have been conducted in order to identify this dimer-like band. This dimer is maximized when the anionic sites are about 50 mol%, indicating it is positively charged species. Efforts to isolate a crystal have failed possibly because this dimer is in equilibrium with monomers under given conditions. However, formation of the fluoro-dimer is indirectly supported by an observation that a covalently linked di[Ga(III)TPP] complex (**4b**) exhibits enhanced fluoride selectivity over other anions (See Section 5.3.3). These observations suggest that fluoride is forming a dimeric complexed species as well as a monomeric complex:

$$L_2OH^+ + F^-_{(aq)} \rightleftharpoons LF + L^+ + OH^-_{(aq)} \qquad (rxn\ 5.1)$$

$$LF + L^+ \rightleftharpoons L_2F^+ \qquad (rxn\ 5.2)$$

105
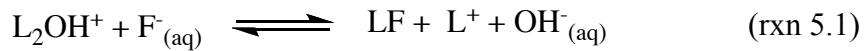
where the species in the aqueous phase are denoted with (aq) and the species without (aq) are in the organic film phase. L^+ denotes the non-ligated Ga(III) porphyrin, L_2OH^+ is the hydroxo-bridged dimer, and L_2F^+ is for the fluoro-bridged dimer. This feature is distinct from Sc(III)OEP where a F-dimer is the only species observed in the film in response to fluoride (see Chapter 3), and from In(III)OEP where a chlorinated In(III)OEP only exists in monomeric form.

Currently, a dimer-monomer equilibrium of a metalloporphyrin within an anion-selective polymeric film has been the subject of various studies [14, 15, 17-24, 29, 30]. A dimer-monomer process throughout the membrane is the reason why the response time is so slow for electrochemical sensors based on porphyrins that exhibit such behavior. In contrast, the Soret band shift upon dimer-monomer conversion is an efficient optical transduction mechanism where the ionophore (i.e., metalloporphyrins) is also a chro-moionophore that do not require any additional dye in the sensing film [21, 22]. A closer look at the mechanistic aspects of the dimer-monomer equilibrium may revise our under-standing regarding its effect on the detection limit and the selectivity of both electro-chemical and optical sensors.

In order to understand how dimer-monomer equilibrium affects the detection limit and the selectivity for optical sensing films, response functions for an anion in the ab-sence of dimerization and in the presence of dimerization must be compared. For this purpose, response functions should be expressed by formation constants of the complexes involved in the response mechanism and the dimerization constants. For simplicity of this discussion, activity coefficients are assumed to be unity and concentrations are consid-ered instead of activities. Formation constants for each complexes are defined as follows:

$$L^+ + OH^- \overset{\beta_{LOH}}{\rightleftharpoons} LOH \qquad \text{(rxn 5.3)}$$

$$L^+ + X^- \overset{\beta_{LX}}{\rightleftharpoons} LX \qquad \text{(rxn 5.4)}$$

$$2L^+ + OH^- \xrightleftharpoons{\beta_{L2OH}} L_2OH^+ \qquad \text{(rxn 5.5)}$$
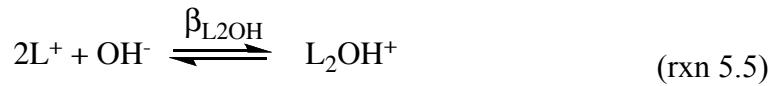
where

$$\beta_{LOH} = \frac{[LOH]}{[L^+][OH^-]} \qquad \text{(Eq. 5.1)}$$

$$\beta_{LX} = \frac{[LX]}{[L^+][X^-]} \qquad \text{(Eq. 5.2)}$$

$$\beta_{L2OH} = \frac{[L_2OH^+]}{[L^+]^2[OH^-]} \qquad \text{(Eq. 5.3)}$$

A dimerization constant can be defined as:

$$LOH + L^+ \xrightleftharpoons{K_{L2OH}} L_2OH^+ \qquad \text{(rxn 5.6)}$$
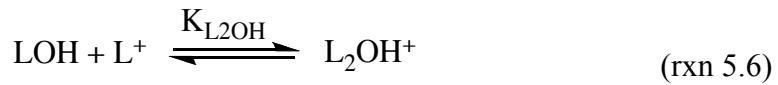
where

$$K_{L2OH} = \frac{[L_2OH^+]}{[L^+][LOH]} \qquad \text{(Eq. 5.4)}$$

and by Eq. 5.1, 5.3, and 5.4,

$$\beta_{L2OH} = K_{L2OH}\beta_{LOH} \qquad \text{(Eq. 5.5)}$$

Now, if a sensor based on the following equilibrium in the absence of dimer-monomer equilibrium is considered,

$$LOH + X^-_{(aq)} \xrightleftharpoons{K_{X1}} LX + OH^-_{(aq)} \qquad \text{(rxn 5.7)}$$
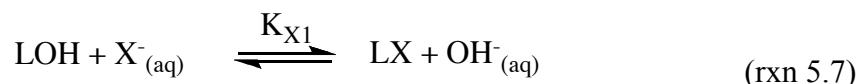
the response function for X⁻ is described by:

$$[X^-_{(aq)}] = \frac{1}{K_{X1}} \times \frac{[LX]}{[LOH]} \times [OH^-_{(aq)}] \qquad \text{(Eq. 5.6)}$$

where K_{X1} can be rewritten in terms of formation constants and ion-exchange constant:

$$K_{X1} = \frac{\beta_{LX}}{\beta_{LOH}} \times K_{exchange} \qquad \text{(Eq. 5.7)}$$

where $K_{exchange}$ is defined by the following ion-exchange process:

$$OH^- + X^-_{(aq)} \xrightleftharpoons{K_{exchange}} OH^-_{(aq)} + X^- \qquad \text{(rxn 5.8)}$$
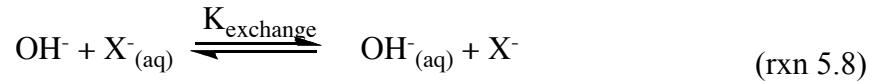
$$K_{exchange} = \frac{[X^-]}{[OH^-]} \times \frac{[OH^-_{(aq)}]}{[X^-_{(aq)}]} \qquad \text{(Eq. 5.8)}$$

When a dimer-monomer equilibrium takes place, the response equilibrium would be:

$$L_2OH^+ + X^-_{(aq)} \xrightleftharpoons{K_{X2}} LX + L^+ + OH^-_{(aq)} \qquad \text{(rxn 5.9)}$$
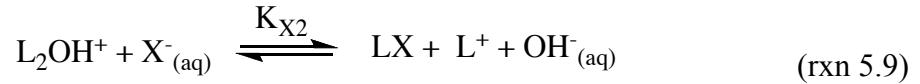
where the response function is:

$$[X^-_{(aq)}] = \frac{1}{K_{X2}} \times \frac{[LX][L^+]}{[L_2OH^+]} \times [OH^-_{(aq)}] \qquad \text{(Eq. 5.9)}$$

and K_{X2} can be rewritten as:

$$K_{X2} = \frac{\beta_{LX}}{\beta_{L2OH}} \times K_{exchange} = \frac{\beta_{LX}}{K_{L2OH}\beta_{LOH}} \times K_{exchange} \qquad \text{(Eq. 5.10)}$$

In order to compare the detection limit of anion X^- for the two mechanisms (rxn 5.7 and rxn 5.9), the concentration of the anion required to give the same degree of response can be compare. For this purpose, points of the half response (i.e., the concentration of an anion in the solution that gives half of the ionophore ligated to the anion) are considered:

$$[X^-_{(aq)}]^{\text{no dimer}}_{\alpha=\frac{1}{2}} = \frac{1}{K_{X1}} \times [OH^-_{(aq)}] \tag{Eq. 5.11}$$

$$[X^-_{(aq)}]^{\text{dimer}}_{\alpha=\frac{1}{2}} = \frac{1}{K_{X2}} \times \frac{[L_T]}{4} \times [OH^-_{(aq)}] \tag{Eq. 5.12}$$

and

$$\frac{[X^-_{(aq)}]^{\text{dimer}}_{\alpha=\frac{1}{2}}}{[X^-_{(aq)}]^{\text{no dimer}}_{\alpha=\frac{1}{2}}} = \frac{K_{X1}}{K_{X2}} \times \frac{[L_T]}{4} = \frac{K_{L2OH}[L_T]}{4} \tag{Eq. 5.13}$$

Eq. 5.13 indicates that the detection limit for X^- in the dimer-monomer mechanism (rxn 5.9) is higher that that in the non-dimer mechanism (rxn 5.7) by $K_{L2OH}[L_T]/4$. This means that when a dimer-monomer equilibrium is present, in order for X^- to replace OH^- on L^+, not only does the bond between OH^- and the metal ion need to be broken, but also the interaction between LOH and L^+ must be broken. Therefore, the calibration curve will shift to the higher concentration range due to the formation of the hydroxo-dimer.

Meanwhile, if the analyte (e.g., fluoride) bridges two monomers, this analyte-induced dimerization enhances the response. Rxn 5.1 and 5.2 gives:

$$L_2OH^+ + F^-_{(aq)} \xrightleftharpoons{K_F} L_2F^+ + OH^-_{(aq)} \tag{rxn 5.10}$$
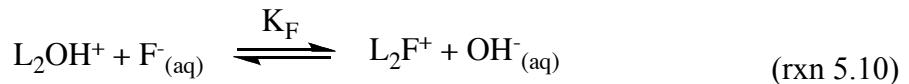
and the response function for F^- is:

$$[F^-_{(aq)}] = \frac{1}{K_F} \times \frac{[L_2F^+]}{[L_2OH^+]} \times [OH^-_{(aq)}] \tag{Eq. 5.14}$$

When the half responses between the response mechanism for X^- and F^- based on the dimer-monomer equilibrium (rxn 5.9 and rxn 5.10), a similar form as Eq. 5.13 is obtained:

$$\frac{[X^-_{(aq)}]^{dimer}_{\alpha=\frac{1}{2}}}{[F^-_{(aq)}]_{\alpha=\frac{1}{2}}} = \frac{K_F}{K_{X2}} \times \frac{[L_T]}{4} = \frac{K_{L2F}[L_T]}{4K'_{exchange}} \qquad (Eq.\ 5.15)$$

where K_{L2F} is the dimerization constant for L_2F^+ (Eq. 1.2) and $K'_{exchange}$ is the ion-exchange process between $F^-_{(aq)}$ and $X^-_{(aq)}$. Eq. 5.15 indicates that the response for F^- will be greater than the response for X^- and thus the selectivity of F^- over X^- will be increased by $K_{L2F}[L_T]/(4K'_{exchange})$. Since $K'_{exchange}$ is only dependent on the nature of anions (i.e., hydration energies of anions), in order to improve selectivity for F^- over X^-, K_{L2F} and/or $[L_T]$ should be increased. The dimerization constant (K_{L2F}) can be enhanced by employing the membrane solvent that favors the dimer or by doping anionic sites that stabilize the positively charged dimeric structure better than KTFPB or by covalently connecting two metalloporphyrins with an appropriate linker.

In summary, dimer-monomer equilibria may be carefully controlled according to the nature of analyte: if the anion of interest breaks the hydroxo-dimer, the membrane environment that weakens dimerization will lower the detection limit, and if the anion of interest is bridging two monomers, any approach that enhances dimerization should improve selectivity. Ga(III) porphyrins as fluoride ionophores are examined here for both purposes, since they can form both monomeric fluoride complexes and dimeric fluoride complexes in plasticized PVC films.

5.3.2 Optical fluoride sensors based on dimer-monomer equilibrium of Ga(III)OEP

As discussed previously, weakening hydroxo-dimer will improve sensitivities toward anions that break this dimeric structure. In this section, optical sensors based on Ga(III)OEP in the plasticized PVC film with appropriate additives are studied. As In(III)OEP has been applied for an optical chloride sensor based on dimer-monomer mechanism, optical fluoride sensors based on Ga(III)OEP are now investigated in the same configuration. Fig. 5.2 illustrates the anionic response of a film composed of

110

Ga(III)OEP/KTFPB/o-NPOE/PVC. Various ionic additives other than KTFPB and non-ionic additives such as polyurethane (SG-80A) are examined in order to create an environment that does not favor the dimeric structure in the film.
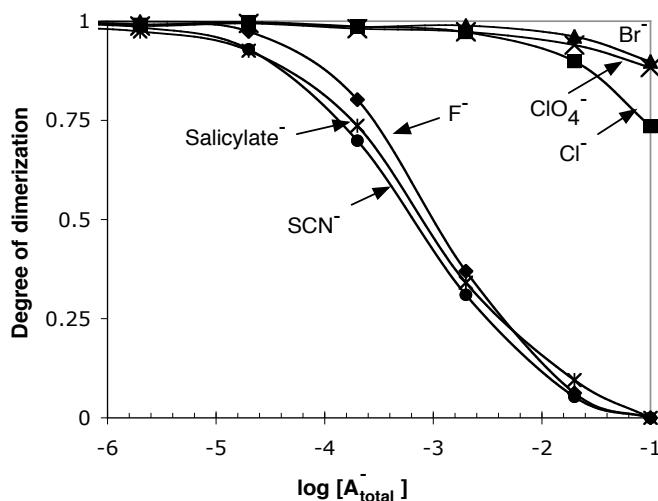
Figure 5.2 Anionic optical response based on the dimer-monomer equilibrium of Ga(III)OEP in the film containing Ga(III)OEP-OH (1 mg)/KTFPB (45 mol%)/o-NPOE (66 mg)/PVC (33 mg). Degree of dimerization was calculated based on the absorbance change at 384 nm (dimeric band) and illustrated as a function of total concentration of anion in the buffer (0.05 M phosphate buffer, pH 3.0).

One of the most plausible approaches that weakens dimeric structure of Ga(III)OEP is to dope the film with an anionic site that has an interaction to some degree with the dimeric structure. When the positively charged hydroxo-dimer is formed in the film, this positive charge should be balanced by anionic sites and the dimer-monomer equibrium should be rewritten as:

$$LOH + L^+ R^- \rightleftharpoons L_2OH^+ R^-$$
(rxn 5.11)

where L^+ indicates $Ga(III)OEP^+$ without any anionic ligand on the metal cation, LOH is Ga(III)OEP with hydroxide, L_2OH^+ is the hydroxo-dimer, and R^- is an anionic site. If interaction between L_2OH^+ and R^- is significant enough to overcome the solvent layer around the L_2OH^+ and R^-, L_2OH^+ will be broken into LOH and L^+R^- as separate complexes. However, if the interaction is so strong to break almost all the L_2OH^+ in the film, this system is not applicable to the dimer-monomer-based optical transduction. Therefore, the interaction between L_2OH^+ and R^- should be weak enough to keep the concentration of

L_2OH^+ at an appreciable level, but should also be strong enough to help promote monomer formation in the plasticized film, when the analyte is added.

The anionic sites should be highly lipophilic so they do not leach out of the film into aqueous phase and should not ligate onto the central metal cation otherwise the dimer is broken by the anionic sites from the beginning. A certain class of organic anions are poor ligands but still keep an ability to bind to the metal ion center. For example, conjugate bases of strong organic acids (e.g., benzene sulfonic acids) are poor anionic ligands but interactions with metalloporphyrins can be improved by the organic structure where the benzene group will have a π-π interaction with the porphyrin. When members of lipophilic benzene sulfonic acids such as dodecylbenzene sulfonic acid and dinonylnaphthalene sulfonic acid (DNNS) were tested as anionic additives, DNNS provided the most stable sensor response with a certain degree of interaction with the dimeric Ga(III)OEP. Therefore, instead of KTFPB, DNNS was doped in the optical sensing film to study the effect of weakening dimerization.

When DNNS is incorporated in the plasticized PVC membrane instead of KTF-PB, the degree of dimerization in the absence of fluoride or any analyte should be high. Fig. 5.3 shows the absorbance change of the Soret band with various amount of DNNS. Since DNNS used in this work is an industrial grade reagent, the purity of DNNS in the reagent is in question. According to Fig. 5.3, 38 mol% of DNNS (mol % was calculated based on the concentration written on the label) maximizes the dimerization. Comparing the initial dimer formation with KTFPB where almost 100 % dimerization was observed, DNNS provides about 70 % dimerization. Hence, dimerization is now weaker than the dimer with KTFPB yet still a significant amount of dimer remains in the film. The calibration curves in Fig. 5.4 show that all the anionic response has been shifted to lower concentrations by about 1.5 order of magnitude. Fig. 5.5 shows the reproducible optical responses for 10^{-3} M and 10^{-5} M F^-, using DNNS as the anionic additives of the sensing film.
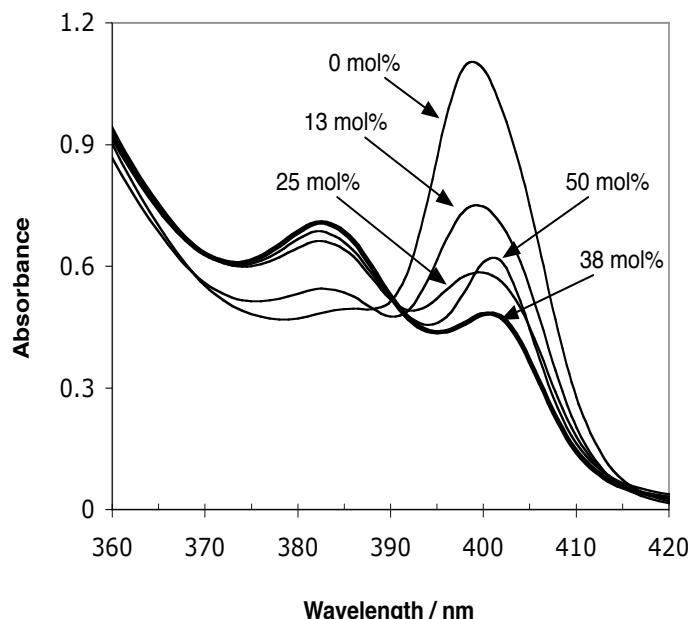
Figure 5.3 Spectral changes based on dimer-monomer equilibrium of the film (Ga(III)OEP-OH (1 mg)/DNNS (0 ~ 50 mol%)/*o*-NPOE (66 mg)/PVC (33 mg)) with various mol% of DNNS to Ga(III)OEP-OH. As an anionic site, DNNS can stabilize the dimeric form in the plasticized PVC film.
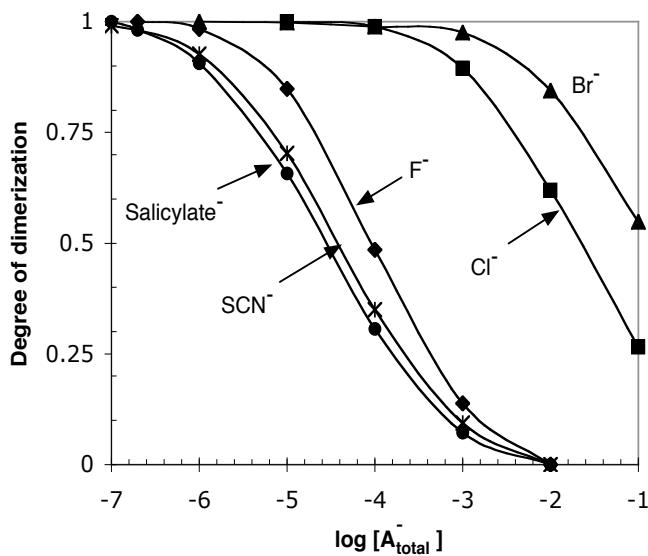
Figure 5.4 Anionic response based on the dimer-monemer equilibrium of Ga(III)OEP in the film containing Ga(III)OEP-OH (1 mg)/DNNS (40 mol%)/o-NPOE (66 mg)/PVC (33 mg). Degree of dimerization was calculated based on the absorbance change at 384 nm (dimeric band) and illustrated in the function of total concentration of anion in the buffer (0.05 M phosphate buffer, pH 3.0). Note that responses for all the anions are shifted to the lower concentration.
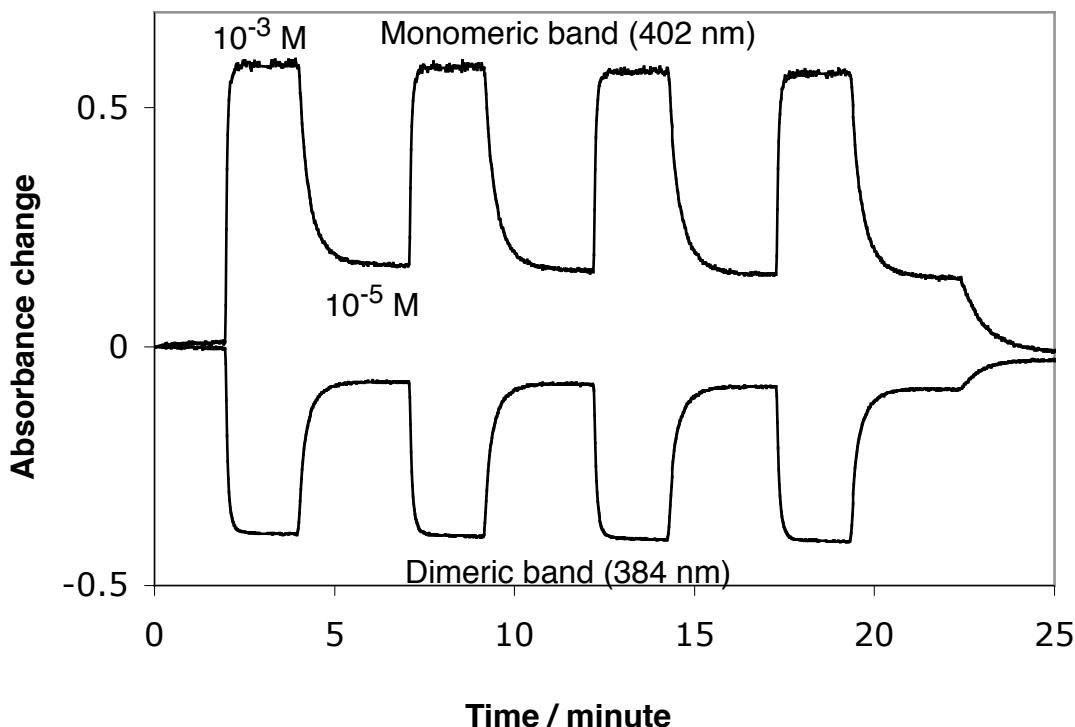
Figure 5.5 Absorbance changes at dimeric band (384 nm) and monomeric band (402 nm) upon responses between 10^{-3} M and 10^{-5} M [F^-_{total}] in 0.05 M phosphate buffer (pH 3.0).

The lipophilic polyurethane SG-80A has also been reported to destabilize dimerization of In(III) porphyrins [31]. This observation suggests that addition of appropriate amount of SG-80A in the plasticized PVC film will create an solvent environment that weakens the dimeric form of Ga(III)OEP. Fig. 5.6 shows the initial dimerization of Ga(III)OEP when contacting buffer with various content of SG-80A in the plasticized PVC film containing Ga(III)OEP and 45 mol% of KTFPB. As shown, between 0.3 - 3 wt% of SG-80A allows a significant degree of dimer formation. In Fig. 5.7, fluoride responses in the presence of 0, 0.03, 0.3, and 3 wt% of SG-80A in the films shows that detection limit is definitely lower than the film without polyurethane. One possible explanation for the effect of SG-80A is that the terminal group (e.g., amine or alcohol) of the polyurethane [32, 33] can behave like a ligand and weakens the dimerization in the film.
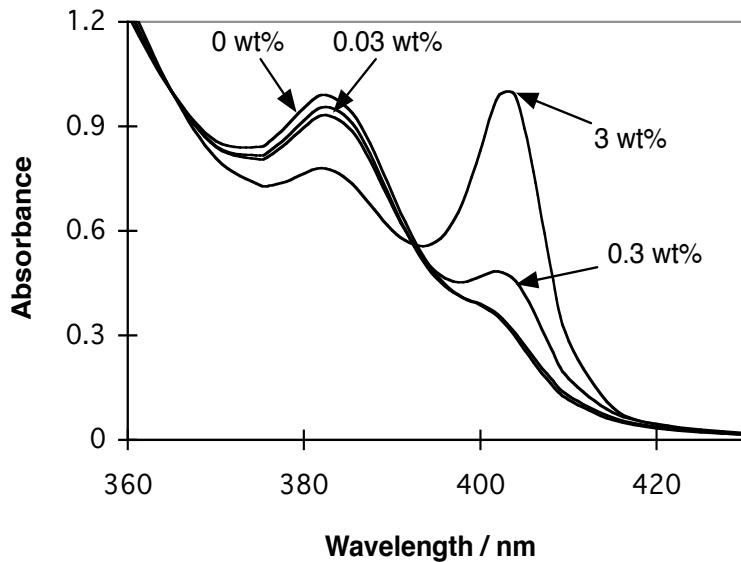
Figure 5.6 Initial dimerization of Ga(III)OEP in a polymer film (Ga(III)OEP-OH (1 mg)/ KTFPB (45 mol%)/SG-80A (0, 0.03, 0.3, and 3 mg)/o-NPOE (66 mg)/PVC (33 mg)) when the film is conditioned in the 0.05 M phosphate buffer (pH 3.0).
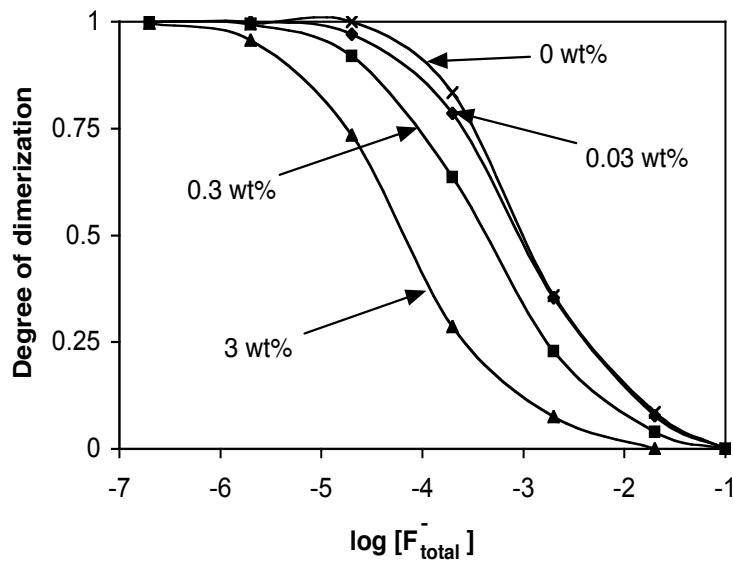
**Figure 5.7 Fluoride responses of the films (Ga(III)OEP-OH (1 mg)/KTFPB (45 mol%)/ SG-80A (0, 0.03, 0.3, and 3 mg)/o-NPOE (66 mg)/PVC (33 mg)) in the 0.05 M phosphate buffer (pH 3.0). Note that the detection limit is lowered as the amount of polyurethane (SG-80A) is increased.**

In summary, the dimer-monomer equilibrium of Ga(III)OEP can be weakened by incorporating DNNS or polyurethane within the polymeric film in order to improve sensitivity for detecting anions that break the dimeric structure. As can be seen in Figures 5.4 and 5.7, fluoride responses are lowered by about 1 - 1.5 decades with DNNS and polyurethane-doped films. However, this approach also increases the sensitivities for other anions and the selectivity for the fluoride is therefore not improved. In the following section, an effort to improve selectivity for fluoride is made by enhancing the dimer formation via fluoride serving as a bridging ligand for new diporpyrin structures.

5.3.3 Ion-selective electrodes based on the fluoro-bridged complexes of di-Ga(III) porphyrins

When an anion of interest forms a bridged dimer species with given metalloporphyrins, the selectivity for the anion will have additional selectivity enhancement by a factor of K_{L2F} as suggested via Eq. 5.15 in Section 5.3.1. In this section, experimental approaches to facilitate dimerization are examined. Since Ga(III) porphyrins appear to form a fluoro-bridged dimer, fluoride-selectivity would be improved by increasing K_{L2F}. The simplest way to increase dimerization is to increase the overall concentration (L_T) of the Ga(III) porphyrin in the film. However, this may cause an aggregation problem such as crystal growth of the metalloporphyrin in the film. Covalently linked porphyrin dimers would be a possible way to increase K_{L2F} if the linker provides a stable dimeric conformation. Therefore, a series of covalently linked Ga(III)TPP dimers should be studied to find an appropriate dimeric structure. It should be also noted that an optical transduction with this dimer-dimer mechanism would not be desirable due to the overlap of dimeric bands between the hydroxo-dimer and the fluoro-dimer. Therefore, ion-selective electrodes based on the di-Ga(III) TPPs are employed for the demonstration of selectivity improvement by enhancing the dimerization constants.

The response mechanism of the plasticized PVC films doped with Ga(III)TPPs and KTpClPB were examined with respect to relative lipophilic anionic levels in the films. Depending on mol% of KTpClPB to Ga(III)TPPs, the response mechanism can be

varied. For example, when F^- is introduced to the membrane containing greater than 50 mol% of anionic sites, fluoro-bridged dimer is formed (rxn 5.10). In this mechanism, the selectivity for F^- will be increased because F^- facilitates dimer formation while other anions can not form dimers. Therefore, the selectivity for F^- of the film containing 50 mol% or more anionic sites will be improved by $K_{L2F}[L_T]/4$ (See Section 5.3.1). However, as can be seen in Fig. 5.8, selectivity for fluoride with the Ga(III)TPP-based membrane are not significantly altered by varying the amount of anionic sites. One possible explanation is that since $K_{L2F}[L_T]/4 \approx 1$ or less, dimerization by fluoride is not important in the response mechanism. Considering that the amount of dimeric form is comparable to the amount of monomeric form (Fig. 5.1), it is a reasonable approximation that $K_{L2F} \approx [L_T] \approx 10^2 \ M^{-1}$ in rxn 5.2. Therefore, in order to improve selectivity for fluoride, K_{L2F} should be increased. One of the possible approaches is to utilize a covalently-connected di[Ga(III)TPP] species, that has a high intramolecular μ-fluoro-dimerization constant.
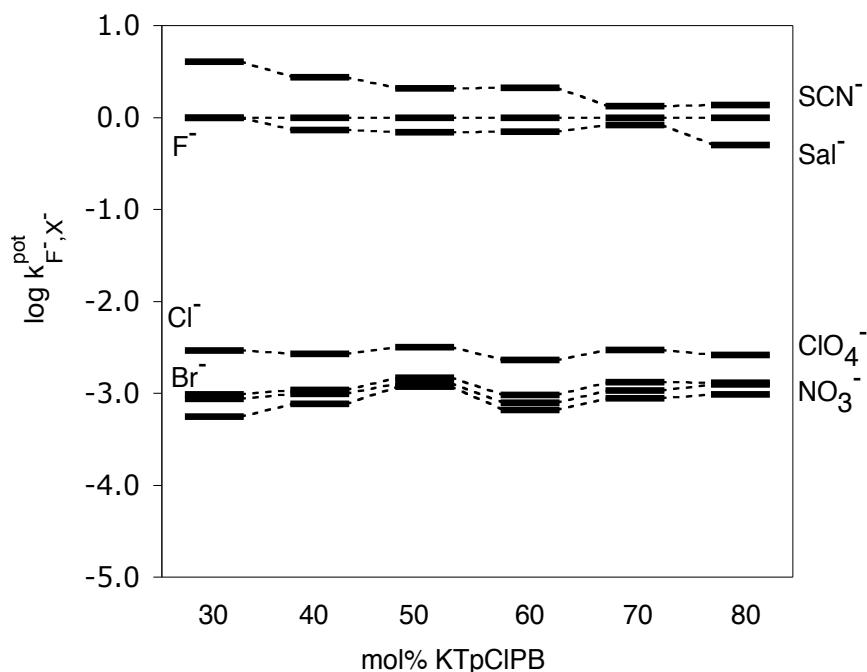
Figure 5.8 Selectivity for F^- with the ion-selective electrode membrane containing Ga(III)TPP(1 mg)/KTpClPB (30 ~ 80 mol%)/o-NPOE (66 mg)/PVC (33 mg).

When two metalloporphyrins are covalently connected via an organic spacer, depending on the stability of the molecular structure of the bridged dimer, and depending on the degree of freedom of each rotational bond in the spacer, the dimeric form can be

more or less favored than dimerization of two separate molecules (see Fig. 5.9). For example, if two porphyrin rings are connected via a long alkyl change, even though it can provide a stable bridged dimeric form, the free rotation of each C-C bond will entropically favor the separated porphyrins conformation and thus if a dimer is formed, it is more likely to have an inter-molecular dimerization rather than an intra-molecular dimerization.
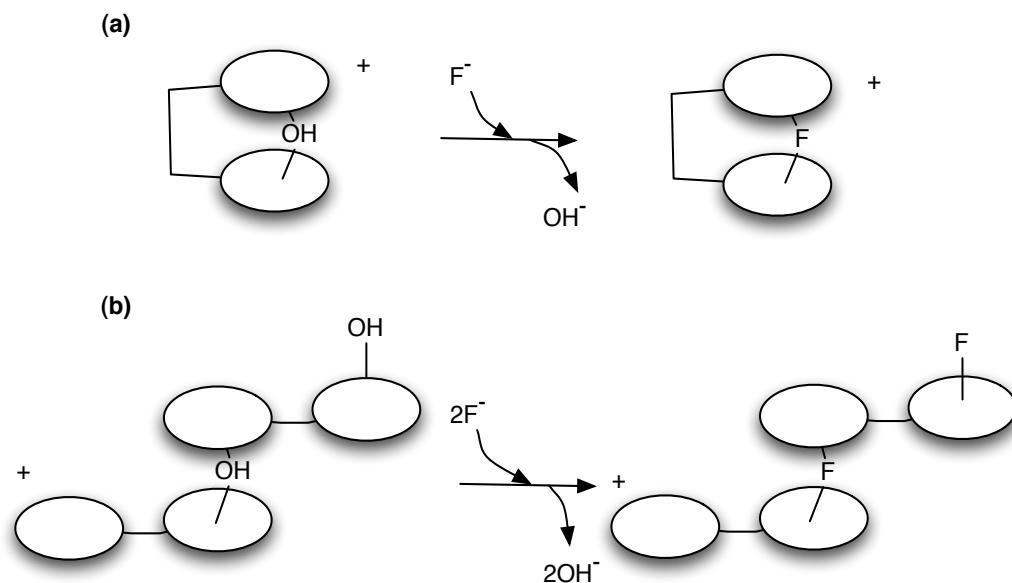
Figure 5.9 Response mechanism of covalently connected di[Ga(III)TPP] via intramolecular dimerization (a) and intermolecular dimerization (b).

Therefore, in this work, four different spacer groups (see scheme 5.1) were prepared to see which spacer will exhibit higher dimerization constant than that of the free metalloporphyrin. If intra-dimerization is dominant over inter-species-dimerization, the dimerization constant of covalently linked dimer is higher that that of free Ga(III)TPP, and the dimer-monomer equilibrium is no longer a concentration dependent process. With the covalently connected dimer, the amount of borate and the response mechanism must also be considered. The only difference is that, to achieve the effect of 50 mol% of anionic sites with GaTPP, 100 mol% of anionic sites are required with the (GaTPP)-link-(GaTPP) species as the ionophore.

Selectivity for fluoride in the presence of the optimal borate level is illustrated in Fig. 5.10 for membranes formulated with [GaTPP]$_2$-C$_4$H$_8$ (**2**) and [GaTPP]$_2$-*o,m,p*-xylene (**4**). These selectivities are compared to membranes doped with free GaTPP in terms of selectivity for fluoride at their optimal compositions. Among the covalently linked GaTPPs, *m*-xylene-link exhibits the most improved selectivity for fluoride over other anions. Figure 5.11 illustrates response curves of various anions using ISE membranes doped with Ga(III)TPP-OH (a) and [Ga(III)TPP-OH]$_2$-*m*-xylene (b) at optimized membrane compositions. The lower detection limit (LDL) for fluoride with both membranes are about 10^{-4} M. However, LDLs for salicylate and thiocyanate with a membrane containing *m*-xylene-linked porphyrin (b) are substantially higher that those with a membrane containing Ga(III)TPP-OH (a). Therefore, relative binding strength for fluoride over salicylate and thiocyanate with this diporphyrin must be enhanced due to having *m*-xylene link between two gallium(III) porphyrins.
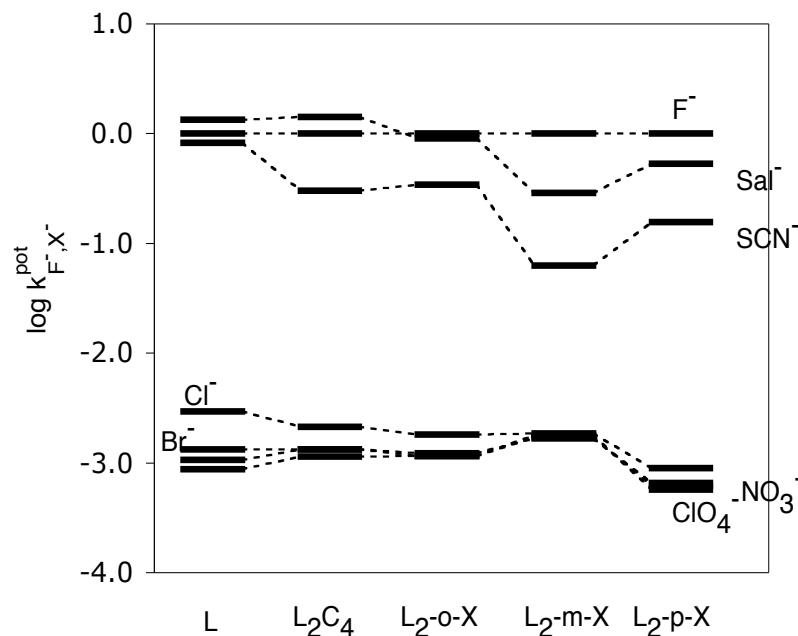
Figure 5.10 Membrane selectivity change for diporphyrin species made with different linkers. L indicates a Ga(III)TPP unit. The mol% of anionic sites are 70 mol% for Ga(III)TPP-doped film and 140 mol% for di(Ga(III)TPP)$_2$-doped films.
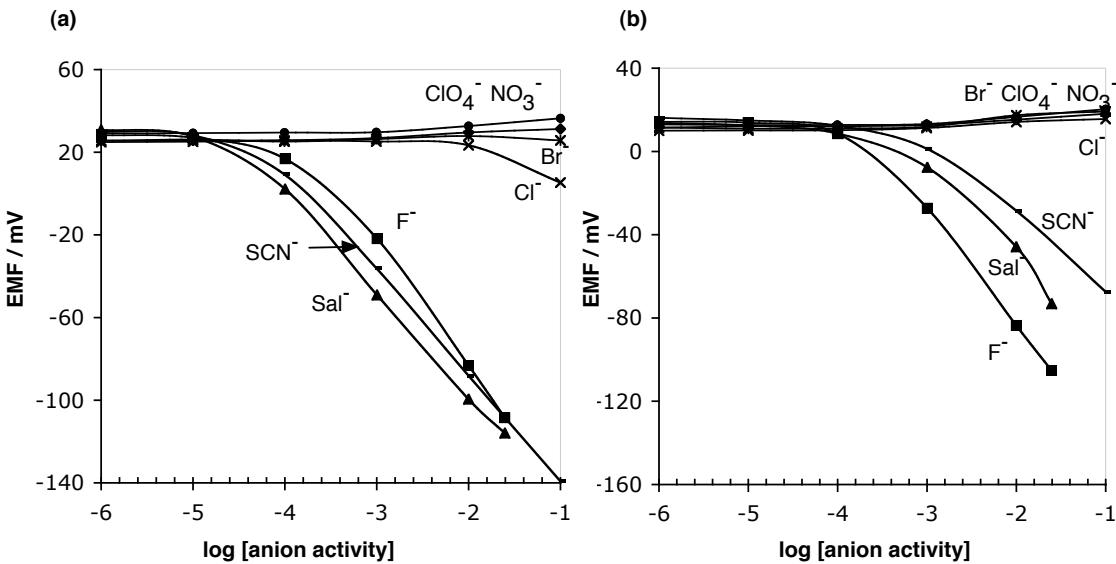
Figure 5.11 Calibration curves with membranes doped with Ga(III)TPP-OH (2 mg)/ KTpClPB (70 mol%)/*o*-NPOE (132 mg)/PVC (66 mg) (a) and [Ga(III)TPP-OH]₂-*m*-xylene (4b, 2.2 mg)/KTpClPB (140 mol%)/o-NPOE (132 mg)/PVC (66 mg) (b).

As discussed in the Section 5.3.1 and in the beginning of Section 5.3.3, if this enhancement of selectivity is achieved by the increased dimerization constant for fluoride, this improvement should be observed when film composition stabilizes dimeric species in the plasticized membrane. Indeed, as can be seen in Fig. 5.12, a significant selectivity shift occurs when KTpClPB is added at levels >100 mol%. In this composition, the following equilibrium dominates the membrane response for fluoride:

$$DOH^+ + F^-_{(aq)} \rightleftharpoons DF^+ + OH^-_{(aq)} \qquad \text{(rxn 5.12)}$$
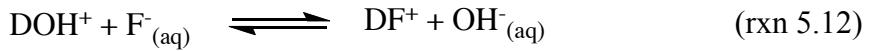
where DOH^+ and DF^+ indicates intra-dimerization via OH^- and F^-, respectively. The equilibrium in rxn 5.12 also explains why lower detection limit for fluoride is not decreased. Since hydroxide also can form a bridged dimer, binding with a hydroxide is also improved by the enhanced dimerization. Assuming dimerization strengths for bridging anions (i.e., OH^- and F^-) are comparable, covalently connecting two porphyrins will not lower detection limit for the anion that can form a dimer. However, an anion, X^-, that cannot form a dimeric structure should break the dimer to bind with one of the Ga(III)TPP-units:

120

$$DOH^+ + X^-_{(aq)} \rightleftharpoons X\text{-}L\text{-}L^+ + OH^-_{(aq)} \qquad \text{(rxn 5.13)}$$
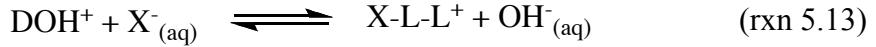
where XL-L$^+$ denotes a di-Ga(III)TPP with X$^-$ ligated to one of the central metal ions. The selectivity coefficient for X$^-$ over F$^-$ is then given by:

$$k^{pot}_{F^-,X^-} = \frac{\beta_{X\text{-}L\text{-}L^+}}{\beta_{F\text{-}L\text{-}L^+}} \times \frac{1}{K_{DF}K'_{exchange}} \qquad \text{(Eq. 5.16)}$$

where $\beta_{X\text{-}L\text{-}L+}$ and $\beta_{F\text{-}L\text{-}L+}$ are formation constants of the complex of diporphyrin with anion X$^-$ and F$^-$, respectively. K_{DF} is the dimerization constant of the reaction:

$$F\text{-}L\text{-}L^+ \xrightarrow{K_{DF}} DF^+ \qquad \text{(rxn 5.14)}$$

Assuming $\beta_{X\text{-}L\text{-}L+}/\beta_{F\text{-}L\text{-}L+}$ is comparable to β_{LX}/β_{LF}, the selectivity for fluoride is increased by K_{DF} ($\sim 10^3$), which is the intramolecular dimerization constant for fluoride.
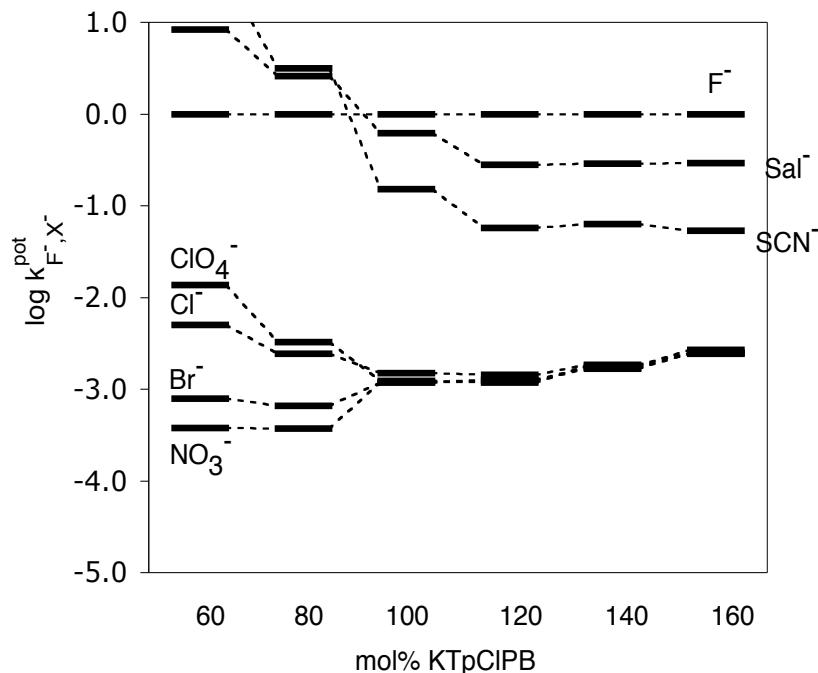
Figure 5.12 Selectivity for F$^-$ with the film ([Ga(III)TPP]$_2$-*m*-xylene(1 mg)/KTpClPB (60 ~ 160 mol%)/o-NPOE (66 mg)/PVC (33 mg)).

Covalently linked metalloporphyrins have their own unique advantages over other conventional metal complex-type anion ionophore. The selective response for bridging anions can be achieved by incorporating an appropriate linker between two porphyrins. Detection of fluoride in this work is a good example of this approach. There are many bridging anions such as imidazole, dicarboxylic acids, diamines, and bifunctional anionic drugs that are potential analytes for such a tweezer-type dimer-monomer response mechanism.

5.4   Conclusions

Since the dimer-monomer equilibrium of metalloporphyrins in plasticized PVC films is now understood in the case of ion-selective electrodes, many efforts have been made in order to suppress the dimerization or to utilize such dimerization in an optical transduction mode. Based on the detailed understanding of dimer-monomer equilibrium and new findings that fluoride also forms bridged dimers, further efforts to take full advantage of dimer-monomer equilibrium of Ga(III) porphyrins have been made in this chapter. By destabilizing the dimeric form in the plasticized membrane, lower detection limits have been achieved for optical fluoride sensing when maintaining a sufficient amount of initial hydroxo-dimer in the film. However, this approach also lowers detection limits for interfering ions. Therefore, in the subsequent work, dimerization was enhanced by designing an appropriate covalently connected dimeric Ga(III) porphyrin molecule. Since only fluoride among the anions tested forms the bridged dimeric conformation, enhanced dimerization improves selectivity for fluoride over other anions by about 10 fold in the case of potentiometric sensing of fluoride. This work provides further insight into designing anion-selective ionophores with metal ion complexes.

5.5 References

[1] Schmidtchen, F.P.; M. Berger, Chem. Rev. 97 (1997) 1609.

[2] Gale, P., Coord. Chem. Rev. 199 (2000) 181.

[3] Gale, P., Coord. Chem. Rev. 213 (2001) 79.

[4] Gale, P., Coord. Chem. Rev. 240 (2003) 191.

[5] Ripa, L.W., J. Public Health Dent. 53 (1993) 17.

[6] Mcdonagh, M.S.; P.F. Whiting; P.M. Wilson; A.J. Sutton; I. Chestnutt; J. Cooper; K. Misso; M. Bradley; E. Treasure; J. Kleijnen, Br. Med. J. 321 (2000) 855.

[7] Harrison, P.T.C., J. Fluorine Chem. 126 (2005) 1448.

[8] Ayoob, S.; A.K. Gupta, Crit. Rev. Environ. Sci. Technol. 36 (2006) 433.

[9] Frant, M.S.; J.W. Ross, Science 154 (1966) 1553.

[10] Bakker, E.; P. Bühlmann; E. Pretsch, Chem. Rev. 97 (1997) 3083.

[11] Bühlmann, P.; E. Pretsch; E. Bakker, Chem. Rev. 98 (1998) 1593.

[12] Hofmeister, F., Arch. Exp. Pathol. Pharmakol. 24 (1888) 247.

[13] Steinle, E.D.; U. Schaller; M.E. Meyerhoff, Anal. Sci. 14 (1998) 79.

[14] Malinowska, E.; L. Gorski; M.E. Meyerhoff, Anal. Chim. Acta 468 (2002) 133.

[15] Gorski, L.; E. Malinowska, Anal. Chim. Acta 540 (2005) 159.

[16] Badr, I.H.A.; M.E. Meyerhoff, Anal. Chim. Acta 553 (2005) 169.

[17] Badr, I.H.A.; M.E. Meyerhoff, Anal. Chem. 77 (2005) 6719.

[18] Mitchell-Koch, J.T.; M. Pietrzak; E. Malinowska; M.E. Meyerhoff, Electroanalysis 18 (2006) 551.

[19] Kang, Y.; J.W. Kampf; M.E. Meyerhoff, Anal. Chim. Acta 598 (2007) 295.

[20] Steinle, E.D.; S. Amemiya; P. Bühlmann; M.E. Meyerhoff, Anal. Chem. 72 (2000) 5766.

[21] Zhang, W.; E. Rozniecka; E. Malinowska; P. Parzuchowski; M.E. Meyerhoff, Anal. Chem. 74 (2002) 4548.

[22] Qin, W.; P. Parzuchowski; W. Zhang; M.E. Meyerhoff, Anal. Chem. 75 (2003) 332.

[23] Gorski, L.; E. Malinowska; P. Parzuchowski; W. Zhang; M. Meyerhoff, Electroanalysis 15 (2003) 1229.

[24] Qin, Y.; E. Bakker, Anal. Chem. 76 (2004) 4379.

[25] Ab, P.G.P.; J. Kampf; E. Rozniecka; Y. Kondratenko; E. Malinowska; M. Meyerhoff, Inorg. Chim. Acta 355 (2003) 302.

[26] Zhang, X.; B. Wayland, Inorg. Chem. 39 (2000) 5318.

[27] Witowska-Jarosz, J.; L. Gorski; E. Malinowska; M. Jarosz, J. Mass Spectrom. 37 (2002) 1236.

[28] Witowska-Jarosz, J.; L. Gorski; E. Malinowska; M. Jarosz, J. Mass Spectrom. 38 (2003) 1265.

[29] Park, S.B.; W. Matuszewski; M.E. Meyerhoff; Y.H. Liu; K.M. Kadish, Electroanalysis 3 (1991) 909.

[30] Malinowska, E.; J. Niedziolka; E. Rozniecka; M. Meyerhoff, J. Electroanal. Chem. 514 (2001) 109.

[31] Malinowska, E.; J. Niedziolka; M. Meyerhoff, Anal. Chim. Acta 432 (2001) 67.

[32] Boretos, J.; W. Pierce, Science 158 (1967) 1481.

[33] Gunatillake, P.; D. Martin; G. Meijs; S. Mccarthy; R. Adhikari, Aust. J. Chem. 56 (2003) 545.

Chapter 6

Conclusions and Future Directions

6.1   Conclusions

In this dissertation work, optical and electrochemical sensors based on metalloporphyrins and an In(III) texaphyrin were examined. Research has focused on understanding the underlying chemistry of metalloporphyrins in the plasticized polymeric films, including interactions between metalloporphyrins and anions, conformational processes such as dimerization via hydroxide or fluoride bridges, and effects of added ionic sites on the stability of either cationic or anionic forms of metalloporphyrins. Based on the knowledge of these chemical processes, the dissertation work focused on designing sensors for target analytes and improving sensing properties by: 1) modifying the dimension of a sensing film (i.e., reducing the thickness of the film for fast response); 2) by incorporating an appropriate metal ion center (i.e., scandium(III) in the porphyrin ring as a fluoride ionophore); 3) by adopting a novel ligand structure (i.e., texaphyrin as a lipophilic ligand that holds metal cation in the plasticized polymeric film); and 4) by manipulating dimer-monomer equilibrium of metalloporphyrin in the polymeric phase.

In Chapter 2, optical sensors with rapid response times (1~2 s) toward solution phase chloride and gas phase amine species were studied. The sensors were based on the incorporation of indium(III) octaethylporphyrin (In(III)[OEP]) within ultra-thin polymeric films (< 0.5 μm) deposited via spin coating on a planar fused silica waveguide. The In(III)[OEP] formed a hydroxide ion bridged dimer when lipophilic anion sites in the form of a lipophilic borate derivative (i.e., potassium tetrakis([3,5-bis(trifluoromethyl)phenyl]borate (KTFPB)) were added to the plasticized films. Selective chloride or amine extraction into the films resulted in a change in the optical

absorption spectrum of the metalloporphyrin owing to ligation of these species to the In(III) center, forcing the formation of monomeric In(III)[OEP] species. These ligation reactions were completely reversible. One of the key fundamental questions answered in this work was how fast the optical response could be based on this dimer-monomer equilibrium of In(III)OEP for aqueous chloride and gaseous amine vapor detection. The use of the waveguide sensing configuration exhibited extremely fast response times (~ 2 sec) without loss in sensitivity since the optical path-length is significant (e.g., absorbance is enhanced about 20 times even when 0.3 µm-thick film is employed). The fast response times of the sensors makes such devices potentially useful as detectors in flow-through analytical systems such as flow-injection analysis (FIA) or gas/liquid phase chromatography.

However, issues associated in using a very thin film were also recognized. Especially loss of o-NPOE plasticizer from the film was a primary factor that limits the lifetime of these sensors. Employing more viscous plasticizers partially solves this problem. Studies regarding the humidity effect on the dimer-monomer equilibrium revealed its fundamental role in the sensor chemistry. Water from air plays two important functions regarding the dimer-monomer equilibrium of metalloporphyrins: water provides OH^- to the metal complexes and water also solvates ionic species in the hydrophobic polymer film. Depending on the degree of hydration of ions, ion-ion interaction can vary significantly and also the dimer-monomer equilibrium can be affected. At a very low humidity, the dimer was broken into monomers, which can be ascribed to the increased interaction between positively charged In(III)OEPs and added lipophilic borate species. At a high humidity, the dimer is stabilized even when the anionic sites are present at 100 mol%, which indicates that H_2O is dissociated into H^+. In this case, OH^- and H^+ is counter-balanced by anionic sites in the film and OH^- is ligated to In(III)OEP to form the dimer, whose formation constant was estimated to be about 10^{16} M^{-2} [1].

In Chapter 3, scandium(III) porphyrins were prepared and characterized as ionophores in optical and electrochemical fluoride sensors. As predicted based on a hard-

soft acid-base perspective, sensors with Sc(III)OEP were found to be comparable to sensors with Al(III) porphyrins as most promising ionophores for fluoride detection [2-6]. In addition, a bis(μ-fluoride) dimer of Sc(III)OEP was isolated and characterized by X-ray crystallography. This is the first report of a dimeric structure of metalloporphyrin bridged by two fluoride ligands. In both optical and electrochemical sensors, selectivities for fluoride were excellent over other inorganic anions tested. Only salicylate exhibited a severe interference with a response comparable to fluoride. In the optical sensing film containing Sc(III)OEP and ETH 7075, salicylate can be discriminated from fluoride since fluoride initiates dimerization of the Sc(III)OEP which causes a blue shift of the Soret band while salicylate does not shift the Soret band at all. Therefore, by monitoring absorbance bands of the Sc(III)OEP dimer (at 393 nm) and ETH 7075 (at 550 nm), selectivity can be further enhanced for fluoride over interfering anions (i.e., salicylate). Electrochemical sensors based on Sc(III)OEP exhibited reversible and fast fluoride response. Fluoro-bridged dimerization was confirmed in these films but does not lead to super-Nernstian response. In contrast, as shown previously, anion-selective electrodes based on In(III) porphyrins, Ga(III)porphyrins, and Zr(IV) porphyrins exhibit super-Nernstian response and slow recovery time because of dimerization of metalloporphyrins. Binding constants of Sc(III)OEP with various anions determined by the sandwich membrane method showed the highest binding affinity between fluoride and Sc(III)OEP, as expected.

Chapter 4 described a study demonstrating the use of an expanded porphyrin as a lipophilic ligand that holds a metal cation as an anion ionophore. Lipophilized indium(III) texaphyrin was prepared to prevent leaching from the hydrophobic polymer phase, and the resulting polymeric films were characterized in optical and electrochemical sensing configurations. In optical anion sensors, only one axial site in In(III) texaphyrin was available for the anion binding when ETH 7075 was doped in the polymeric film. This optical sensor showed good response to thiocyanate and exhibited a non-Hofmeister selectivity pattern. Electrochemical sensors based on the In(III) texaphyrin were also studied with varying ionic sites and results suggest a charged carrier ionophore mechanism, where the positively charged In(III) texaphyrin binds directly with

anions. Selectivity of this electrode was observed to depend on the relative amount of anionic additives, where the polymer membrane with lower anionic sites (< 50 mol%) preferentially responded to thiocyanate and, at higher anionic concentration (> 50 mol%) in the membrane, fluoride response became more significant. Comparison of various indium(III) complexes as ionophores reported in the previous literature provided valuable insights on understanding the ligand effect on the central metal cation with respect to its preference to anions.

Chapter 5 reported on an effort to understand and utilize, advantageously, a dimer-monomer equilibrium in anion sensor development. The tendency of a metalloporphyrin to form a bridged dimer in a polymeric membrane via a certain anion can both be beneficial and detrimental depending on the nature of anion that is to be measured. Ga(III) porphyrins were studied as model compounds that suffer significant interference from SCN$^-$ and salicylate when films doped with Ga(III) porphyrins were used for the fluoride detection. Ga(III) porphyrins also exhibit intermediate dimerization tendancy where fluoride promotes both monomeric fluoro-complex and fluoro-bridged dimer in the polymer membrane. If fluoride breaks the dimeric structure of Ga(III)OEP, manipulation of membrane compositions (by doping DNNS or KTFPB/polyurethane) that do not favor dimerization in the membrane should improve sensitivity for the anion. Optical fluoride sensors based on the film with Ga(III)OEP and appropriate dopants that weakened dimerization were shown to exhibit improved sensitivity for the fluoride. Since weakening dimerization improved sensitivities for all the anions except for the bridging anion (i.e., OH$^-$), weakening dimerization resulted in lower detection limits for all the anions except for OH$^-$. However, if fluoride also promotes dimerization, enhancing dimerization constant by covalently connecting two metalloporphyrins together with an appropriate linking structure should improve selectivity for fluoride. A series of di(Ga(III)TPP)s were prepared and Ga(III)TPP connected via *m*-xylene was shown to exhibit much improved selectivity for fluoride over thiocyanate and salicylate, when potentiometric sensors were prepared using these novel compounds as ionophores.

The studies of anion sensors based on metalloporphyrins and metallotexaphyrins in

optical and electrochemical sensing configurations conducted in this dissertation work provide insightful understanding and valuable experimental results on the chemistry of metalloporphyrins in polymeric matrices. This information will be an important resource in designing sensors for better response time, better sensitivity, and better selectivity for target analyte anions. Efforts should continue to examine various metal-complexes as anion acceptors, to understand the fundamental chemistry of those compounds in the given sensor system, and to establish approaches to modify components for optimal sensor performance.

6.2   Future directions

6.2.1   Polymeric matrices for optical sensors based on ultra-thin films

Issues that emerged in Chapter 2 regarding loss of plasticizers into the sample phase may be resolved if a plasticizer-free matrix is used. Polymethylmethacrylate [7-9], silicone rubber [10-13], and polyurethane [14] have been employed previously as plasticizer-free polymeric matrices for ionophore-based sensors. The success of these materials can be partially attributed to polymeric structures that do not interfere with the interaction between ionophores and analytes. However, when a dimer-monomer equilibrium occurs, interactions between the ionophore and the polymer backbone may not be negligible. A preliminary study in the course of this dissertation work using silicone rubber showed that dimerization of In(III)OEP was not favored and a crystallization of metalloporphyrin occurred in the matrix. A hydrophobic polyurethane (SG-80A) also destabilized dimeric forms of metalloporphyrins. Therefore, to utilize a dimer-monomer equilibrium of a metalloporphyrin for sensing purposes, the choice of polymeric matrices is limited.

In order to have dimeric forms of metalloporphyrins in a plasticizer-free polymer matrix, not only does the polymeric matrix need to be flexible (with low T_g), but also it should not contain any possible ligation unit in the backbone structures such as amines, amides, and alcohols. A polymer with high dielectric constant will solvate

129

metalloporphyrins well enough to prevent crystallization. Copolymers of a flexible unit and a high dielectric unit should be examined. For example, polymethylmethacrylate and methylmethacrylate copolymers (e.g., with polyethylene oxide) should be examined as a matrix for dimer-monomer equilibrium of In(III)OEP. To characterize the polymeric matrix, the stability of metalloporphyrin in the given polymeric film should be studied in detail. Trace amounts of the initiator may facilitate decomposition of the metalloporphyrin. Once stability of the ionophores are found to be adequate for sensor testing, selectivity, reversibility, response time, and lifetime should be characterized. The polymeric matrix may have different innate partition pattern for anions, may have too slow mass transport in the film, and may contain some endogenous ionic groups. All of these could influence properties of sensors prepared with these materials. The plasticizer-free polymeric film, however, can ultimately still provide a fast responding optical sensors based on use of ultra-thin film coatings on the waveguide configuration.

6.2.2 Utilizing dimer-monomer equilibria of metalloporphyrins for detection of gaseous analytes and various organic anions

One great advantage of having a dimer-monomer equilibrium within the polymer film is that response to neutral ligands may be possible without requiring co-extraction of protons to observe optical changes of a chromoionophore [15]. The dimer-monomer equilibrium of In(III)OEP has already been utilized for gaseous amine detection [16]. In the same configuration, Sc(III)OEP can be employed for gaseous HF detection or other neutral gaseous ligand species (amines, CO, or NO). Gas phase selectivity can be characterized in this configuration. The advantage of using Sc(III)OEP over In(III)OEP is that dimers of Sc(III)OEP are neutral species and thus humidity effects may be relatively small. In handling HF gas, great care will need to be taken in building the flowing gas system for generation of $HF_{(g)}$, and to quench $HF_{(g)}$ at the outlet [17]. In order to obtain a calibration curve, an independent method to quantify HF in the flowing gas phase must be devised. Monitoring fluoride with a LaF_3 electrode in the HF-quenching buffer solution would be a simple way to determine the HF concentration in the gas phase.

Covalently connected diporphyrin species will also provide an alternative approach for designing ionophores for a certain class of anions (e.g., dicarboxylic acid, diamines, or organic drugs that have two or more metal ion binding sites). Depending on the metal cation in the porphyrin and the linking structure, selectivity for anions can be modulated to improve the response for the target anion or to suppress interference from other anions in the sample. Zn(II) porphyrin-dimers via imidazole bridges will be a good first example for this approach [18]. Figure 6.1 illustrates candidate dimeric structures of metalloporphyrins [19-23] for such studies. Of course, the Zn(II) centers could be changed to other metal cations that interact more favorably with the target analyte anion.

Before employing these dimeric complexes as ionophores, solubility in the plasticized polymeric film must be confirmed. Due to the increased molecular weight, solubility in organic solvents (i.e., $CHCl_3$, CH_2Cl_2, and THF) can be reduced significantly. If metallation of the given dimeric porphyrin is not reported, metallation

(a) face-to-face pophyrin via urea-link [19] **(b) porphyrin dimer via calix[4]arene [20]**
(Porf=tetraphenylporphyrin)

(c) porphyrin co-facial dimer [21] **(d) porphyrin dimer via L-lysine [22]**
(M=Zn, Ni)
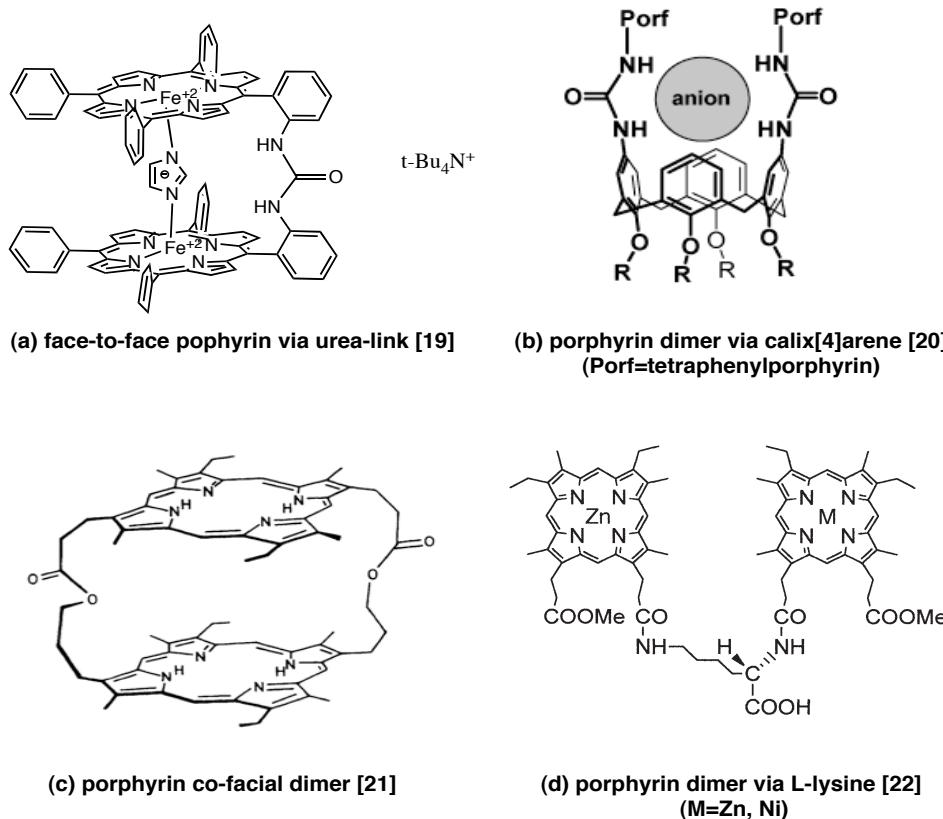
Figure 6.1 A few examples of dimeric structures of metalloporphyrins found in literature that may be of interest in testing as ionophores for anion sensors

may be a problem. Since solubility of ligand can be limited, the rate of metallation reaction can be quite slow under conditions that use acetic acid as the solvent. In such a case, addition of a chlorinated solvent with an appropriate boiling point will increase the solubility of the diporphyrin ligand maintaining solubility of metal salts in the reaction mixture (see Chapter 5, Section 5.2.2).

6.2.3   Further studies on metallated expanded porphyrins

The study of In(III) texaphyrin in this dissertation research was the first effort to utilize a metallated expanded porphyrin as an ionophore in anion selective sensors. Even though the results with In(III) texaphyrin are not superior to the known ionophores for fluoride or thiocyanate, the work provided valuable insights on the ligand effect of texaphyrin on the central metal cation when the anion selectivity of the In(III) texaphyrin-based ISE was compared to those of Ga(III) porphyrin and In(III) porphyrin ionophores. Therefore, the next stages of sensor studies using metallotexaphyrins should focus on examining other metal ions such as Mn(II), Y(III), and lanthanides(III) as the central metal cation in the lipophilized texaphyrin structure. Selectivity patterns in optical and electrochemical modes using such texaphyrins should provide preliminary information about the preferred anion ligation chemistry of these structures.

Other than metallotexaphyrins, pyrrole-based conjugated cyclic ligands such as various metallated expanded porphyrins [24-28] as well as contracted porphyrins [29, 30] have been reported (see Fig. 6.2). Especially a boron(III) subporphyrin would be an interesting candidate for a fluoride sensor since hardness of central metal cation would be even higher than Al(III) porphyrins. Indeed, organoboron compounds have been studied as fluoride binding agents for many years [30-35]. If the well-known oxophilicity of boron is comparable to "fluorophilicity" of the given boronic structure, it should exhibit good fluoride sensitivity. In order to examine the metallocomplexes shown in Fig. 6.2 as ionophores, each compound should exhibit a reversible ligand exchange and the central metal cation should stay in the core of the ligand irreversibly. The redox state must also be stable, the complex should be inert to acid or base from the sample solution, and the

species should not decompose under light. Once these basic properties are confirmed, the metal complexes can be doped in polymeric films for anionic response testing. By doping the film with appropriate additives or by modifying the peripheral structure of the ligand or by employing an appropriate polymeric matrix, the anion sensor could be optimized. The selectivity patterns, reversibility, and lifetime of sensors based on these structures can then be characterized.

(a) dimetal macrocyclic complexes from reference [24, 27, 28]

(b) boron(III) subporphyrins [29]
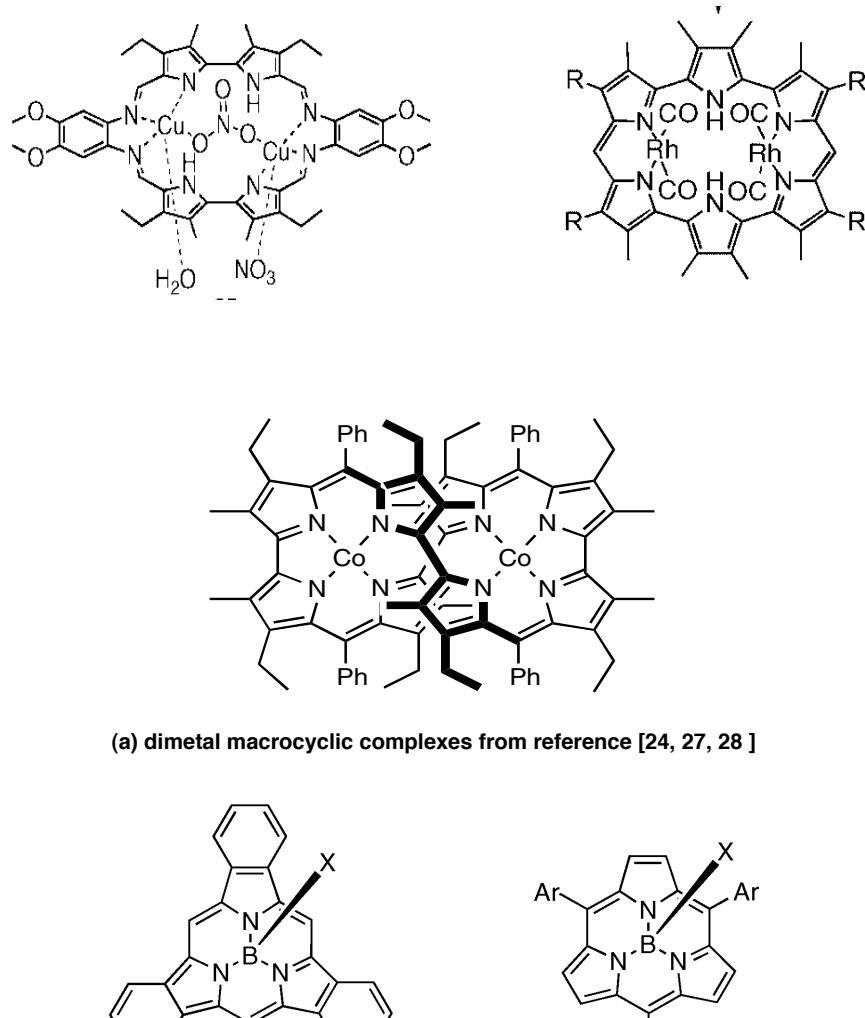
Figure 6.2 Dimetal expanded porphyrins (a) and boron(III) subporphyrins (b).

6.3 References

[1] Steinle, E.D.; S. Amemiya; P. Bühlmann; M.E. Meyerhoff, Anal. Chem. 72 (2000) 5766.

[2] Badr, I.H.A.; M.E. Meyerhoff, J. Am. Chem. Soc. 127 (2005) 5318.

[3] Badr, I.H.A.; M.E. Meyerhoff, Anal. Chim. Acta 553 (2005) 169.

[4] Badr, I.H.A.; M.E. Meyerhoff, Anal. Chem. 77 (2005) 6719.

[5] Mitchell-Koch, J.T.; M. Pietrzak; E. Malinowska; M.E. Meyerhoff, Electroanalysis 18 (2006) 551.

[6] Pietrzak, M.; M. Meyerhoff; E. Malinowska, Anal. Chim. Acta 596 (2007) 201.

[7] Ambrose, T.; M. Meyerhoff, Electroanalysis 8 (1996) 1095.

[8] Malinowska, E.; L. Gawart; P. Parzuchowski; G. Rokicki; Z. Brzozka, Anal. Chim. Acta 421 (2000) 93.

[9] Qin, Y.; S. Peper; E. Bakker, Electroanalysis 14 (2002) 1375.

[10] Tsujimura, Y.; M. Yokoyama; K. Kimura, Anal. Chem. 67 (1995) 2401.

[11] Tsujimura, Y.; T. Sunagawa; A. Yokoyama; K. Kimura, Analyst 121 (1996) 1705.

[12] Shin, J.H.; D.S. Sakong; H.Y. Nam; G.S. Cha, Anal. Chem. 68 (1996) 221.

[13] Bakker, E.; P. Buhlmann; E. Pretsch, Electroanalysis 11 (1999) 915.

[14] Malinowska, E.; J. Niedziolka; M.E. Meyerhoff, Anal. Chim. Acta 432 (2001) 67.

[15] Seiler, K.; W. Simon, Anal. Chim. Acta 266 (1992) 73.

[16] Qin, W.; P. Parzuchowski; W. Zhang; M.E. Meyerhoff, Anal. Chem. 75 (2003) 332.

[17] Franks, A.; P. Harper; M. Bilo, J. Hazard. Mater. 51 (1996) 11.

[18] Zhang, Y.; R. Yang; F. Liu; K. Li, Anal. Chem. 76 (2004) 7336.

[19] Landrum, J.; D. Grimmett; K. Haller; W. Scheidt; C. Reed, J. Am. Chem. Soc. 103 (1981) 2640.

[20] Dudic, M.; P. Lhotak; I. Stibor; K. Lang; P. Proskova, Org. Lett. 5 (2003) 149.

[21] Cowan, J.; J. Sanders, J. Chem. Soc., Perkin Trans. 1 (1987) 2395.

[22] Takeuchi, Y.; H. Watanabe; A. Kashiwada; M. Nagata; T. Ohtsuka; N. Nishino; H. Kawai; T. Nagamura; Y. Kurono; N. Oku; M. Nango, Chem. Lett. (2002) 848.

[23] Yagi, S.; I. Yonekura; M. Awakura; M. Ezoe; T. Takagishi, Chem. Commun. (2001) 557.

[24] Sessler, J.; E. Tomat, Acc. Chem. Res. 40 (2007) 371.

[25] Mori, S.; K.S. Kim; Z. Yoon; S.B. Noh; D. Kim; A. Osuka, J. Am. Chem. Soc. 129 (2007) 11344.

[26] Mori, S.; S. Shimizu; J. Shin; A. Osuka, Inorg. Chem. 46 (2007) 4374.

[27] Sessler, J.; P.J. Melfi; E. Tomat; V. Lynch, J. Chem. Soc., Dalton Trans. (2007) 629.

[28] Setsune, J.I.; M. Mori; T. Okawa; S. Maeda; J. Lintuluoto, J. Organomet. Chem. 692 (2007) 166.

[29] Inokuma, Y.; Z. Yoon; D. Kim; A. Osuka, J. Am. Chem. Soc. 129 (2007) 4747.

[30] Li, Y.; S. Xu; X. Li; K. Chen; H. Tian, Chem. Lett. 36 (2007) 664.

[31] Arimori, S.; M. Davidson; T. Fyles; T. Hibbert; T. James; G.I. Kociok-Kohn, Chem. Commun. (2004) 1640.

[32] Sole, S.; F. Gabbai, Chem. Commun. (2004) 1284.

[33] Liu, Z.Q.; M. Shi; F. Li; Q. Fang; Z. Chen; T. Yi; C. Huang, Org. Lett. 7 (2005) 5481.

[34] Zhou, Z.; F. Li; T. Yi; C. Huang, Tetrahedron Lett. 48 (2007) 6633.

[35] Agou, T.; J. Kobayashi; Y. Kim; F. Gabbai; T. Kawashima, Chem. Lett. 36 (2007) 976.